

National Chiao Tung University

Department of Materials Science and Engineering

Ph.D. Thesis

**Synthesis, Characterization, and Applications of Low Band-Gap
Bithiazole-Based Polymers and their Supramolecular Networks
Complexed with H-Bonded Cross-Linkers for Polymer Solar
Cells**

合成含 **Bithiazole** 低能隙高分子及與氫鍵交聯體形成超分子網狀結構在太陽能高分子

電池之應用

Dhananjaya Patra (達南杰)

Advisor: Hong-Cheu Lin, Ph.D. (林宏洲 教授)

December, 2011

Synthesis, Characterization, and Applications of Low Band-Gap Bithiazole-Based Polymers and their Supramolecular Networks Complexed with H-Bonded Cross-Linkers for Polymer Solar Cells

合成含 **Bithiazole** 低能隙高分子及與氫鍵交聯體形成超分子網狀結構在太陽能高分子

電池之應用

Student: Dhananjaya Patra (達南杰)

Advisor: Hong-Cheu Lin, Ph.D. (林宏洲 教授)

A Thesis submitted to
Department of Materials Science and Engineering
College of Engineering
National Chiao Tung University
In partial fulfillment of the requirement for the degree of
Doctor of Philosophy
In materials science and engineering

December, 2011



“In a day when you don't come across any problems — you can be sure that you are traveling in the wrong path”.

(Swami Vivekananda)

Abstract

Prime aim of this dissertation is to bring together the areas of low band-gap conjugated (LBG) polymers and their supramolecular networks complexed with π -conjugated cross-linkers for the applications of organic solar cells. These D-A conjugated polymers/their supramolecular networks possessed broad absorption sensitization in the region of 300-750 nm, having the lowest optical band gaps as low as 1.68 eV. Both highest occupied molecular orbital (HOMO) and lowest unoccupied molecular orbital (LUMO) energy levels of the LBG polymers/their supramolecular networks were within the desirable range of ideal energy levels. Hole and electron mobilities of these polymers/their supramolecular networks are in the range of 10^{-6} - 10^{-8} cm^2/Vs , which were calculated from the space-charge limited current experiments. Because of these properties, these were applied to polymer solar cell (PSC) as electron donors with (6,6)-phenyl- C_{61} -butyric acid methyl ester (PC_{61}BM) or (6,6)-phenyl- C_{71} -butyric acid methyl ester (PC_{71}BM) as an acceptor.

First, a series of LBG donor-acceptor conjugated main-chain copolymers (**P1-P4**) containing planar 2,7-carbazole as electron donors and bithiazole units (4,4'-dihexyl-2,2'-bithiazole and 4,4'-dihexyl-5,5'-di(thiophen-2-yl)-2,2'-bithiazole) as electron acceptors were synthesized and studied for the applications in PSC. The effects of electron deficient bithiazole units on the thermal, optical, electrochemical, and photovoltaic properties of these LBG copolymers were investigated. The photovoltaic device bearing an active layer of polymer blend **P4**: PC_{71}BM (1:1.5 w/w) showed the best power conversion efficiency (PCE) value of 1.01% with a short circuit current density (J_{sc}) of $4.83 \text{ mA}/\text{cm}^2$, a fill factor (FF) of 35%, and $V_{\text{oc}} = 0.60 \text{ V}$ under $100 \text{ mW}/\text{cm}^2$ of AM 1.5 white-light illumination. Again, five LBG conjugated polymers (**P1-P5**) consisting of one dithieno[3,2-b:2',3'-d]pyrroles (DTP) unit as an electron donor and various bithiazole units as electron acceptors were designed. The PSC device containing an active layer of **P5**: PCBM =1:1 exhibited a best PCE of 0.69%, with a V_{oc} of 0.40 V, a J_{sc} of $4.0 \text{ mA}/\text{cm}^2$, and a FF of 43% under the illumination of AM 1.5, $100 \text{ mW}/\text{cm}^2$.

Furthermore, a conjugated main-chain copolymer (**PBT**) consisting of bithiazole, DTP, and pendent melamine units was synthesized by Stille polymerization, which can be hydrogen-bonded (H-bonded) with proper molar amounts of bi-functional π -conjugated cross-linker **F** (i.e.,

two uracil motifs covalently attached to a fluorene core through triple bonds symmetrically) to develop a novel supramolecular polymer network (**PBT/F**). The effects of multiple H-bonds on light harvesting capabilities, HOMO levels, and photovoltaic properties of polymer **PBT** and H-bonded polymer network **PBT/F** are investigated. The preliminary results show that the solar cell device containing 1:1 wt. ratio of **PBT/F** and PC₇₁BM offers the best power conversion efficiency (PCE) value of 0.86% with a J_{sc} of 4.97 mA/cm², an V_{oc} of 0.55 V, and FF of 31.5%. Besides, Stille polymerization was employed to synthesize another LBG conjugated main-chain polymer **PBTH** consisting of bithiazole, DTP, and pendent melamine derivatives. Novel supramolecular polymer networks **PBTH/C** and **PBTH/F** were developed by mixing proper molar amounts of polymer **PBTH** (containing melamine pendants) to be hydrogen-bonded (H-bonded) with complementary uracil-based conjugated cross-linkers **C** and **F** (i.e., containing two symmetrical uracil moieties connected with carbazole and fluorene units through triple bonds). The formation of multiple H-bonds between polymer **PBTH** and cross-linkers **C** or **F** was confirmed by FT-IR measurements. In contrast to polymer **PBTH**, the supramolecular design with multiple H-bonds can enhance the photovoltaic properties of PSC devices containing H-bonded polymer networks **PBTH/C** and **PBTH/F** by tuning their light harvesting capabilities, HOMO energy levels, and crystallinities. The PCE values of PSC devices containing supramolecular polymer networks **PBTH/C** and **PBTH/F** (as polymer:PC₇₁BM=1:1 w/w) are found to be 0.97 and 0.68%, respectively, in contrast to 0.52% for polymer **PBTH**. The highest PCE value of 1.56% with J_{sc} value of 7.16 mA/cm², a V_{oc} value of 0.60 V, and a FF of 0.36 was obtained in the PSC device containing supramolecular polymer networks **PBTH/C** as polymer:PC₇₁BM=1:2 w/w.

摘要

主要的研究方向是利用共軛性高的分子，及超分子的作用力，連結低能隙的高分子(LBG)，形成交聯的結構後，在有機太陽電池上的應用。這些 D-A 共軛高分子和其交聯的結構，皆具有寬廣的吸收帶(300~750 nm)，其中最低光學能隙為 1.68 eV，且它們的 HOMO 和 LUMO 皆位於理想的能階，電子與空穴的遷移率在 10^{-6} - 10^{-8} cm^2/Vs ，由於以上之理想的條件，將之運用於有機太陽能電池，並以 PC₆₁BM 作為電子受體。

首先，合成以 LBG 為骨幹的高分子，平面的 carbazole 為電子予體，bithiazole 為電子受體的共軛高分子(P1-P4)，做光伏元件的研究。其中 bithiazole 對耐熱性、光學、電化學、光伏性質等主體結構的影響皆被研究。其光伏元件以 P4:PC₇₁BM (1:1.5 w/w)得到最佳效率(PCE) 為 1.01%、短路電流(J_{sc}) 為 4.83 mA/cm^2 ，曲線因子(FF) 35%，和開路電壓(V_{oc})= 0.60 V。同樣地，包含 dithieno[3,2-b:2',3'-d]pyrroles (DTP)為電子予體的高分子(P1-P5)，最佳光電轉換效率為 P4:PCBM=1:1，PCE=0.69%、短路電流(J_{sc}) 為 4.0 mA/cm^2 ，曲線因子(FF) 43%，和開路電壓(V_{oc})= 0.40 V。

另外，也合成包含 bithiazole, DTP, 和 pendent melamine 為主幹的共軛高分子(PBT)，此系列高分子可以與具可配對氫鍵官能基的分子 F，進一步形成超分子的交聯結構(PBT/F)。研究發現，多重氫鍵可以影響吸收光譜的範圍，HOMO 能階，和光伏的性質。最佳光電轉換效率為 PBT/F : PC₇₁BM =1:1，PCE=0.86%、短路電流(J_{sc}) 為 4.97 mA/cm^2 ，曲線因子(FF) 31.5%，和開路電壓(V_{oc})= 0.55 V。此外，進一步合成以 LBG 為主幹，包含 bithiazole、DTP、和 pendent melamine 的新穎高分子 PBTH，並以具可配對氫鍵官能基的分子 F、C 形成交聯結構 PBTH/C 和 PBTH/F(C 和 F 分別為 carbazole and fluorene 並含 uracil 官能基)。其多重氫鍵的結構利用 FT-IR 去證明，實驗結果證明，以超分子作用力行程共軛的交聯結構，可以增加可見光，改變 HOMO 和晶體結構，進而提升光伏效應。以重量比 polymer:PC₇₁BM=1:1，其 PBTH/C、PBTH/F 和 PBTH 的光電轉換效率分別為 0.97、0.68 和 0.52%，以重量比 PBTH/C:PC₇₁BM=1:2，最佳光電轉換效率為 1.56%、短路電流(J_{sc}) 為 7.16 mA/cm^2 ，曲線因子(FF) 36%，和開路電壓(V_{oc})= 0.60 V。

Acknowledgement

I am deeply indebted to my Professor Hong-Cheu Lin who has been unstinting in his encouragement and constructive criticism, well beyond the call of duty. He has taught me, how good research could be done both deliberately and instinctively. I appreciate all his contributions of time, ideas, and valuable discussion to make my Ph.D. experience productive and stimulating. The contentment and enthusiasm he has for exceptional research was infectious and motivational for me, even during tough times in the Ph.D. pursuit.

I owe my deepest gratitude also to Dr. Chih-Wei Chu and his group members for their support in a number of ways including device fabrications and characterizations. My thanks and appreciation goes to my thesis committee members, for their encouragement, insightful comments, and suggestions. I owe my deepest gratitude to Prof. Kung-Hwa Wei (Chairman), and all professors and secretaries of Department of Materials Science and Engineering, NCTU for their support.

I am deeply obliged to Dr. Sahu who has shown me the stepping stone by introducing me with my advisor and also being with me in all my ups and downs during stay at Taiwan. The members of our group have contributed immensely to my personal as well as professional life during my four years at NCTU. The group has been a source of friendships as well as good advice and collaboration. I have been enjoying collaboration with our group members including Dr. Hari, Dr. Rajan, Hsuan-Chih, Wei-Hong, Yen-Hsing, Hsiao-Ping, Mutheya, Rudrakanta, Ashutosh, Ramesh, Murali, Raju, I-Hung, Han, Chong-Lun, Chung-Ji, Ming-shaw, Shin-Chieh, Chia-Lin, Kuan-Ying, Li-Han, and Dr. Yang.

The financial support of my Ph.D. work by grant form National Science Council (NSC), Office of International Affairs and National Chiao Tung University, Taiwan, R.O.C. is gratefully acknowledged.

Last but not least, I would like to thank my whole family. A special deliberation is devoted to my mother for her never-ending support. The encouragement of my brothers Bada bhai, Pana bhai and Muna and my only sister Nani is the powerful sources of inspiration and energy. Furthermore, I want to thank International service centre and all of my friends who made my life in Taiwan easy, enjoyable and sociable.

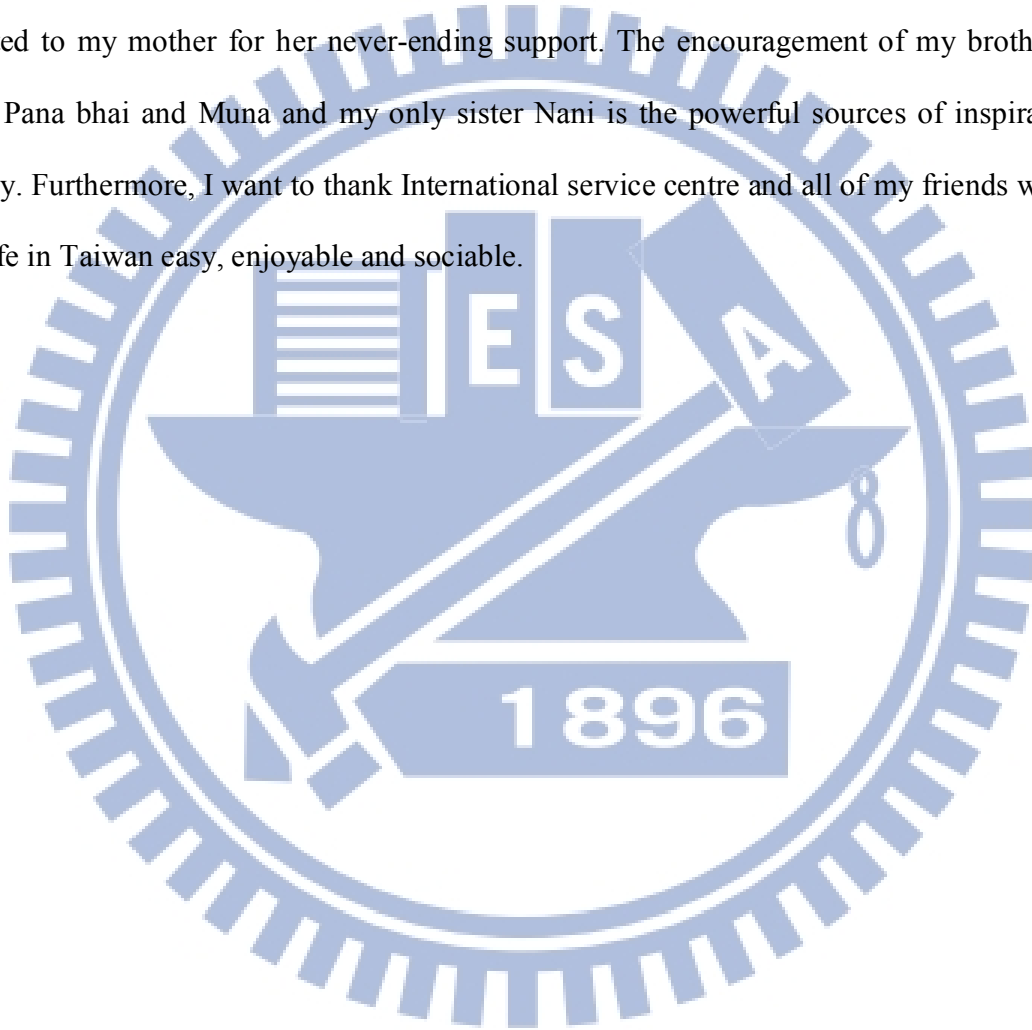


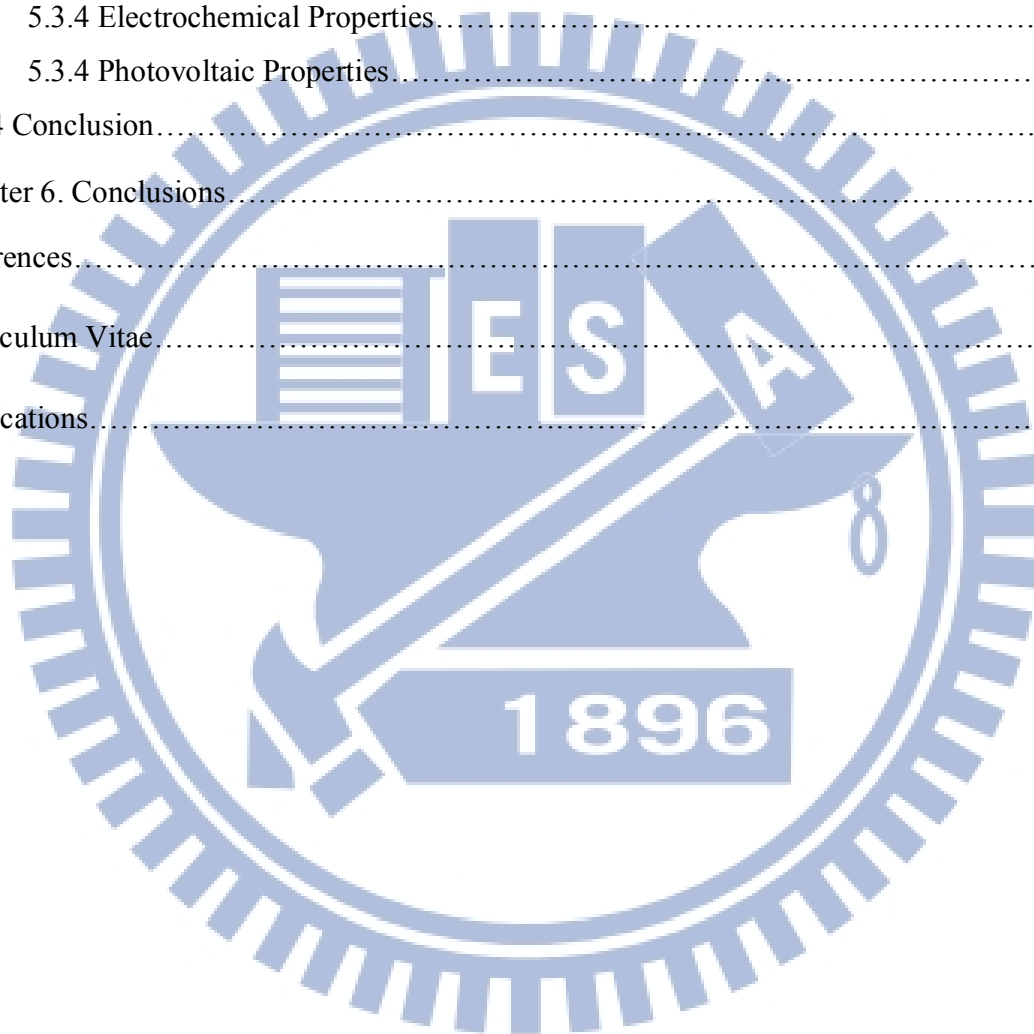
Table of Contents

Abstract.....	I
摘要.....	III
Acknowledgements.....	IV
List of Figures.....	X
List of Tables.....	XIV
Chapter 1.....	1
1.1 Introduction.....	1
1.2 Solar Cell.....	3
1.3 Bulk-Heterojunction Solar Cells (BHJs).....	5
1.3.1 General Device Structures of Bulk-Heterojunction Solar Cells.....	5
1.3.2 Basic Mechanistic Principles of Organic Solar Cells.....	7
1.4 Determination of Solar Cell Performances.....	9
1.4.1 Short Circuit Current (I_{sc}).....	9
1.4.2 Incident Photon-to-Current Conversion Efficiency (IPCE).....	11
1.4.3 Open Circuit Voltage.....	11
1.4.4 Fill Factor.....	12
1.4.5 Organic photovoltaic Device Architectures.....	13
1.4.6 Comparison between Organic and Inorganic Solar Cell.....	16
1.5 Literature Survey of Organic Solar Cell Materials.....	17
1.5.1 Design Considerations for Low Band Gap Polymers.....	18
1.5.2 Polymer Solar cell Materials.....	21
1.5.3 Various Low-Band-Gap polymers for solar cells.....	22
1.5.4 Supramolecular Hydrogen-Bonded Polymers for Organic Solar Cells.....	29
1.5.5 Characterization of Active Materials for Polymer Solar Cells.....	31

1.6 Objective and Outline of this Thesis.....	32
Chapter 2. Synthesis and Applications of 2,7-Carbazole-Based Conjugated Main-Chain Copolymers Containing Electron Deficient Bithiazole Units for Organic Solar Cells.....	36
2.1 Introduction	32
2.2 Experimental.....	39
2.2.1 Materials.....	39
2.2.2 Synthesis Measurements and Characterizations.....	39
2.2.3 Device Fabrication and Photovoltaic Measurements of Polymer Solar Cells (PSCs).....	41
2.2.4 Synthesis of Monomers and Polymers	42
2.3 Results and Discussion.....	46
2.3.1 Syntheses and Characterization.....	46
2.3.2 Optical Properties.....	51
2.3.3 Electrochemical Properties.....	54
2.3.4 Photovoltaic Properties.....	56
2.4 Conclusion	61
Chapter 3. Fine Tuning of HOMO Energy Levels for Low-Band-Gap Photovoltaic Copolymers Containing Cyclopentadithienopyrrole and Bithiazole Units.....	62
3.1 Introduction	62
3.2 Experimental Part.....	65
3.2.1 Materials.....	65
3.2.2 Measurements and Characterizations.....	65
3.2.3 Fabrication of Polymer Solar Cells.....	66
3.2.4 Fabrication of Hole- and Electron-Only Devices.....	68
3.2.5 Synthesis of Monomers and Polymers.....	68
3.3 Results and Discussion.....	74
3.3.1 Syntheses and Characterization	74
3.2.1 Optical Properties.....	78

3.3.2 Electrochemical Properties.....	80
3.3.3 Photovoltaic Cell Properties.....	83
3.4 Conclusion.....	87
Chapter 4. Synthesis and Applications of a Novel Supramolecular Polymer Network with Multiple H-bonded Melamine Pendants and Uracil Cross-linkers.....	88
4.1 Introduction	88
4.2 Experimental.....	90
4.2.1 Materials.....	90
4.2.2 Measurements and Characterizations.....	90
4.2.3 Fabrication and Testing of Polymer solar Devices.....	92
4.2.4 Fabrication of Hole-only Devices.....	93
4.2.4 Synthesis of Monomers and Polymers.....	94
4.2.5 Preperation of Supramolecular Polymer Networks (PBT/F).....	98
4.3 Results and Discussion.....	99
4.3.1 Synthesis and Structural Characterization.....	99
4.3.2 Optical Prepoerties.....	103
4.3.3 Electrochemical Properties.....	104
4.3.4 Photovoltaic Properties.....	107
4.4 Conclusions.....	110
Chapter 5. Enhancement of Photovoltaic Properties in Supramolecular Polymer Networks Featuring a Solar Cell Main-Chain Polymer H-Bonded with Conjugated Cross-Linkers.....	112
5.1 Introduction.....	112
5.2 Experimental.....	116
5.2.1 Materials.....	116
5.2.2 Measurements and Characterizations.....	116
5.2.3 Fabrication and Testing of Polymer Solar Cells.....	117
5.2.4 Synthesis of Monomer M1 , Conjugated Cross-Linkers (C and F), and Conjugated Main-Chain Polymer PBTH	118

5.2.5 Preperation of Supramolecular Polymer Networks (PBTH/C and PBTH/F).....	124
5.3 Results and Discussion.....	126
5.3.1 Synthesys and Characterization.....	126
5.3.2 IR Measurements.....	128
5.3.3 Optical Prepoerties.....	129
5.3.4 Electrochemical Properties.....	133
5.3.4 Photovoltaic Properties.....	135
5.4 Conclusion.....	139
Chapter 6. Conclusions.....	140
References.....	143
Curriculum Vitae.....	155
Publications.....	156



List of Figures

Figure 1.1	(a) World energy consumption 1990-2035 (quadrillion Btu) (b) World electricity generation by fuel, 2007-2035 (trillion kilowatthours).....	2
Figure 1.2	Terrestrial cell efficiencies measured under the global AM1.5 spectrum.....	4
Figure 1.3	Recent achievements in organic solar cells.....	4
Figure 1.4	Schematic device structure for bulk heterojunction solar cells.....	6
Figure 1.5	General mechanisms for photoenergy conversion in excitonic solar cells.....	7
Figure 1.6	Current (voltage) characteristics of a typical organic diode shown together with the metal-insulator-metal (MIM) picture for the characteristic points. (a) Short circuit condition. (b) Open circuit condition. (c) Forward bias. (d) Reverse bias.	10
Figure 1.7	Four device architectures of conjugated polymer-based photovoltaic cells: (a) single-layer PV cell; (b) bilayer PV cell; (c) disordered bulk heterojunction; (d) ordered bulk heterojunction.....	13
Figure 1.8	Absorption coefficients of films of commonly used materials in comparison with the standard AM 1.5 terrestrial solar spectrum.....	17
Figure 1.9	Resonance structures in benzo-bis-thiadiazole.....	19
Figure 1.10	Alternating donor–acceptor units lower the effective band gap by orbital mixing.....	19
Figure 1.11	Example of organic semiconductors used in polymer solar cells.....	21
Figure 1.12	Chemical structures of 2,7-Carbazole containing LBG polymers.....	23
Figure 1.13	Chemical structures of DTP containing polymers.....	24
Figure 1.14	Chemical structures of benzodithiophene and dithienosilole containing polymers.....	26
Figure 1.15	Chemical structures of bithizole derivatives containing polymers.....	27
Figure 1.16	Chemical structures of supramolecular H-bonded polymers.....	29
Figure 1.17	Basic investigation techniques required for an extended characterization of active materials for polymer solar cells.....	31
Figure 2.1	Synthetic schemes of compound 5 and polymers P1-P4	48

Figure 2.2	TGA measurements of polymers P1-P4 with a heating rate of 10°C/min.....	49
Figure 2.3	Normalized absorption spectra of P1-P4 (a) in dilute chloroform solutions and (b) solid films.....	51
Figure 2.4	Cyclic voltammograms of P1-P4 in solid films at a scan rate of 100 mV/s.....	54
Figure 2.5	<i>J-V</i> characteristics of ITO/PEDOT:PSS/ P1-P4 :PC ₆₁ BM(1:1 w/w)/Ca/Al under illumination of AM 1.5 at 100 mW/cm ²	57
Figure 2.6	(a) <i>J-V</i> characteristics of ITO/PEDOT:PSS/ P4 :PC ₇₁ BM/Ca/Al under illumination of AM 1.5 at 100 mW/cm ² . (b) EQE curves of PSC devices based on polymer blends P4 :PC ₇₁ BM in various weight ratios.....	59
Figure 2.7	AFM images of blended polymer P4 :PC ₇₁ BM spin coated from DCB in the ratios of (a) 1:1 (w/w), (b) 1:1.5 (w/w), and (c) 1:2 (w/w) with a size of 1×1 μm ²	60
Figure 3.1	Synthesis of M5 and polymers (P1-P5).....	73
Figure 3.2	TGA measurements of polymers P1-P5 with a heating rate of 10°C/min.....	75
Figure 3.3	Normalized UV-vis spectra of polymers in (a) in dilute chlorobenzene solutions and (b) as solid films on glass surfaces, respectively.....	77
Figure 3.4	Cyclic voltammograms of P1-P5 in solid films at a scan rate of 100 mV/s.....	80
Figure 3.5	(a) <i>J-V</i> characteristics of ITO/PEDOT:PSS/ P1-P5 :PCBM (1:1 or 1:2 by wt.)/Ca/Al under illumination of AM 1.5 at 100 mW/cm ² . (b) EQE curves of PSC devices based on polymer blends P4 :PCBM at various weight ratios (1:1 or 1:2)..	82
Figure 3.6	AFM images of blended polymers (a) P1 , (b) P2 , (c) P3 , (d) P4 , and (e) P5 , respectively, blended with PCBM in the ratio of P1-P5 :PCBM=1:1 (w/w) and (f) in another ratio of P4 :PCBM=1:2 (w/w) spin-coated from DCB with a size of 1×1 μm ²	87
Figure 4.1	Schematic representation of PBT/F after complexation with PBT and F	98
Figure 4.2	Synthetic Routes of M1 , F , and Polymer PBT	98
Figure 4.3	TGA thermogram of PBT and PBT/F , recorded at a heating rate of 10 °C min ⁻¹ under N ₂ atmosphere.....	99

Figure 4.4	FT-IR spectra of π -conjugated cross-linker F , polymer PBT , and supramolecular polymer network PBT/F at room temperature.....	100
Figure 4.5	X-ray diffraction patterns of PBT and PBT/F	101
Figure 4.6	Normalized UV-Vis absorption spectra of (a) PBT and H-bonded π -conjugated cross-linker F in dilute dichlorobenzene solutions; and (b) PBT , PBT/F , and F in solid films.....	102
Figure 4.7	Cyclic voltammograms of polymer PBT and supramolecular polymer network PBT/F and cross-linker F	105
Figure 4.8	(a) <i>J-V</i> and (b) EQE characteristic curves of polymer PBT and H-bonded polymer network PBT/F blended with PC ₆₁ BM (or PC ₇₁ BM) in a wt. ratio of 1:1.....	108
Figure 4.9	AFM images of blended polymers (a) PBT and (b) PBT/F mixed with PC ₆₁ BM, respectively; (c) PBT and (d) PBT/F mixed with PC ₇₁ BM, respectively (in a wt. ratio of 1:1 by spin-coating from dichlorobenzene and annealing at 70°C for 30 min.)	109
Figure 5.1	Schematic illustration of conjugated main-chain polymer (PBTH) and supramolecular polymer networks (PBTH/C , and PBTH/F).....	115
Figure 5.2	Synthesis routes of monomer M1 , C , F , and random copolymer PBTH	125
Figure 5.3	TGA plots of polymer PBTH and supramolecular polymer networks (PBTH/C , and PBTH/F) with a heating rate of 10°C/min under N ₂	127
Figure 5.4	FT-IR spectra of polymer PBTH , cross-linkers (C and F), and supramolecular polymer networks (PBTH/C and PBTH/F).....	128
Figure 5.5	Normalized UV-vis spectra of (a) conjugated main-chain polymer PBTH , π -conjugated cross-linkers C and F (in dichlorobenzene solutions and solid films), and (b) supramolecular polymer networks PBTH/C and PBTH/F (in solid films only).....	131
Figure 5.6	Cyclic voltammograms of PBTH , PBTH/C , PBTH/F , C and F in solid films at a scan rate of 100 mV/s.....	132
Figure 5.7	<i>J-V</i> characteristics of PBTH , PBTH/C , and PBTH/F under illumination of AM 1.5 at 100 mW/cm ²	135

Figure 5.8 X-ray diffraction patterns of polymer **PBTH** and supramolecular polymer networks (**PBTH/C** and **PBTH/F**) in solid powders.....138



List of Tables

Table 1.1	Characteristics of PSCs based on 2,7- carbazole derivatives.....	25
Table 1.2	Characteristics of PSCs DTP-based polymers.....	26
Table 1.3	Current status in the development of solar cells	27
Table 1.4	Characteristics of PSCs DTP-based polymers.....	29
Table 2.2	Molecular Weights and Thermal Properties of Polymers P1-P4	49
Table 2.3	Optical and Electrochemical Properties of Polymers P1-P4	52
Table 2.4	Photovoltaic Properties of Polymer Solar Cell (PSC) Devices with a Configuration of ITO/PEDOT:PSS/ P1-P4 :PC ₆₁ BM(1:1 w/w)/Ca/Al.....	56
Table 2.5	Photovoltaic Properties of Bulk-Heterojunction PSC Devices Containing Different Weight Ratios of Blended Polymers P4 :PC ₇₁ BM and blend film roughness by AFM measurements.....	57
Table 3.1	Molecular Weights and Thermal Properties of Polymers (P1-P5).....	76
Table 3.2	Optical and Electrochemical Data of Polymers (P1-P5).....	79
Table 3.3	Electron and Hole Mobilities, Photovoltaic Properties, and Roughnesses (R_{rms}) of Polymers (P1-P5).....	84
Table 4.1	Optical and Electrochemical Properties of Polymer PBT , Cross-Linker F , and H-Bonded Polymer Network PBT/F	103
Table 4.2	Photovoltaic Properties and Film Roughnesses (R_{rms} Measured by AFM) of Bulk-Heterojunction PSC Devices Containing PBT and PBT/F with PC ₆₁ BM and PC ₇₁ BM in a Blending Wt. Ratio of 1:1.....	106
Table 5.1	Optical and Electrochemical Properties of Polymer PBTH and Supramolecular Polymer Networks (PBTH/C and PBTH/F).....	132
Table 5.2	Photovoltaic Properties of Polymer PBTH and Supramolecular Polymer Networks (PBTH/C and PBTH/F).....	136

Chapter 1

1.1 Introduction

Energy is currently the most important problem facing mankind. The “fire age” in which our civilization has been based from the very beginning is approaching its end. Human beings have been burning a wide variety of materials since early times, and with the advent of carbon-based fossil fuels in the last two centuries, their combustion has become nowadays a major problem due to the huge amounts of carbon dioxide emissions produced all over the world. Moreover, nuclear energy has always been subject of intensive public discussion due to the security and health risks of nuclear power stations and the following problems with radioactive waste. Because of the resulting pollution, global warming and degradation of the planet, a new era based on non-contaminating renewable energies is currently a priority. As alternative energy sources, solar energy is regarded as one of the perfect energy resources over the last decades. The Sun, which can be considered as a giant nuclear fusion reactor, represents the most powerful source of energy available in our solar system and, therefore, its use for providing energy to our planet is among the most important challenges nowadays in science. Actually, the energy received from Sun, calculated as 120 000 TW (5% ultraviolet; 43% visible and 52% infrared), surpasses that consumed on the planet over a year by several thousand times.¹ The sun has the potential to make the largest energy contribution: only one hour of sunshine (3.8×10^{23} kW) is more than enough to satisfy the highest human demand for energy for an entire year (1.6×10^{20} kW in 2005).² Huge efforts have been invested in developing highly efficient solar energy conversion technologies and the most prospective approach is converting solar energy into

electricity. The emerging photovoltaic industry has been growing rapidly due to searching for green technology in recent years.

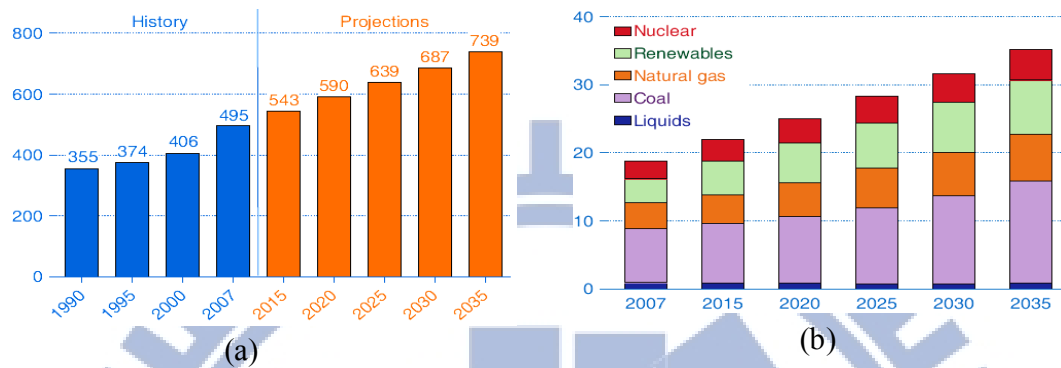


Figure 1.1 (a) World energy consumption 1990-2035 (quadrillion Btu) (b) World electricity generation by fuel, 2007-2035 (trillion kilowatthours)

The state-of-the-art inorganic silicon solar cell technology significantly, convert 15% to 20% of the energy in sunlight to electricity, and their price has been dropping steadily. But many industry observers worry that a price floor could be near, because the cells require expensive clean-room technology to manufacture. Thin films of copper, indium, gallium, and selenium are 15% efficient and cheap, but indium is in short supply. Cadmium-telluride thin films, which rely on rare tellurium, are in much the same boat. The most widely studied organic solar cells are polymer-based solar cells using conjugated polymers. Most conjugated polymers have high absorption coefficient and high percentage of absorbed photons that can produce an excited state (>90%). There are further advantages for using the polymer-based organic solar cells. First, the photo and electronic properties of the conjugated polymers can be fine-tuned by engineering the chemical structures through advances in organic chemistry. Second, simple coating or printing processes can be used which will reduce the cost of the fabrication process. Third, the mechanical flexibility allows the development of flexible devices. Therefore, Organic solar cells

appear to be the highly promising and cost-effective alternative for the photovoltaic energy sector. In this context, bulk heterojunction (BHJ) photovoltaic cells (PVCs) have attracted considerable attention in recent years.

1.2 Solar Cell

A solar cell is a device that converts the energy of sunlight directly into electricity by the photovoltaic effect. The Photovoltaic effect was first observed in 1839 by French physicist Alexander-Edmond Becquerel, when he shined light onto an AgCl electrode in an electrolyte solution and a light-induced voltage was discovered.³ Forty-four years later in 1883, Fritts created the first device made from Se wafers with a power conversion efficiency (PCE) of approximately 1%.⁴ Since 1946, when modern junction semiconductor solar cells were patented by Ohl,⁵ an intensive search for highly efficient photovoltaics has been ongoing. Modern generation of solar cells was born in 1953 when at Bell Laboratories (New Jersey, USA) the first silicon solar cell was developed with a power conversion efficiency of 6%.⁶ After that, many different technologies and materials were developed in order to improve the performance of the device and lower their production cost.

Organic photovoltaic devices have gained a broad interest in the last few years due to their potential for large-area low-cost solar cells. The current status of solar cell is shown in Figure 1.2. The first reports on molecular thin film devices more than 30 years ago, their power conversion efficiencies have increased significantly from 0.001% in 1975⁷ to 1% in 1986⁸. For years the efficiency of polymer-based cells scraped along at a feeble 3% to 5%. But things have improved markedly over the past 2 years. In early April, Mitsubishi Chemical reportedly set a new

efficiency record producing organic solar cells with 9.2% conversion efficiency, according to *The Nikkei*, a Japanese business daily.⁹

Classification ^a	Effic. ^b (%)	Area ^c (cm ²)	V _{oc} (V)	J _{sc} (mA/cm ²)	FF (%)	Test centre (and date)
Cells (silicon)						
Si (MCZ crystalline)	24.7 ± 0.5	4.0 (da)	0.704	42.0	83.5	Sandia (7/99) ^d
Si (moderate area)	23.9 ± 0.5	22.1 (da)	0.704	41.9	81.0	Sandia (8/96) ^d
Si (large crystalline)	23.0 ± 0.6	100.4 (t)	0.729	39.6	80.0	AIST (2/09)
Si (large crystalline)	22.0 ± 0.7	147.4 (t)	0.677	40.3	80.6	FhG-ISE (3/06) ^d
Si (large multicrystalline)	19.3 ± 0.5	217.7 (t)	0.651	38.8	76.4	AIST (7/09)
Cells (other)						
GaInP/GaAs/GaInAs (tandem)	35.8 ± 1.5	0.880 (ap)	3.012	13.9	85.3	AIST (9/09)
CIGS (thin film)	20.1 ± 0.6	0.503 (t)	0.720	36.3	76.8	FhG-ISE (4/10)
a-Si/nc-Si/nc-Si (tandem)	12.5 ± 0.7 ^g	0.27 (da)	2.010	9.11	68.4	NREL (3/09)
Dye-sensitized	11.2 ± 0.3 ^f	0.219 (ap)	0.736	21.0	72.2	AIST (3/06) ^d
Organic	7.9 ± 0.3 ^{fg}	0.0441 (ap)	0.756	14.7	70.9	NREL (11/09)

^a CIGS = CuInGaSe₂.

^b Effic. = efficiency.

^c (ap) = aperture area; (t) = total area; (da) = designated illumination area.

^d Recalibrated from original measurement.

^e Light soaked under 100 mW/cm² white light at 50°C for 1000 h.

^f Stability not investigated.

^g Light soaked under simulated AM1.5 for about 140 h prior to shipment to NREL.

Figure 1.2 Terrestrial cell efficiencies measured under the global AM1.5 spectrum.^{9a}

RECENT EFFICIENCY GAINS		
Company	Date	Efficiency
Solarmer Energy Inc.	July 2010	8.13%
Heliatek	October 2010	8.30%
Konarka	November 2010	8.30%
Mitsubishi Chemical	April 2011	9.2%*

*According to media reports.

Figure 1.3 Recent achievements in organic solar cells.

Figure 1.3 describes recent achievement from, three other companies such as Konarka Technologies in Lowell, Massachusetts; Solarmer Energy Inc. in El Monte, California; and Heliatek in Dresden, Germany are now reporting cells with efficiencies greater than 8%. Many researchers in the field are confident that the figure could soon top 10% and possibly reach 15%.⁹ The progresses in efficiency will possibly make them a competitive alternative to inorganic solar cells in the near future. Different concepts have been published using small molecules¹⁰, conjugated polymers¹¹, combinations of small molecules and conjugated polymers¹², or combinations of inorganic and organic materials¹² as the active layer. “Active layer” refers here to the layer in which the majority of the incident light is absorbed and charges are generated. Small molecules and polymers differ in their molecular weights. Commonly, macromolecules with a molecular weight larger than 10,000 amu are called polymers, whereas lighter molecules are referred to as “oligomers” or “small molecules”. Inspired by the significant progress in solar cell efficiencies with organic materials such as organic electron donor and acceptor molecules in polymer BHJ photovoltaic cells, research have grown rapidly. This technology is relatively new, being actively researched by universities, national laboratories and several companies around the world.

1.3 Bulk-Heterojunction (BHJs) Solar Cells

1.3.1 General Device Structure of BHJs Solar Cells

BHJ solar cells are those solar cells in which semiconducting conjugated polymers or oligomers are applied as active components in the photocurrent generation and power conversion process within thin film photovoltaic devices that convert solar light into electrical energy.¹³ The schematic design of a bulk-heterojunction solar cell (ITO/PEDOT:PSS/Active layer(D-

A)/Al(cathode)) is displayed in Figure 1.4. The core of the cell is the photoactive layer, which is generally composed of a p-type electron-donor compound (D) and an n-type electron-acceptor compound (A). The photoactive layer is usually sandwiched between an indium tin oxide (ITO)-covered substrate (glass or plastic) and a reflective (aluminum) back electrode as cathode. As the ITO substrate is transparent, illumination takes place from this side of the device. The two electrodes may be further modified by the introduction of a PEDOT: PSS (poly[3,4-(ethylenedioxy)thiophene]:poly(styrene sulfonate)) coating on the ITO side. The device architecture of the photoactive layer has a strong impact on charge carrier separation and transport.

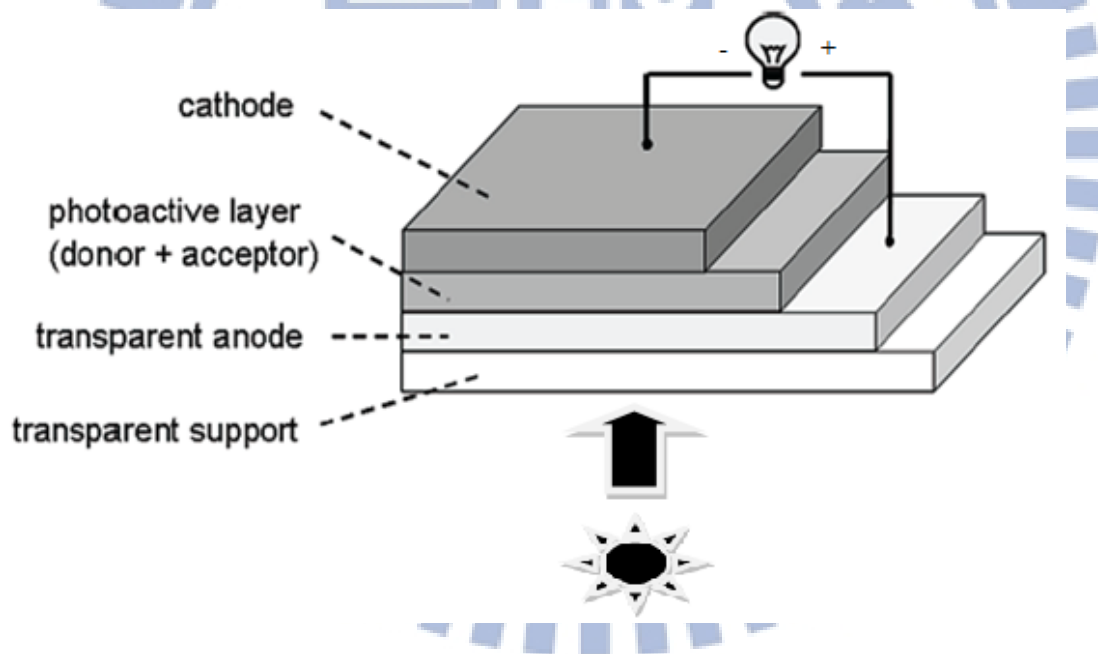


Figure 1.4 Schematic device structure for bulk heterojunction solar cells.¹⁴

1.3.2 Basic Mechanistic Principles of Organic Solar Cells

Figure.1.5 shows the conversion steps of photons into separated charges as it takes place in an organic solar cell. The mechanism of energy conversion in an organic solar cell can be well explained by four fundamental steps.¹⁵

(1) *Absorption of light and generation of excitons*: Photoexcitation of the absorber material(s) causes the promotion of electrons from the ground state, approximated by the highest occupied molecular orbital (HOMO), to the excited state, approximated by the lowest unoccupied molecular orbital (LUMO). These photoexcitation depends upon the value of the optical absorption coefficient and on the thickness of the donor material. Then the excitons are generated which, consists of an electron and a hole paired by an energy that is smaller than the

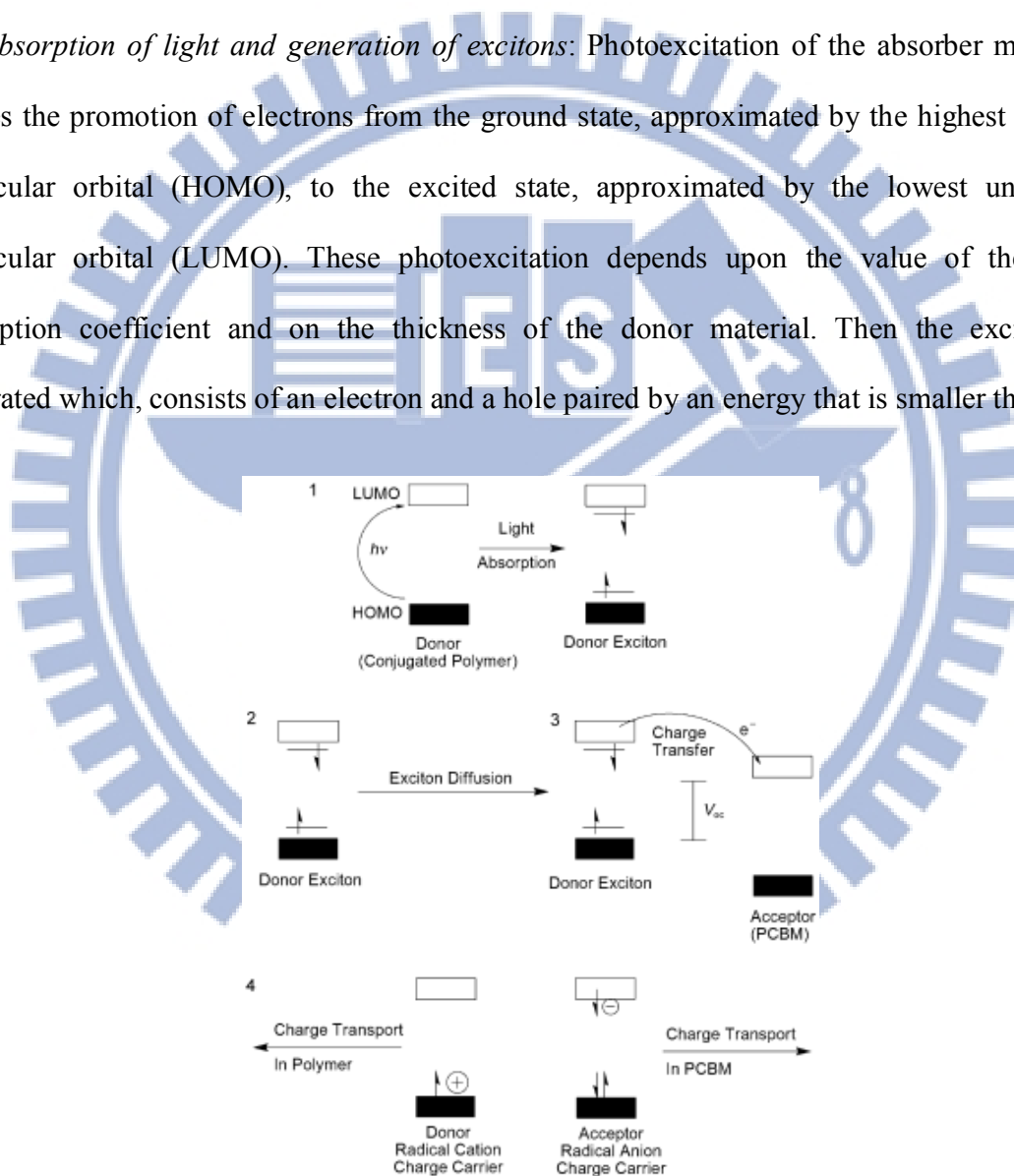


Figure 1.5 General mechanisms for photoenergy conversion in excitonic solar cells.¹⁵

energy gap between the limits of the permitted bands (LUMO and HOMO bands, respectively). The difference between two energies is called exciton binding energy which, is around 0.1-0.2 eV in organic materials. The occupation of these excited states, the LUMO by the electron, and the HOMO by the hole, is termed as nonrecombined excitons.

(2) *Diffusion of the excitons*: Excitons produced within a diffusion length from the D/A interface will have the chance to reach it before decaying, radiatively or not. Diffusion takes place as long as recombination process do not takes place. Forster (long range) or Dexter (between the adjacent molecules) transfers can takes place between an excited molecule.

(3) *Dissociation of the excitons*: If the offsets of the energy levels of the D and the A materials are higher than the exciton binding energy, excitons dissociate at the D/A interface. Excitons photogenerated in the donor side will dissociate by transferring the electron to the LUMO level of the acceptor and retaining the positive charge, while those created in the other side will transfer the hole to the HOMO of the donor while retaining the negative charge. This step leads to the formation of free charge carriers.

(4) *Charge transport and charge collection*: The charge carriers diffuse to the electrodes through the respective materials (electrons in the acceptor and holes in the donor). The charges reach the electrodes and are collected. For this to occur most efficiently, the following conditions must be satisfied:

$$(E_F)_{\text{cathode}} < (E_{\text{LUMO}})_{\text{acceptor}} \text{ and } (E_F)_{\text{anode}} < (E_{\text{LUMO}})_{\text{donor}}.$$

In each of the above steps several phenomena can take place that decrease the efficiency of the global process, so that only a limited portion of the photons reaching the cell are able to generate

“useful” charge carriers. Thus, the optimization of each step is fundamental to extract as much energy as possible from the device.

1.4 Determination of Solar Cell Performances

Besides the insight into the overall photon-to-current conversion efficiency η (or power conversion efficiency, PCE), solar cells are further characterized by measuring the current-voltage I - V curve under illumination of a light source that mimics the sun spectrum. A typical current-voltage I - V curve of a polymer solar cell is shown in Figure 1.6. Since organic semiconductors show very low intrinsic carrier concentration, the metal-insulator-metal (MIM) model seems to be best suited to explain this characteristic. The characteristic points used to characterise a solar cell are labelled in Figure 1.6. In addition, for each of these points, the energy diagram for a single-layer cell with an indium tin oxide (ITO) anode and aluminium cathode is displayed.

1.4.1 Short Circuit Current (I_{sc})

The current delivered by a solar cell under zero bias is called short circuit current (I_{sc}). In this case, exciton dissociation and charge transport is driven by the so-called built-in potential. This can be determined by the product of photoinduced charge carrier density and the charge carrier mobility within the organic semiconductors:

$$I_{sc} = ne\mu E$$

Where, n is the density of charge carriers, e is the elementary charge, μ is the mobility, and E is the electrical field. Therefore, for improving the short circuit current, high mobility/low band gap materials are essential. In the MIM picture, this potential is equal to the difference in work

function (Φ) of the hole- and electron-collecting electrodes. For polymer solar cells, the transparent ITO electrode is often chosen ($\Phi_{\text{ITO}} = 4.7 \text{ eV}$) in combination with a low work function material ($\Phi_{\text{Ca}} = 2.87 \text{ eV}$, $\Phi_{\text{Mg}} = 3.66 \text{ eV}$, $\Phi_{\text{Al}} = 4.24 \text{ eV}$) as counter-electrode to achieve a high internal field.

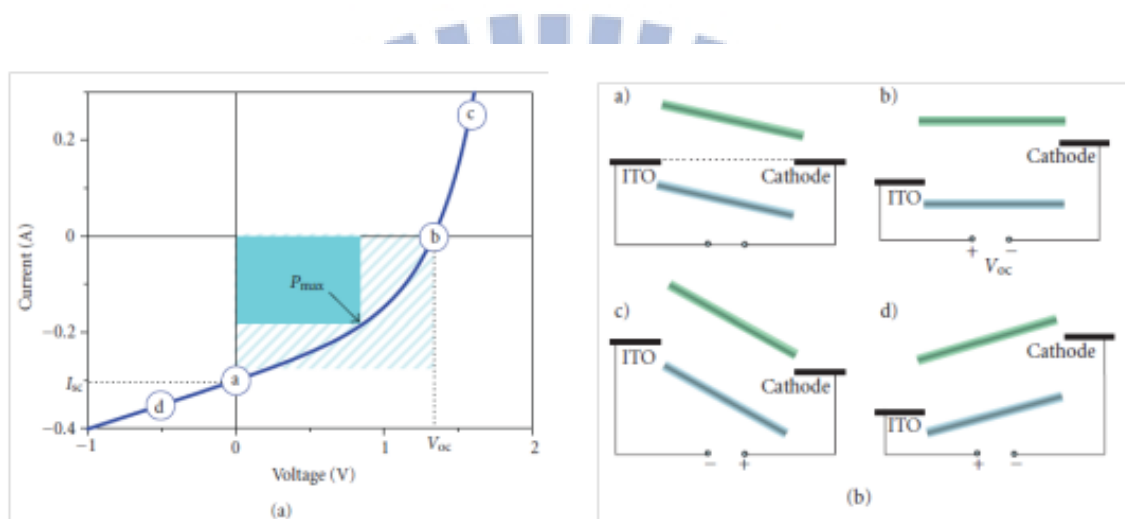


Figure 1.6 Current (voltage) characteristics of a typical organic diode shown together with the metal-insulator-metal (MIM) picture for the characteristic points. (a) Short circuit condition. (b) Open circuit condition. (c) Forward bias. (d) Reverse bias.¹²

1.4.2 Incident Photon-to-Current Conversion Efficiency (IPCE)

The photocurrent action spectrum of solar cells is very informative for the characterization of new materials in a device. It represents the ratio of the observed photocurrent divided by the incident photon flux as a function of the excitation wavelength and is referred to as the incident photon-to-current conversion efficiency (IPCE). The photocurrent which is normally measured is obtained outside the solar cell device; therefore, IPCE can also be named as external quantum efficiency (EQE), e.g. the current obtained outside the photovoltaic device per incoming photon:¹⁰ The IPCE can be calculated by the following equation.

$$\text{IPCE}(\lambda) = \frac{n_{\text{electrons}}}{n_{\text{photons}}} = \frac{I/e}{P/h\nu} = \frac{I}{P} \times \frac{hc}{e\lambda} = \frac{I}{P} \times \frac{1240}{\lambda \text{ (nm)}}$$

Where, I is the photocurrent in A m^{-2} and P is the incident light power in W m^{-2} .

1.4.3 Open Circuit Voltage

In heterojunction solar cells, the open circuit voltage is most often simply estimated to be the difference between the donor HOMO level and the acceptor LUMO level. For example, in the case of polymer: fullerene-based solar cells, the V_{oc} value can be estimated by the following equation:

$$V_{\text{oc}} \approx E_{\text{LUMO,Acceptor}} - E_{\text{HOMO,Donor}} - 0.3 \text{ V}$$

Where, 0.3 V represents the lost energy during the photoinduced charge-generation process. Based on this, Scharber *et al.* found a relationship among (1) the LUMO level of the donors, (2) the band gap of the donors, and (3) the power conversion efficiency of the devices.¹⁶ From the

calculation, the highest power conversion efficiency could be over 10% for single polymer:fullerene bulk-heterojunction solar cells.

1.4.4 Fill Factor

The point where the electrical power $P = I \times V$ reaches the maximum value represents the condition where the solar cell can deliver its maximum power to an external load. It is called the maximum power point. The ratio of this maximum electrical power P_{max} to the product of the short circuit current and the open circuit voltage is termed the fill factor (FF). The fill factor can be calculated by the following equation

$$FF = \frac{P_{max}}{V_{oc} \times I_{sc}}$$

Ideally, the fill factor should be unity, but losses due to transport and recombination result in values between 0.2–0.7 for organic photovoltaic devices. The photovoltaic power conversion efficiency (η) is then calculated for an incident light power P_{in} by following equation.

$$\eta = \frac{V_{oc} \times I_{sc} \times FF}{P_{in}}$$

1.4.5 Organic Photovoltaic Device Architectures

The organic cells reported in the literature can be categorized by their device architecture as having single layer, bilayer, disordered bulk heterojunction; or ordered bulk heterojunction structure (Figure 1.7)

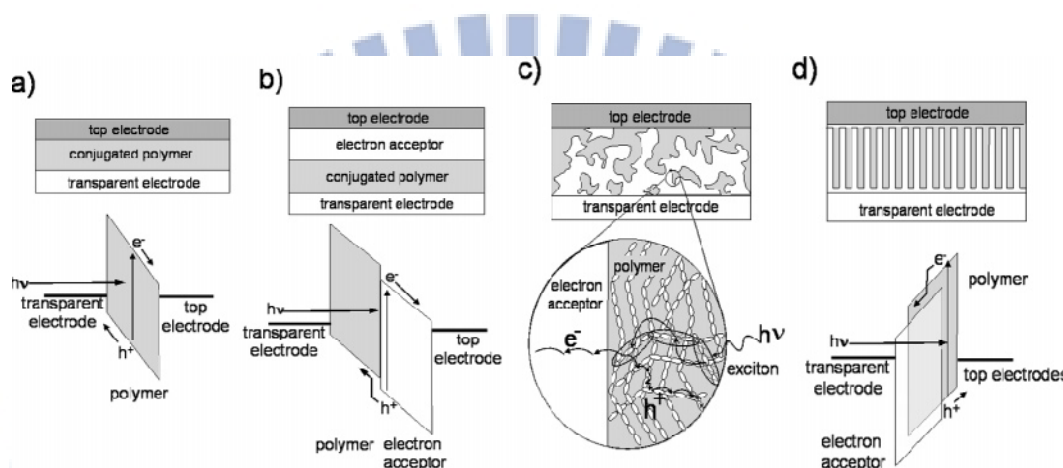


Figure 1.7 Four device architectures of conjugated polymer-based photovoltaic cells: (a) single-layer PV cell; (b) bilayer PV cell; (c) disordered bulk heterojunction; (d) ordered bulk heterojunction.¹⁷

(a) *Single-layer PV cell*: Although it is possible to generate a built-in field in an inorganic semiconductor through the controlled placement of n- and p-type dopant atoms, it is difficult to controllably dope most conjugated polymers. As a result of this, conjugated polymers are usually made as pure as is practically possible and can effectively be considered to be intrinsic semiconductors. Generating built-in electric fields within a film in the dark requires sandwiching the polymer between electrodes with varying work functions or incorporating interfaces with a second semiconductor into the device structure.¹⁸ In single-layer conjugated polymer PV cells, the sign and magnitude of V_{oc} could at least be partially attributed to an electrode work-function

difference. Although single-layer PV cells tend to produce a reasonable V_{oc} , their photocurrent is typically very low.¹⁹

(b) *Bilayer PV cell*: C. W. Tang in 1985 discovered that, by making two-layer PV cells with organic semiconductors that have offset energy bands, the external quantum efficiency of PV cells could be improved to 15% at the wavelength of maximum absorption.²⁰ The improved efficiency resulted from exciton dissociation at the interface between the two semiconductors. Excitons generated within a few nanometers of the heterojunction could diffuse to the interface and undergo forward electron or hole transfer. This process of forward charge transfer led to the spatial separation of the electron and hole, thereby preventing direct recombination and allowing the transport of electrons to one electrode and holes to the other. Because there were essentially no minority free carriers in the undoped semiconductors, there was little chance of carrier recombination once the charges moved away from the interface, despite the long transit times to the electrodes. Sariciftci *et al.* first applied this two-layer technique to a conjugated polymer PV cell by evaporating C_{60} on top of a spin-cast MEH-PPV layer.²¹ However, in the organic PV cell, the excitons in these materials need to be generated near the interface for dissociation to occur before recombination. The exciton diffusion length in several different conjugated polymers has subsequently been measured to be 4–20 nm.²² Because the exciton diffusion length in a conjugated polymer is typically less than the absorption length of the material (~100 nm), the EQE of a bilayer device made with a conjugated polymer and another semiconductor is ultimately limited by the number of photons that can be absorbed within an exciton diffusion length of the interface.

(c) *Disordered bulk heterojunction*: To address the problem of limited exciton diffusion length in conjugated polymers, Yu *et al.*²³ and Halls *et al.*²⁴ independently intermixed two conjugated polymers with offset energy levels so that all excitons would be formed near an interface. They observed that the photoluminescence from each of the polymers was quenched. This implied that the excitons generated on one polymer within the film reached an interface with the other polymer and dissociated before recombining. This device structure, called a bulk heterojunction, provided a route by which nearly all photogenerated excitons in the film could be split into free carriers.

(d) *Ordered bulk heterojunction*: In all of the bulk heterojunction devices that we have described above, the conjugated polymer and electron acceptor have been randomly interspersed throughout the film. The randomly distributed interface between the two semiconductors can lead to incomplete PL quenching in the conjugated polymer in regions of the polymer that are more than an exciton diffusion length away from an acceptor. For these reasons, some have sought to create well-ordered conjugated polymer–electron acceptor films. In an ideal device structure, every exciton formed on the conjugated polymer will be within a diffusion length of an electron acceptor, although quantitative modeling has pointed out that some light emission will still occur in the polymer even if this is the case.²⁵ Polymeric bulk heterojunction devices, whose photoactive layer is composed of a blend of bicontinuous and interpenetrating donor and acceptor, can maximize interfacial area between the donor and the acceptor. In addition, these devices can be processed in solution, such as spin-coating or roll-to-roll printing, thereby contributing several attractive advantages such as low-cost, lightweight, and flexible devices.

1.4.6 Comparison between Organic and Inorganic Solar Cell

The mechanism underneath the operation of a polymer (or an organic) solar cell exhibits, of course, many similarities with that of inorganic cells, but also some distinctions, arising from a few important different characteristics of the materials involved:

(1) While inorganic semiconductors exhibit a band structure, organic semiconductors possess discrete energy levels (molecular orbitals). Nevertheless, the term “bandgap” is often improperly used for organic semiconductors.

(2) In solar cells based on inorganic semiconductors such as silicon, the absorbed photons lead to the direct creation of free charge carriers. In contrast, in organic semiconductors based on π -conjugated systems because of the low dielectric constant of these materials, light absorption leads to the creation of excitons, strongly coulombically bound electron-hole pairs. In organic heterojunctions, the driving force for exciton dissociation is provided by the energy offset between the molecular orbitals of the donor and acceptor. Exciton dissociation into free charge carriers thus represents a key process that imposes one of the major limitations to the power conversion efficiency of organic solar cells.

(c) When a bound hole-electron pair (exciton) is generated in an inorganic semiconductor, its immediate dissociation is observed. Excitons in organic semiconductors are tightly bound (binding energy of around 0.3–0.5 eV) and dissociation must be promoted in some way avoiding radiative recombination.

(d) Compared to inorganics, charge carrier mobilities in organic semiconductors are very low.

(e) Light absorption coefficients of organic materials are much higher than those of inorganics.

1.5 Literature Survey of Polymer Solar Cell Materials

In a typical polymeric BHJ PVC, the photoactive blend layer, sandwiched between an indium tin oxide (ITO) positive electrode and a metal negative electrode, may be composed of a low band gap conjugated polymer donor and a soluble nanosized acceptor.^{11, 15} A fullerene derivative, [6,6]- phenyl-C₆₁-butyric acid methyl ester (PC₆₁BM) or [6,6]- phenyl-C₇₁-butyric acid methyl ester (PC₇₁BM) are widely utilized acceptor. As a component in the active layer, a conjugated polymer donor serves as the main absorber to solar photon flux, as well as the hole transporting phase.²⁶ Thus a low band gap feature to match the solar spectrum (Figure 1.6) and fast hole mobility are basic requirements to design an ideal polymer donor.

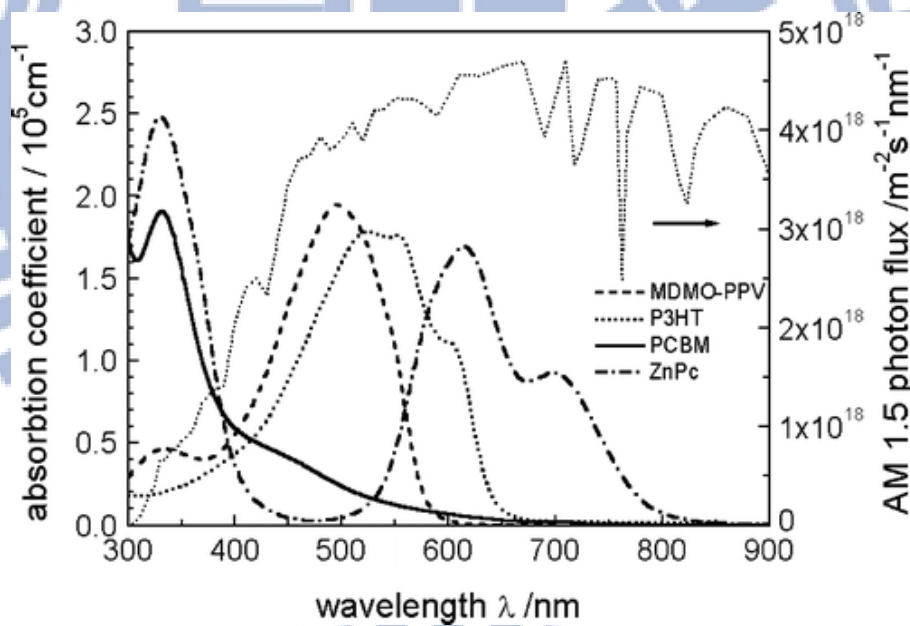


Figure 1.8 Absorption coefficients of films of commonly used materials in comparison with the standard AM 1.5 terrestrial solar spectrum.²⁷

1.5.1 Design Considerations for Low Band Gap Polymers

In recent days, interests in the design and synthesis of conjugated polymers have been increased for the applications of electronic and photonic devices. It remains a key challenge to synthesize ideal low band gap (LBG) polymers with high intrinsic conductivities to develop their potential applications in highly efficient BHJ solar cells. Concerning the band gaps of LBG polymers, the following factors should be taken into the account: intra-chain charge transfers, bond-length alternation, aromaticity, substituents effects, intermolecular interactions, and π -conjugation length etc.^{28, 29}

The low band gap copolymers reported are often based on thiophene but other electron rich aromatic units such as pyrrole are also found. Identical for these copolymers are the alternation between electron donor (electron rich) and electron acceptor (electron deficient) units. The high energy level for the HOMO of the donor and the low energy level for the LUMO of the acceptor results in a lower band gap due to an intra-chain charge transfer from donor to acceptor.²⁹ Planarity along the aromatic backbone results in a low band gap, due to a high degree of delocalization of the π -electrons. The alternation between single and double bonds along the polymer chain has a tendency to increase the band gap. A reduction of the difference in bond length alternation is achieved by the alternation of donor and acceptor units along the conjugated polymer chain thus lowering the band gap. As described interactions between acceptor and donor enhance double bond character between the repeating units, this stabilizes the quinoid form of e.g. benzo-bis(thiadiazole) (Figure 1.7) formed within the polymer backbone, and hence a reduction in band gap is achieved.³⁰

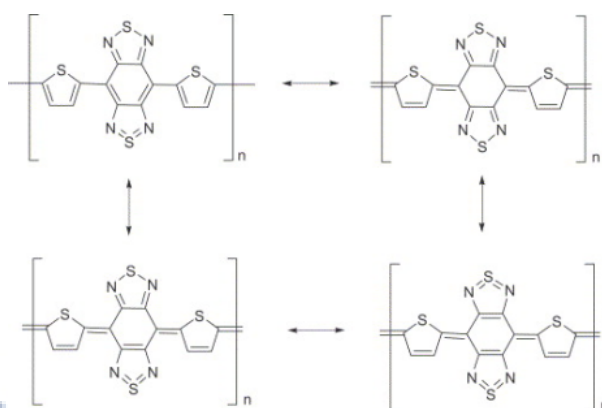


Figure 1.9 Resonance structures in benzo-bis-thiadiazole.³¹

If the HOMO level of the donor and the LUMO level of the acceptor are close in energy it results in a low band gap as shown in (Figure 1.8). Therefore, to achieve a lower band gap the strength of the donor and the acceptor must be increased. This is efficiently achieved by using electron withdrawing groups such as CN, NO₂, quinoxalines, pyrazines or thiadiazole on the acceptor and electron donating groups such as thiophene or pyrrole on the donor.³⁰

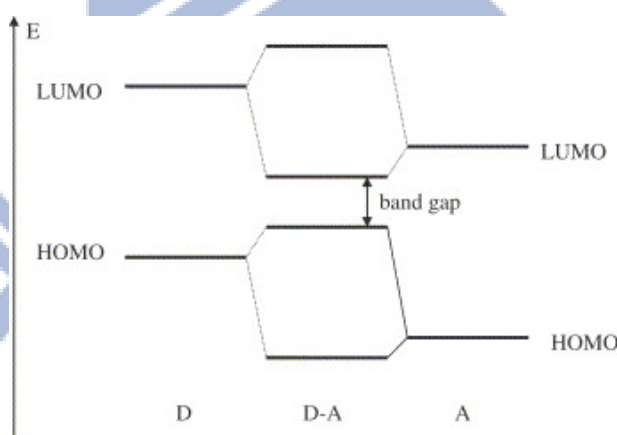


Figure 1.10 Alternating donor–acceptor units lower the effective band gap by orbital mixing.³¹

In order to increase the PCE in BHJ solar cells, some important characteristics of LBG polymers need to be dealt, such as: (i) a more favorable overlap of the absorption spectrum of the

active layer with the solar emission³² – Many classes of LBG polymers with the absorption edges extended into the near-infrared regions have been synthesized and investigated.³³ (ii) a better charge carrier mobility³⁴ – This can be improved by optimization of intra-chain ordering (co-planarity and conjugation length) and inter-chain stacking, which often can be increased upon annealing the BHJ solar cell devices.³⁵ (iii) an optimized relative positions of the energy levels of the electron donors and acceptors³⁶ – The maximization of the open circuit voltage (V_{oc}) is correlated to have more efficient charge separation between electron-donor polymers and electron-acceptor PCBM. For this purpose, the donor polymer should exhibit a band gap between 1.2 and 1.9 eV, which corresponds to a HOMO energy level between -5.8 and -5.2 eV and LUMO energy level between -4.0 and -3.8 eV.³⁷ In order to achieve higher efficiencies of BHJ solar cell devices, the difference of the LUMO levels between donor polymer and acceptor PCBM needs to be at least 0.3 eV.³⁸ Otherwise, the driving force for charge separation will be decreased, and also V_{oc} will be reduced by raising the HOMO level of the donor polymer. Therefore, in order to synthesize LBG polymers, the design rules described above suggest that the optimization of HOMO and LUMO levels of LBG polymers is the most promising strategy to develop BHJ solar cells with high efficiencies. However, it is difficult to synthesize the LBG polymers with all three properties like broad absorption spectra, high carrier mobilities, and appropriate molecular energy levels.

1.5.2 Polymer Solar Cell Materials

Generally, organic materials having delocalized π electrons, absorbing sunlight, creating photo generated charge carriers and transporting these charge carriers can be used for fabrication of polymer solar cells. These materials are classified to the electron donors and the electron acceptors.

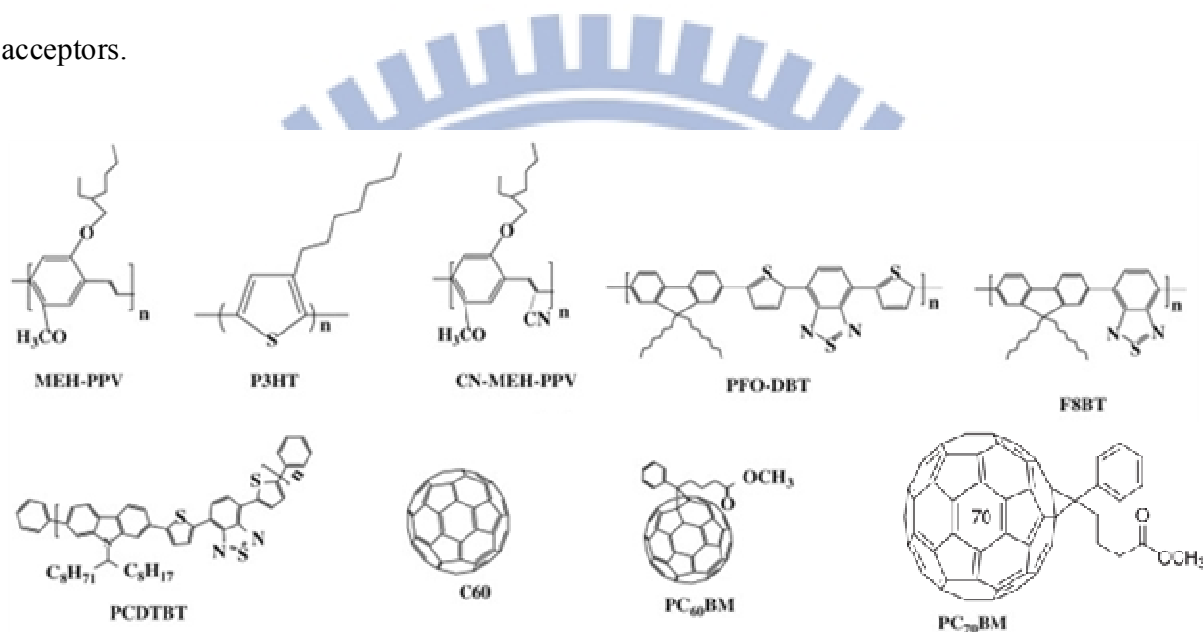


Figure 1.11 Example of organic semiconductors used in polymer solar cells.³⁹

Most of semiconducting polymers are hole-conductors. This kind of semiconducting polymers was named as the electron donor polymers. Figure 1.11 shows some representative semiconducting polymers. Four important representatives of electron donor polymers are MEH-PPV, P3HT, PFO-DBT and PCDTBT. The electron acceptor polymers like CN-MEH-PPV, F8TB, and small molecules, C60 and soluble derivatives of C60 and C70, namely PC₆₀BM and PC₇₀BM, are also shown in Figure 1.11. Fullerenes are considered to be the best electron acceptors so far. This is because: (i) ultrafast (50 fs) photo induced charge transfer was happened

between the donor polymers and fullerenes; (ii) fullerenes exhibited high mobility, for example, PC₆₀BM shown electron mobility up to $1 \text{ cm}^2 \text{ V}^{-1} \text{ s}^{-1}$ measured by field effect transistors; (iii) fullerenes shown a better phase segregation in the blend film.⁴⁰

Dialkoxy-substituted poly(para-phenylene vinylene)s (PPVs), for example, poly[2-methoxy-5-(2-ethyl-hexyloxy)-1,4-phenylene vinylene] (MEH-PPV) and poly[2-methoxy-5-(3',7'-dimethyloctyloxy)-1,4-phenylene vinylene] (MDMOPPV) shows strong absorption in the visible light band. Notable PCE values of 2-3% have been reproducibly achieved.^{41, 42}

1.5.3 Various Low-band-gap polymers for solar cells

The efficient BHJ PSC device architectures were obtained by using an active layer of poly (3-hexylthiophene) (P3HT) as an electron donor and PC₆₁BM as an electron acceptor, which were able to reach PCE values up to 5%.⁴³ The main disadvantage of P3HT is appreciably wide band gap (1.9 eV) and able to absorb only 22% of influx from solar spectrum because the maximum photon fluxes from the sun to earth surface is ca. 1.8 eV (i.e., 700 nm). In such conjugated polymers, electron-donating groups and electron-withdrawing groups are substituted alternatively in the polymer backbones to lower HOMO energy levels.⁴⁴ Therefore, the molecular design of D-A alternating architectures in polymer backbones have received considerable attention to organic chemists for the developments and applications of new low band gap conjugated polymers in photovoltaic devices. Followings are new class of LBG materials has attracted much interest from the scientific community with their promising results for commercial applications.

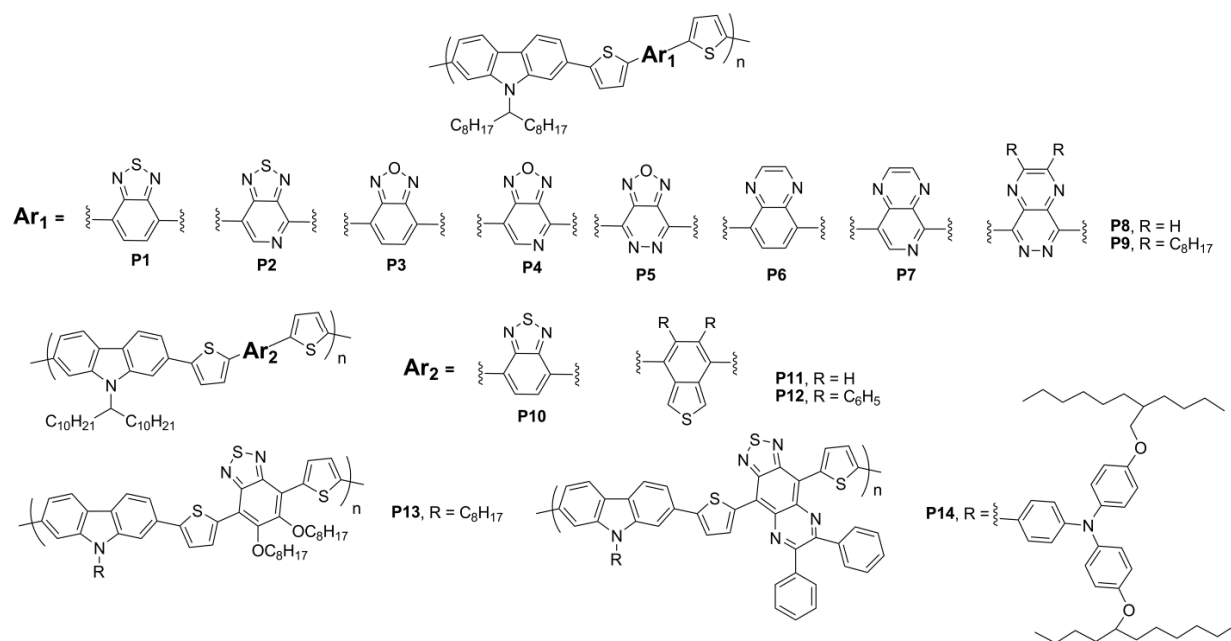


Figure 1.12 Chemical structures of 2,7-Carbazole containing LBG polymers.

Polycarbazoles (i.e. polyvinylcarbazoles) were first reported as photoconductive materials in photocopiers. Since then, different families of poly(carbazole)s have been reported in the literature such as poly(3,6-carbazole)s, poly(1,8-carbazole)s, and poly(2,7-carbazole)s. This last class of materials was found to exhibit interesting features that make these polymers attractive for photovoltaic applications. Indeed, poly (2,7-carbazole)s possess low HOMO energy levels which lead to air-stable materials and to high open circuit voltage (V_{oc}). Upon structure modifications, those materials can be easily fine tuned to match the optimal solar spectra emission. The main reasons for using a carbazole unit over a fluorene unit is that they are reported to have better hole transporting properties with respect to the fluorene unit, while maintaining the stability.⁴⁵ They can also exhibit good hole mobility values. Also, the 2,7-carbazole ring is fully aromatic, which provides a better chemical stability. Figure 1.12 and

Table 1.1 shows chemical structures of some 2,7- carbazole containing LBG polymers for PSC applications.

Table 1.1 Characteristics of PSCs based on 2,7- carbazole derivatives.

Polymer	Mn/ kgmol ⁻¹	PDI	Eg/eV	V _{oc} / V	J _{sc} /mA cm ⁻²	FF	PCE (%)	Ref.
P1	36	1.5	1.88	0.88	10.6	0.66	6.1	46
P2	4.0	1.5	1.75	0.71	2.9	0.32	0.7	45
P3	9.0	1.5	2.02	0.95	3.0	0.56	1.8	45
P4	4.5	1.3	1.67	0.85	1.4	0.60	0.8	45
P5	4.8	1.9	1.57	0.82	1.52	0.38	0.5	47
P6	26.0	1.9	1.87	0.96	3.7	0.60	2.4	45
P7	11.0	1.7	1.89	0.90	2.6	0.44	1.1	45
P8	3.5	2.5	1.91	0.66	0.55	0.35	0.1	47
P9	4.4	1.8	1.79	0.91	0.86	0.44	0.4	47
P10	16.5	1.5	1.72	0.80	7.66	0.50	3.0	48
P11	6.6	1.6	1.57	0.56	4.41	0.41	1.0	48
P12	7.8	1.8	1.46	0.62	3.94	0.37	0.9	48
P13	16.6	3.1	1.95	0.81	9.6	0.69	5.4	49
P14	3.3	1.6	1.10	0.41	5.16	0.29	0.6	50

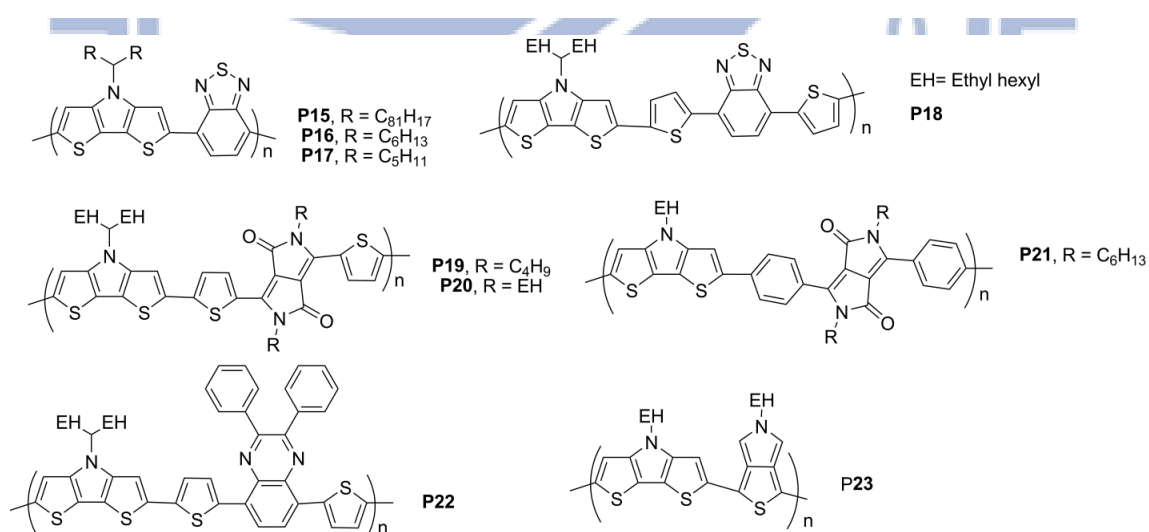


Figure 1.13 Chemical structures of DTP containing polymers.

Table 1.2 Characteristics of PSCs DTP-based polymers.

Polymer	Mn/ kgmol ⁻¹	PDI	Eg/eV	V _{oc} / V	J _{sc} / mA cm ⁻²	FF	PCE (%)	Ref.
P15	14.9	1.37	1.41	0.43	6.19	0.46	1.23	51
P16	15.6	1.36	1.42	0.43	11.1	0.43	2.06	51
P17	17.9	1.63	1.43	0.54	11.9	0.44	2.80	51
P18	100.0-1.0	3.4	1.46	0.52	9.17	0.44	2.18	52
P19	18.9	2.04	1.13	0.38	14.87	0.48	2.71	53
P20	8.5	1.70	1.13	0.44	4.47	0.57	1.12	54
P21	8.8	1.13	1.69	0.61	6.67	0.30	1.32	55
P22	8.1	1.4	1.61	0.46	7.78	0.49	1.77	56
P23	4.1	1.3	1.62	0.70	6.97	0.39	1.90	57

An enhanced intermolecular π -stacking, long-range order, and solution processable electron donating dithieno[3,2-b:2',3'-d]pyrroles (DTP) unit one kind of electron rich building block containing fused thiophene units, offer great processabilities by attaching various alkyl chains to N-substituents of the pyrrole rings without affecting their conjugation lengths can be co-polymerized with various electron-deficient units to generate LBG polymers for PSC applications. Figure 1.13 and Table 1.2 demonstrates DTP containing LBG polymer and their properties.

Figure 1.14 and Table 1.3 are some of the benzodithiophene and dithienosilole containing polymer structures, developed in recent years have seen a dramatic improvement in the efficiency of polymer solar cells. Maximizing the open-circuit voltage in low-band gap polymers is one of the critical factors towards enabling high-efficiency solar cells. Study of the relation between open-circuit voltage and the energy levels of the donor/acceptor in bulk heterojunction polymer solar cells has stimulated interest in modifying the open-circuit voltage by tuning the energy levels of polymers. Recently, by tuning the open-circuit voltage of polymer

solar cells based on the structure of a LBG polymer **P27**, yielded power conversion efficiency as high as 7.7%, as certified by the National Renewable Energy Laboratory.

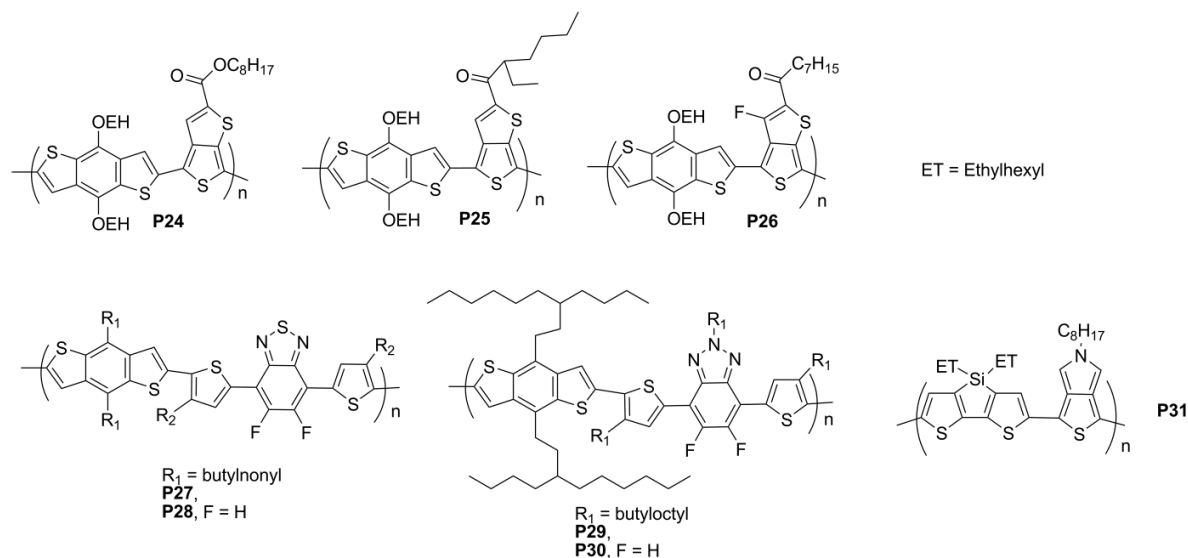


Figure 1.14 Chemical structures of benzodithiophene and dithienosilole containing polymers.

Table 1.3 Characteristics of PSCs benzodithiophene and dithienosilole containing polymers.

Polymer	Mn/ kgmol ⁻¹	PDI	E _g /eV	V _{oc} / V	J _{sc} /mA cm ⁻²	FF	PCE (%)	Ref.
P24	-	-	-	0.62	13.2	0.63	5.1	11a
P25	16.7	1.8	1.61	0.7	14.7	0.64	6.6	11a
P26	-	-	-	0.76	15.2	0.68	7.7	11a
P27	33.8	2.6	1.70	0.91	12.91	0.61	7.2	58
P28	41.2	1.7	1.75	0.87	10.03	0.57	5.0	58
P29	42.2	2,4	2.0	0.79	11.83	0.73	7.1	59
P30	47.6	2.6	1.98	0.70	11.14	0.55	4.3	59
P31	28.0	1.6	1.73	0.88	12.2	0.68	7.3	60

Various electron-accepting moieties reported so far, such as benzothiadiazole,⁴⁵ thiazole,⁶² triazole,⁵⁹ and quinoxaline,⁴⁵ to manipulate the HOMO level of polymers. Thiazole unit is one of the five-membered azaheterocycles with electron deficient characteristics, which contains an electron-withdrawing imine ($-C=N$) in place of the carbon atom at the 3-position of thiophene.^{62,63} Moreover, the thiazole-based polymers showed high oxidative stabilities which minimized the HOMO energy levels and to induce the high V_{oc} values. Followings are some bithazole containing polymer reported in recent years. Figure 1.15 and Table 1.4 are few examples of bithazole derivative containing LBG polymers for solar cells.

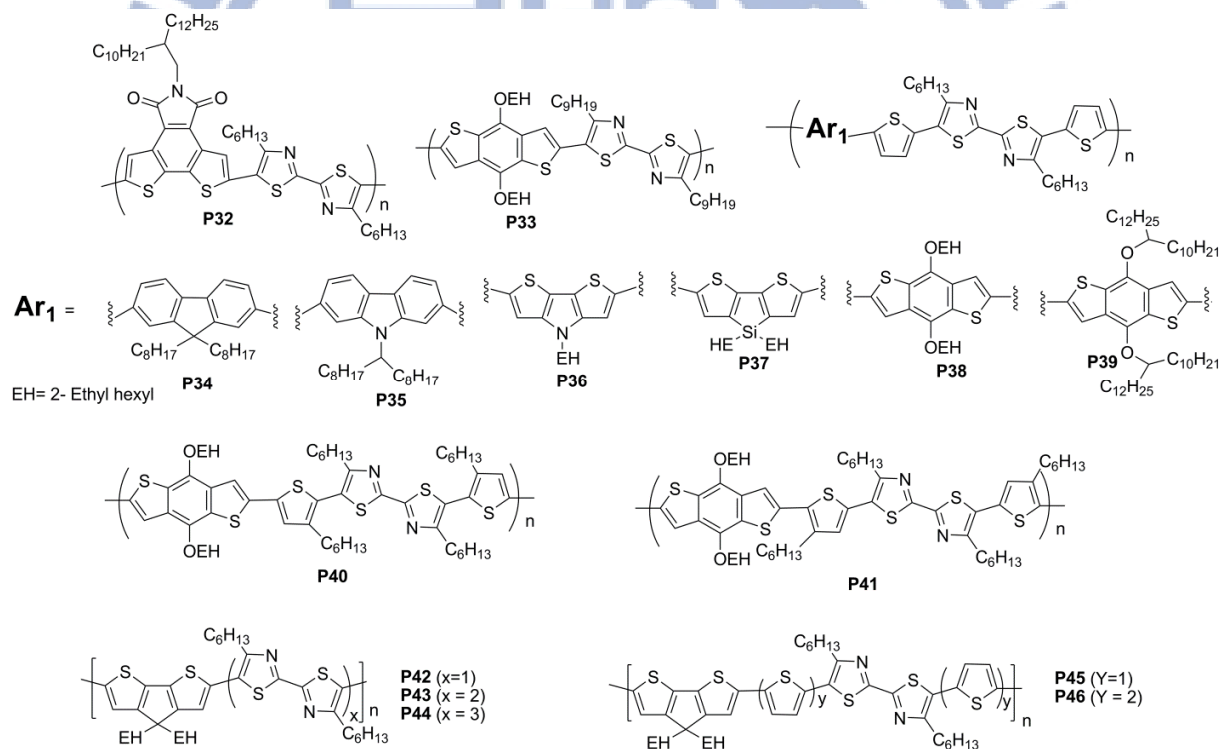


Figure 1.15 Chemical structures of bithiazole derivatives containing polymers.

Table 1.4 Characteristics of PSCs bithizole derivatives containing polymers.

Polymer	Mn/ kgmol ⁻¹	PDI	Eg/eV	V _{oc} / V	J _{sc} /mA cm ⁻²	FF	PCE (%)	Ref.
P32	9.9	1.43	2.09	-	-	-	-	61
P33	6.9	1.4	2.0	0.73	6.63	0.42	2.03	62
P34	49.3	2.08	2.21	0.76	1.70	0.40	0.52	63
P35	73.7	3.4	2.21	0.82	1.24	0.30	0.30	64
P36	4.6	1.78	1.68	0.28	0.51	0.34	0.06	64
P37	5.6	1.7	1.85	0.68	7.85	0.54	2.86	64
P38	3.3	1.95	1.97	0.86	7.84	0.57	3.82	65
P39	8.7	1.3	1.93	0.91	3.30	0.38	1.14	66
P40	7.4	1.5	1.94	0.44	0.44	0.25	0.09	66
P41	6.9	1.4	1.99	0.82	6.64	0.47	2.54	66
P42	15.1	1.34	1.94	0.73	6.34	0.53	2.45	67
P43	38.0	1.37	1.90	0.77	5.26	0.52	2.12	67
P44	42.1	1.66	1.83	0.82	4.43	0.49	1.78	67
P45	17.7	1.81	1.84	0.70	8.0	0.53	3.04	67
P46	9.5	1.47	1.70	0.73	3.03	0.36	0.80	67



1.5.4 Supramolecular Hydrogen-Bonded Polymers for Organic Solar Cells

Nanostructured materials with tailor-made properties and functions can be developed by exploiting the supramolecular approach through molecular recognition.⁶⁸ In fact, the hierarchical self-assembly of multivalent molecular modules through the concerted action of multiple non-covalent interactions represents a very powerful approach as it makes possible the simultaneous organization of various molecular systems into intrinsically defect-free 2D architecture featuring a long-range order.⁶⁹

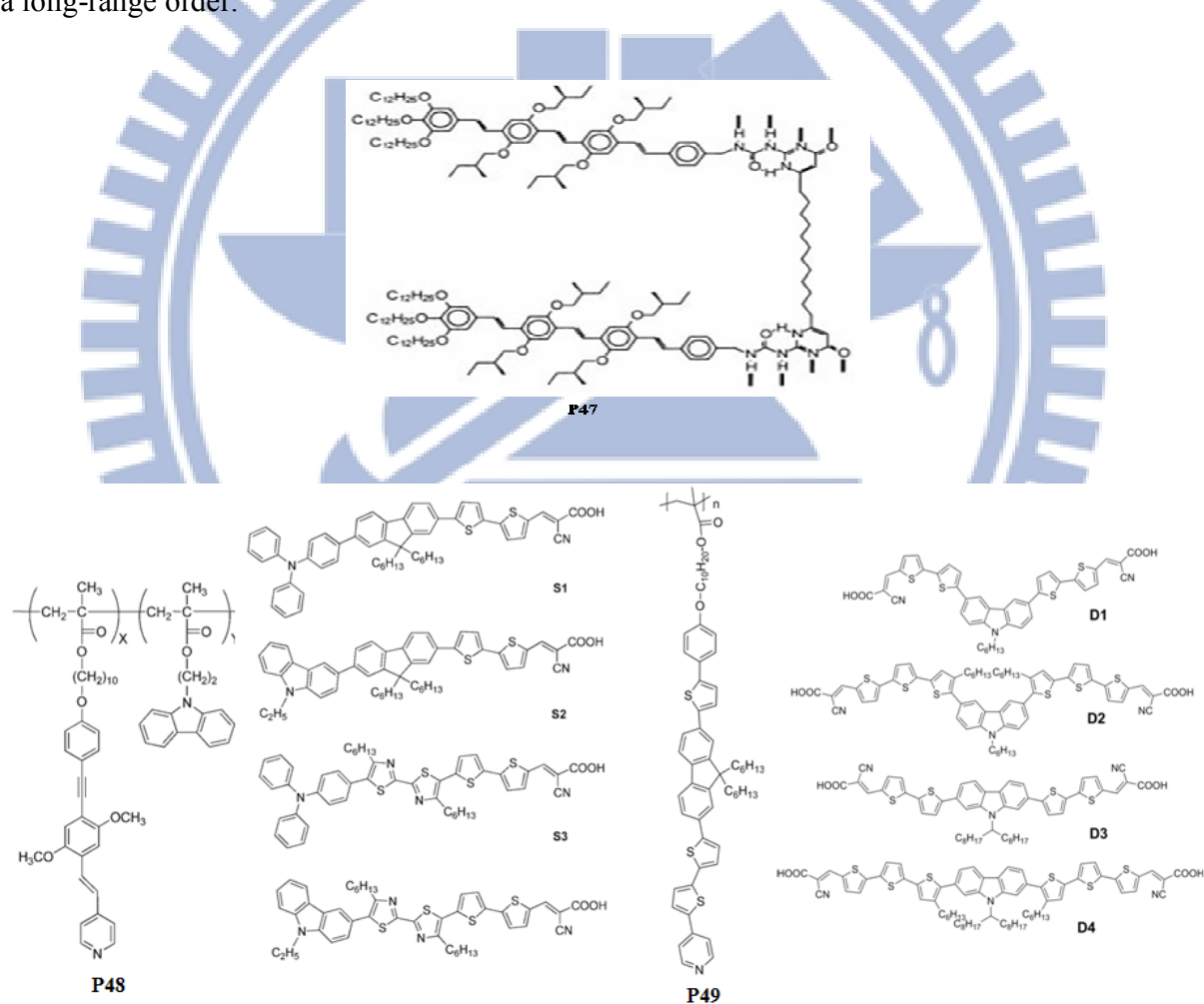


Figure 1.16 Chemical structures of supramolecular H-bonded polymers.

Hitherto a large variety of interactions have been employed in order to hold together molecular modules forming targeted self-assembled mono-component architectures at surfaces including dipolar forces,⁷⁰ coordination bonds,⁷¹ metal bonds,⁷² H-bonds,⁷³ and more recently covalent interactions.¹¹ Among the proposed approaches, the use of H-bonding is very promising since this type of interaction features very high directionality and selectivity, along with a reversible character, providing access to a vast variety of sophisticated functional assemblies and materials barely accessible through conventional covalent synthesis.⁷³

The design of supramolecular D-A systems was recognized as a promising strategy via the charge-transfer processes between donor and acceptor units.⁷³ Würthner, Schenning, and Meijer reported well-defined mesoscopic assemblies by using complementary H-bonded moieties of perylene bisimide and melamine derivatives. Meijer et al. reported a PCE value of 0.25% for the polymer solar cell (PSC) device by utilizing a main-chain H-bonded polymer **P47** containing oligo(p-phenylene vinylene) and ureido-pyrimidinone units (as H-bonded groups).⁷⁴ Small molecules and their polymer analogues have attracted exceptional attentions in the recent days owing to their corresponding advantages, including high purities and (hole and electron) mobilities for small molecules, and easy processing capabilities and low costs for polymers.⁷⁵ Therefore, one of the attractive approaches is to achieve advanced π -conjugated materials by the combination of both small molecular and polymeric designs through supramolecular architectures. Figure 1.16 demonstrates some of supramolecular hydrogen bonded cross-linking polymers for solar cell applications. Cross-linking polymer **P48/S3** and **P49/D2** shows higher PCE of 0.50 and 0.31% among the above serie of cross-linking polymers.⁷⁶

1.5.5 Characterization of Active Materials for Polymer Solar Cells

The molecular design of D/A pairs for high efficiency PSC has to meet a lot of optoelectronic requirements, other than an excellent processability from solution, very high chemical purity, etc. To this end, an extensive characterization of the newly synthesized materials is required, involving multidisciplinary expertise (Figure 1.17), to assess their potentials as promising donors or acceptors for polymer solar cells. Chemists are making a great effort in the direction of energy level engineering and a variety of fullerene derivatives and p-type conjugated polymers (vide infra) have been proposed as functional materials toward high efficiency PSC.

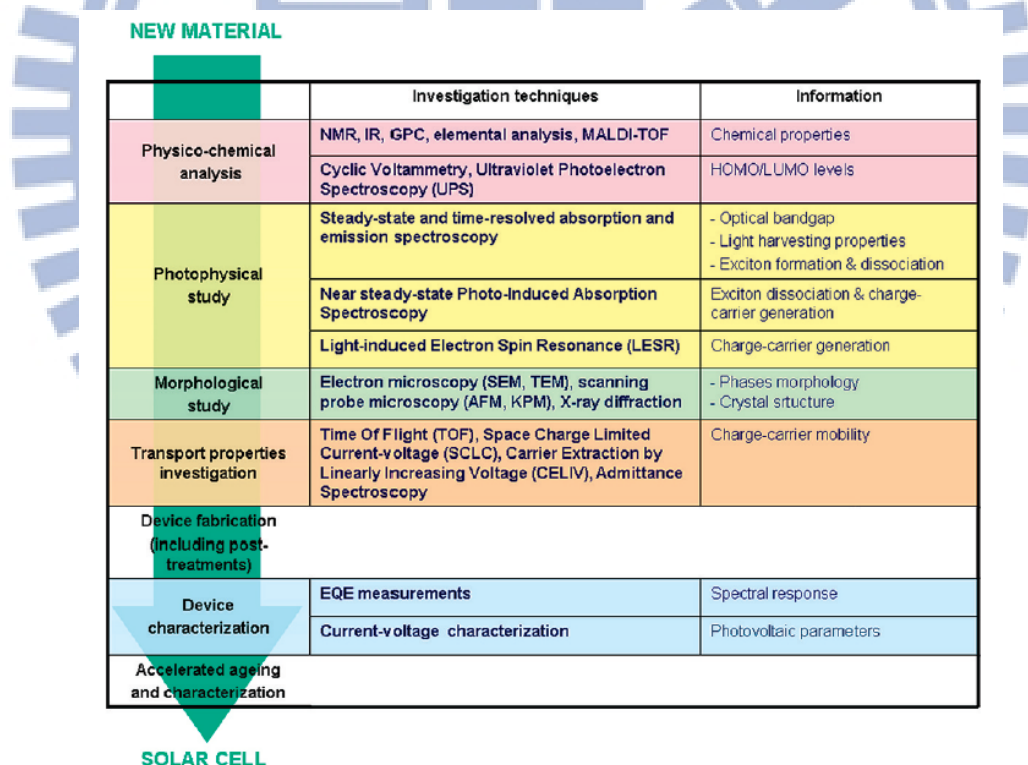


Figure 1.17 Basic investigation techniques required for an extended characterization of active materials for polymer solar cells.⁷⁷

1.6 Objective and Outlines of this Thesis

The main objective of this dissertation is to construct the donor-acceptor polymers or supramolecular polymer networks by mixing proper molar ratio of polymer and conjugated cross-linkers and further to study their performances in BHJ PSCs as electron donors with fullerene derivatives as electron acceptors.

In wide bandgap polymers there is a disadvantage of less light harvesting from the solar spectrum range though the larger gap between the HOMO and the LUMO on the polymers provide an opportunity to increase the open circuit voltages. In order to increase the V_{oc} while holding the band gap constant, the energy levels of both the HOMO and LUMO of the conjugated polymer must be decreased simultaneously. Thus, electron-withdrawing groups would need to be added to the polymer.⁵⁸ Conjugated polymers having D-A architectures have been extensively studied by utilizing fused heterocyclic electron rich segments, such as carbazole,⁴⁵⁻⁴⁸ cyclopentadithiophene,⁶⁷ dithienopyrrole,⁵²⁻⁵⁴ dithienosilole,⁶⁰ fluorene,⁶³ and benzodithiophene^{58, 59} as an electron donating building block for PSCs and organic field effect transistors (OFETs). Owing to the easy modulations of physical properties, it has been proven that, 2,7-carbazole derivatives are the excellent potential donor candidates for BHJ solar cells.⁴⁵ Using 2,7-carbazole and benzothiadiazole with improving absorption characteristics and charge-carrier mobilities, Heeger *et al.* reported an ever high PSC device containing PCDTBT with a PCE value of 6.1% and an internal quantum efficiency approaching ca. 100%.⁴⁶ The five-membered heterocyclic electron deficient moiety, i.e., thiazole, induces larger π - π stacking and higher co-planarity⁶⁵⁻⁶⁷ in D-A polymers so as to have a stronger tendency to self-assemble into stacked solid structures, which not only minimize steric hindrances but also provide extended

conjugation lengths. Introduction of thiazole units with electron-withdrawing imine nitrogen ($\text{C}=\text{N}$) generally enhances the electron-accepting (n-doping) properties of the D-A polymers.⁶⁵ Moreover, thiazole-based polymers exhibit high oxidative stabilities which favor the polymers to lower its HOMO energy level and thus to increase their open circuit voltages.⁶⁵

In chapter 2 copolymers consisting of a planar 2,7-carbazole moiety with conducting thiophene (thiophene or bithiophene) as electron-donating segments and bithiazole derivatives as electron-accepting segments, were synthesized by Pd(0)-catalyzed Stille coupling polymerization. The effects of electron deficient bithiazole units on the thermal, optical, electrochemical, and photovoltaic properties of these LBG copolymers were investigated.

DTPs, one kind of electron rich building block containing fused thiophene units, offer great processabilities by attaching various alkyl chains to N-substituents of the pyrrole rings without affecting their conjugation lengths.⁷⁸ However, due to high values of HOMO levels in DTP-based polymers, they showed relatively low V_{oc} values (less than 0.6 V) and thus to induce low PCE values.⁵¹⁻⁵⁶ This problem is expected to be solved by using various electron-deficient units to manipulate their HOMO energy levels.^{57, 79} In Chapter 3, a series of alternative D-A conjugated DTP-based polymers containing the electron-rich DTP block (with a minimum branched alkyl chain length) and electron-deficient bithiazole along with various conducting thiophene lengths were synthesized via Suzuki coupling polymerization. The manipulation of optical, electrochemical, and photovoltaic properties by copolymerizing with electron-deficient bithiazole derivatives were discussed.

During the past decade, semi-conducting polymers containing supramolecular structures, including hydrogen-bonds (H-bonds), are one of the key targets for sensors and optoelectronic

devices.⁸⁰ Owing to the self-assembly behavior, high specificity, and directionality of H-bonds,⁶⁹ well-defined nanostructures and mesoscopic assemblies are generated by utilizing complementary hydrogen-bonding concept. Due to self-assembly between complementary molecular components, various kinds of non-covalent interactions, such as hydrogen-bonds (H-bonds),⁷³ ionic forces,⁷⁴ and metal-coordinations,⁷³ can give rise to unique properties, which are not possessed by their individual components. Small molecules and their polymer analogues have attracted exceptional attentions in the recent days owing to their corresponding advantages, including high purities and (hole and electron) mobilities for small molecules, and easy processing capabilities and low costs for polymers.⁷⁵ Consequently, one of the attractive approaches is to achieve advanced π -conjugated materials by the combination of both small molecular and polymeric designs through supramolecular architectures, so the H-bonded polymer networks are explored.⁷⁶

In chapter 4, we could tune molecular energy levels, morphologies, and device preferemances by a new and straight-forward approach to introducing multiple H-bonded supramolecular structures. The broader light absorption (an extra blue absorption from H-bonded crosslinker **F** and the red-shifted absorption from H-bonded main-chain polymer **PBT**), lower HOMO level (to have a higher V_{oc} value), higher hole mobility, larger crystallinity, and better morphorlogy in H-bonded polymer network **PBT/F** induces better photovoltaic properties than that containing polymer **PBT** were discussed.

In chapter 5 we synthesized a conjugated main-chain polymer **PBTH**, in which the melamine pendants can be H-bonded with complementary uracil-based conjugated cross-linkers **C** and **F** (in proper molar amounts), i.e., the symmetrical uracils of cross-linkers **C** and **F** are

linked to central carbazole and fluorene units, respectively, through triple bonds, to generate supramolecular polymer networks **PBTH/C** and **PBTH/F**. We studied the effect of light harvesting capabilities, manipulation of HOMO energy levels, and power conversion efficiencies of conjugated main-chain polymer **PBTH** and supramolecular polymer networks **PBTH/C** and **PBTH/F**.



Chapter 2

Synthesis and Applications of 2,7-Carbazole-Based Conjugated Main-Chain Copolymers Containing Electron Deficient Bithiazole Units for Organic Solar Cells

2.1 Introduction

In the 21st century, to reduce carbon emissions and green house effects, solar energy is one of the “green” and “sustainable energy” sources to create better environment. Recently, organic semiconducting materials, including π -conjugated polymers,^{11a,46,58,60,81} and small molecules,^{75,82} have been utilized in various optical and electronic devices due to their unique advantages, such as light weight, low-cost production, and large area device fabrication by solution process.^{11,14,15,81} The highly efficient organic solar cell devices belong to the bulk heterojunction (BHJ) solar cells, in which π -conjugated polymers are used as electron donors and the fullerene derivatives, such as [6,6]-phenyl-C₆₁-butyric acid methyl ester (PC₆₁BM) or [6,6]-phenyl-C₇₁-butyric acid methyl ester (PC₇₁BM), as electron acceptors. After an extensive investigation on polymer solar cells (PSCs), the BHJ devices based on polymer blends (with various weight ratios and thicknesses) of poly(3-hexylthiophene) (P3HT) and PC₆₁BM were taken as standard devices. However, the enhancements of power conversion efficiency (PCE) values in these devices are quite difficult due to low open circuit voltage (V_{oc}) values (~0.6 V) and large band gaps, which limit their net light harvesting capabilities. Hence, the utilization of newly developed low band gap (LBG) conjugated polymers likely to be the promising alternatives of P3HT for PSCs. Recently, PCE values up to 6.0-7.7% were obtained by using

LBG conjugated polymers in the BHJ solar cells as electron donors.^{11,15} Nevertheless, these power conversion efficiencies are not sufficient for commercialization of polymer solar cells (PSCs). Therefore, promising efforts are required to develop new donor-acceptor (D-A) polymer structures with higher molecular crystallinity which can result in better π - π stacking, extended absorption, higher mobility, and balanced charge transport to get higher PCE values in PSCs.^{81c}

Later, there were several reports on D-A polymer solar cells,⁴⁵⁻⁶² which harvest maximum solar spectrum ranging from visible to near infra-red absorptions which appealed high short circuit current density (J_{sc}) values. It has been verified that V_{oc} is directly proportional to the difference between the highest occupied molecular orbital (HOMO) levels of donor polymers and the lowest unoccupied molecular orbital (LUMO) levels of acceptor PCBM derivatives.⁸¹ In BHJ solar cells, where PCBM is used as an acceptor, the ideal band gap (in order to achieve a high V_{oc} value) of donor polymer should be in the range of 1.2-1.9 eV which corresponds to a HOMO energy level between -5.8 and -5.2 eV and a LUMO energy level between -4.0 and -3.8 eV.^{45,81} Furthermore, to facilitate efficient electron transfer from donor to acceptor, the minimum energy difference between LUMO levels of electron donor and acceptor should be ca. 0.3 eV.^{45,81} Consequently, in order to obtain the desired molecular energy levels of the conjugated LBG polymers, electron-donating groups or electron-withdrawing groups can be substituted alternatively in the polymer backbones either to raise the HOMO energy level or to reduce the LUMO energy level.

Conjugated polymers having D-A architectures have been extensively studied by utilizing fused heterocyclic electron rich segments, such as carbazole,⁴⁵⁻⁴⁸ dibenzosilole,⁸³ cyclopentadithiophene,^{67,84} dithienopyrrole,⁵²⁻⁵⁴ dithienosilole,⁶⁰ fluorene,^{63,85} and

phenothiazine⁸⁶ as an electron donating building block for PSCs as well as organic field effect transistors (OFETs). Owing to the easy modulations of physical properties, it has been proven that 2,7-carbazole derivatives are one of the excellent potential donor candidates for BHJ solar cells. Using 2,7-carbazole based alternating copolymer (PCDTBT) as an electron donor, Leclerc *et al.* achieved a PCE value of 3.6%.⁸⁷ Hence, with improving absorption characteristics and charge-carrier mobilities, Heeger *et al.* reported an ever high PSC device containing PCDTBT with a PCE value of 6.1% and an internal quantum efficiency approaching ca. 100%.⁴⁶

The five-membered heterocyclic electron deficient moiety, i.e., thiazole, induces larger π - π stacking and higher co-planarity in D-A polymers so as to have a stronger tendency to self-assemble into stacked solid structures, which not only minimize steric hindrances but also provide extended conjugation lengths. Introduction of thiazole units with electron-withdrawing imine nitrogen ($-C=N$) generally enhances the electron-accepting (n-doping) properties of the D-A polymers. Moreover, thiazole-based polymers exhibit high oxidative stabilities which favor the polymers to lower its HOMO energy level and thus to increase their open circuit voltages.^{63,88} Though Shim *et al.* firstly reported that the polymer containing bithiazole and fluorine units achieved a low PCE value of 0.52%,⁶³ we reached a much higher PCE value of 3.04% utilizing a copolymer containing bithiazole and cyclopentadithiophene units recently.⁶⁷ As a consequence, the copolymers containing the planar electron-withdrawing bithiazole units as acceptors and 2,7-carbazole units as donors to produce D-A polymers will be very interesting LBG polymers for the applications of PSCs. In addition, Li *et al.* have newly reported one D-A copolymer containing 2,7-carbazole and bithiazole moieties as electron-donor and electron-acceptor segments, respectively, but only possessed a maximum PCE value of 0.30%.⁶⁴

In this article, we synthesized and characterized a series of copolymers consisting of a planar 2,7-carbazole moiety with conducting thiophene (thiophene or bithiophene) as electron-donating segments and bithiazole derivatives as electron-accepting segments. The copolymers were synthesized by Pd(0)-catalyzed Stille coupling polymerization with 1:1 (molar ratio) donor-acceptor ratio. The resulting polymers **P1-P4** exhibited broad absorption bands located in the UV-visible regions from 300 to 600 nm with optical band gaps of 1.99-1.93 eV. From the preliminary investigation, the photovoltaic performance of the PSC device containing **P4** (as an electron donor) blended with PC₇₁BM (as an acceptor) showed the best PCE value of 1.01% with a $V_{oc} = 0.60$ V, a $J_{sc} = 4.83$ mAcm⁻², and a fill factor (FF) of 35.0% measured under 100 mW/cm² of AM 1.5 white-light illumination.

2.2 Experimental Section

2.2.1 Materials

All chemicals and solvents were reagent grades and purchased from Aldrich, ACROS, Fluka, TCI, TEDIA, and Lancaster Chemical Co. Toluene and THF were distilled from sodium-benzophenone under nitrogen prior to use. Unless otherwise specified, the other solvents were degassed by nitrogen 1 h prior to use. All of the other chemicals were used as received.

2.2.2 Measurements and Characterization

¹H & ¹³C NMR spectra were recorded on a Varian Unity 300 MHz spectrometer using CDCl₃ solvent and chemical shifts were reported as δ values (ppm) relative to an internal tetramethylsilane (TMS) standard. Elemental analyses were performed on a HERAEUS CHN-OS RAPID elemental analyzer. Thermogravimetric analyses (TGA) were conducted with a TA

Instruments Q500 at a heating rate of 10°C/min under nitrogen. Gel permeation chromatography (GPC) analyses were conducted on a Waters 1515 separation module using polystyrene as a standard and THF as an eluant. UV–Visible (UV-vis) absorption spectra were recorded in dilute THF solutions (10^{-6} M) on a HP G1103A spectrophotometer. Thin films for UV–vis measurements were spin-coated on a glass substrate from THF solutions with a concentration of 5 mg/mL. Cyclic voltammetry (CV) measurements were performed using a BAS 100 electrochemical analyzer with a standard three-electrode electrochemical cell in a 0.1 M tetrabutylammonium hexafluorophosphate (TBAPF₆) solution (in acetonitrile) at room temperature with a scanning rate of 100 mV/s. During the CV measurements, the solutions were purged with nitrogen for 30 s. In each case, a carbon working electrode coated with a thin layer of copolymers, a platinum wire as the counter electrode, and a silver wire as the quasi-reference electrode were used, and Ag/AgCl (3M KCl) electrode was served as a reference electrode for all potentials quoted herein. The redox couple of ferrocene/ferrocenium ion (Fc/Fc⁺) was used as an external standard. The corresponding highest occupied molecular orbital (HOMO) and lowest unoccupied molecular orbital (LUMO) levels were calculated using $E_{\text{ox/onset}}$ and $E_{\text{red/onset}}$ for experiments in solid films of polymers, which were performed by drop-casting films with the similar thickness from THF solutions (ca. 5 mg/mL). The LUMO levels of PC₆₁BM or PC₇₁BM employed were in accordance with the literature data. The onset potentials were determined from the intersections of two tangents drawn at the rising currents and background currents of the CV measurements.

2.2.3 Device Fabrication and Photovoltaic Measurements of Polymer Solar Cells (PSCs)

The polymer photovoltaic (PV) cells in this study were composed of an active layer of blended polymers (**P1-P4**:PCBM) in solid films, which were sandwiched between a transparent indium tin oxide (ITO) anode and a metal cathode. Prior to the device fabrication, ITO-coated glass substrates ($1.5 \times 1.5 \text{ cm}^2$) were ultrasonically cleaned in detergent, deionized water, acetone, and isopropyl alcohol sequentially. After routine solvent cleaning, the substrates were treated with UV ozone for 15 min. Then, a modified ITO surface was obtained by spin-coating a layer of poly(ethylene dioxythiophene):polystyrenesulfonate (PEDOT:PSS) ($\sim 30 \text{ nm}$). After baking at 130°C for one hour, the substrates were transferred to a nitrogen-filled glove box. The PSC devices were fabricated by spin-coating solutions of blended polymers (**P1-P4**):PCBM (with various weight ratios of a copolymer and one of PCBM_s, i.e., PC₆₁BM or PC₇₁BM) onto the PEDOT:PSS modified substrates at 1500 rpm for 60 s (ca. 80 nm), and placed in a covered glass Petri dish. Initially, the blended polymer solutions were prepared by dissolving both copolymers and PC₆₁BM (with a 1:1 weight ratio) initially and then with various weight ratios for the optimum copolymer with PC₇₁BM in 1,2 dichlorobenzene (DCB) (20 mg/mL), followed by continuous stirring for 12 h at 50°C . In the slow-growth approach, blended polymers in solid films were kept in the liquid phase after spin-coating by using the solvent with a high boiling point. Finally, a calcium layer (30 nm) and a subsequent aluminum layer (100 nm) were thermally evaporated through a shadow mask at a pressure below 6×10^{-6} Torr. All PSC devices were prepared and measured under ambient conditions, where the active area of the devices was 0.12 cm^2 . The solar cell testing was done inside a glove box under simulated AM 1.5G irradiation (100 mW/cm^2) using a Xenon lamp based solar simulator (Thermal Oriel 1000W).

The external quantum efficiency (EQE) action spectrum was obtained at short-circuit condition. The light source was a 450 W Xe lamp (Oriol Instrument, model 6266) equipped with a water-based IR filter (Oriol Instrument, model 6123NS). The light output from the monochromator (Oriol Instrument, model 74100) was focused onto the photovoltaic cell under test.

2.2.4 Synthesis of Monomers and Polymers

4,4'-Dibromo-2-nitrobiphenyl (1)

4,4'-Dibromobiphenyl (20 g, 64 mmol) in 300 mL of glacial acetic acid was heated (100°C) to dissolve completely. Then, 90 mL of fuming nitric acid was added dropwise for a period of 30 min. The resulting mixture was further stirred vigorously for 1 h at 100°C to get a reddish brown precipitate. The reaction mixture was cooled to room temperature and poured into ice cold water. The precipitate was filtered and washed with excess of water, then the obtained product was further purified by recrystallization from ethanol to get a yellow solid (20.30 g, 88.72%). ¹H NMR (300 MHz, CDCl₃), δ (ppm): 8.03 (d, *J* = 3.0 Hz, 1H), 7.75 (dd, *J* = 9.0 Hz, *J* = 3.0 Hz, 1H), 7.55 (d, *J* = 9.0 Hz, 2H), 7.30 (d, *J* = 9.0 Hz, 1H), 7.15 (d, *J* = 6.0 Hz, 2H).

2,7-Dibromocarbazole (2)

Mixture of compound 2 (20 g, 56.02 mmol) and triphenylphosphine (36.73 g, 140.05 mmol) were dissolved in 220 mL of DCB and the reaction mixture was refluxed for 12 h. The excess DCB was removed by high vacuum distillation and the residue was purified by column chromatography (Silica gel) using a mixture of hexane:ethyl acetate (7:3) to get a white solid (12.90 g, 70.87%). ¹H NMR (300 MHz, CDCl₃), δ (ppm): 8.08 (br, 1H), 7.87 (d, *J* = 8.7 Hz, 2H), 7.56 (d, *J* = 1.5 Hz, 2H), 7.35 (dd, *J* = 1.8 Hz, *J* = 8.4 Hz, 2H).

1-Hexylheptanol (3)

In a 500 mL flame-dried two-neck round bottom flask, ethyl formate (10 mL, 123.78 mmol) was dissolved in 100 mL of anhydrous THF and cooled to -78°C under N_2 atmosphere. A freshly prepared hexylmagnesium bromide, which was obtained by adding 1-bromohexane (48.90 mL, 346.59 mmol) to a suspension of magnesium turning (10.40 g, 433.24 mmol) in dry THF (150 mL), was added dropwise into the previous solution, and then the reaction mixture was stirred overnight at room temperature. The reaction was quenched by the addition of MeOH, and then followed by adding saturated aqueous NH_4Cl . The crude compound was extracted three times with ethyl acetate. The combined organic fractions were washed with brine, dried over MgSO_4 , and concentrated by rotary evaporation. After vacuum distillation, the final compound was isolated as a white solid (21.87 g, 87.94%). ^1H NMR (CDCl_3 , 300 MHz): δ (ppm): 3.58 (m, 1H), 1.46–1.25 (m, 21H), 0.87 (t, $J = 6.4$ Hz, 6H).

Tridecan-7-yl 4-methylbenzenesulfonate (4)

In a 250 mL flame-dried two neck round bottom flask, 1-hexylheptanol (10.0 g, 49.91 mmol), Et_3N (17.40 mL, 124.77 mmol), and $\text{Me}_3\text{N}\cdot\text{HCl}$ (4.77 g, 49.91 mmol) were mixed in 40 mL of CH_2Cl_2 and then cooled to $0-5^{\circ}\text{C}$. A solution of *p*-toluenesulfonyl chloride (11.90 g, 62.38 mmol) in CH_2Cl_2 (39 mL) was added dropwise over 90 min and kept the reaction at room temperature. After 2 h, water was added and the crude compound was extracted with CH_2Cl_2 . The organic fraction was washed with water and brine, and dried over MgSO_4 , and concentrated by rotary evaporation. Subsequently, the crude product was purified by column chromatography (Silica gel, hexane/ethylacetate 9:1) to yield a viscous colorless liquid (15.15 g, 85.60%). ^1H

NMR (300 MHz, CDCl₃): δ (ppm): 7.79 (d, J = 8.2 Hz, 2H); 7.32 (d, J = 8.1 Hz, 2H); 4.53 (m, J = 6.0 Hz, 1H); 2.43 (s, 3H); 1.52 (m, 4H); 1.22 (m, 20H); 0.88 (t, J = 6.9 Hz, 6H).

2,7-Dibromo-9-(tridecan-7-yl)-9H-carbazole (5)

2,7-Dibromocarbazole (4.0 g, 12.30 mmol) and potassium hydroxide powder (3.45 g, 61.50 mmol) were dissolved in 50 mL of DMSO at 60°C. Then, a solution of tridecan-7-yl 4-methylbenzenesulfonate (6.25 g, 18.45 mmol) with 30 mL of DMSO was added dropwise through a dropping funnel over 1.5-2 h and stirred overnight. The reaction mixture was cooled to room temperature and poured into 500 mL of water. The crude compound was extracted with ethylacetate and washed with brine. The combined organic layer was dried over MgSO₄ and concentrated in rotary evaporator. The crude compound was purified by column chromatography (Silica gel) using hexane as an eluant to give a white solid (4.62 g, 74.03%). ¹H NMR (300 MHz, CDCl₃): δ (ppm): 7.90 (br, 2H); 7.70 (s, 1H); 7.54 (s, 1H); 7.33 (d, J = 6.0 Hz, 2H); 4.42 (m, 1H); 2.19 (m, 2H); 1.91 (m, 2H); 1.15 (m, 16H); 0.83 (t, J = 6.3 Hz, 6H). ¹³C NMR (75 MHz, CDCl₃): δ (ppm): 130.61; 130.15; 122.58; 121.71; 121.48; 114.75; 112.39; 57.22; 33.76; 31.79; 29.25; 26.98; 22.76; 14.23; EIMS (m/z): Anal. Calcd for C₂₅H₃₃Br₂N: C, 59.18; H, 6.56; N, 2.76. Found: C, 59.58; H, 6.12; N, 2.77. MS (FAB): m/z [M⁺] 505.0; calcd m/z [M⁺] 505.10.

General Synthetic Procedures of Polymers P1-P4

The synthetic route of copolymers is shown in Scheme 1. Into a 25 mL two-neck flask, 2,7-dibromo-9-(tridecan-7-yl)-9H-carbazole, 2,5-bis(tributylstannyl)thiophene (or 5,5'-bis(tributylstannyl)-2,2'-bithiophene), and 5,5'-dibromo-4,4'-dihexyl-2,2'-bithiazole (or 5,5'-bis(5-bromothiophen-2-yl)-4,4'-dihexyl-2,2'-bithiazole) were added. The mixture was

deoxygenated with nitrogen for 30 min, after which dry toluene (15 mL) and Pd(PPh₃)₄ (1 mol %), was transferred into the mixture in a dry environment. The reaction mixture was stirred at 110°C for 3 days, and then an excess amount of 2-bromothiophene was added to end-cap the trimethylstannyl groups for 4 hr. The reaction mixture was cooled to 40°C and added slowly into a vigorously stirred mixture of methanol/acetone (3:1). The polymers were collected by filtration and reprecipitation from methanol. The crude polymers were further purified by washing with acetone and EA for 2 days in a Soxhlet apparatus to remove oligomers and catalytic residues.

P1

Following the general polymerization procedure, compound **5** (0.5 equiv), **M1** (0.5 equiv), and compound **6** (1.0 equiv) were used in this polymerization to acquire a red powder. Yield: 72%. GPC: *M_w*: 41,900; PDI: 1.62; ¹H NMR (300 MHz, CDCl₃): δ (ppm) 8.10 (broad), 7.79-7.39 (broad), 7.12 (s), 4.62 (broad), 2.84 (broad), 1.83 (broad), 1.75-0.80 (broad), 0.77-0.61(broad). Anal. Calcd for (C₅₁H₆₅N₃S₄)_n: C, 72.21; H, 7.72; N, 4.95. Found: C, 71.81; H, 7.59; N, 4.87.

P2

Following the general polymerization procedure, compound **5** (0.5 equiv), **M2** (0.5 equiv), and compound **7** (1.0 equiv) were used in this polymerization to acquire a deep red powder. Yield: 69%. GPC: *M_w*: 25,100; PDI: 1.36; ¹H NMR (300 MHz, CDCl₃): δ (ppm) 8.10 (broad), 7.89-7.22 (broad), 7.12 (broad), 4.62 (broad), 2.97 (broad), 1.83 (broad), 1.75-0.80 (broad), 0.77-0.61(broad). Anal. Calcd for (C₅₉H₆₉N₃S₆)_n: C, 69.98; H, 6.87; N, 4.15. Found: C, 69.18; H, 6.79; N, 4.25.

P3

Following the general polymerization procedure, compound **5** (0.5 equiv), **M1** (0.5 equiv), and compound **6** (1.0 equiv) were used in this polymerization to acquire a black powder. Yield: 66%. GPC: M_w : 8,880; PDI: 1.20; ^1H NMR (300 MHz, CDCl_3): δ (ppm) 8.10 (broad), 7.79-7.19 (broad), 7.15 (broad), 4.62 (broad), 2.99 (broad), 1.85 (broad), 1.75-0.80 (broad), 0.77-0.61 (broad). Anal. Calcd for $(\text{C}_{59}\text{H}_{69}\text{N}_3\text{S}_6)_n$: C, 69.98; H, 6.87; N, 4.15. Found: C, 69.30; H, 6.98; N, 4.22.

P4

Following the general polymerization procedure, compound **5** (0.5 equiv), **M2** (0.5 equiv), and compound **7** (1.0 equiv) were used in this polymerization to acquire a black powder. Yield: 64%. GPC: M_w : 8,600; PDI: 1.19; ^1H NMR (300 MHz, CDCl_3): δ (ppm) 8.10 (broad), 7.79-7.39 (broad), 7.11 (broad), 4.59 (broad), 2.97 (broad), 1.81 (broad), 1.75-0.80 (broad), 0.77-0.61 (broad). Anal. Calcd for $(\text{C}_{67}\text{H}_{73}\text{N}_3\text{S}_8)_n$: C, 68.38; H, 6.25; N, 3.57. Found: C, 67.82; H, 6.38; N, 3.64.

2.3 Results and Discussion

2.3.1 Syntheses and Characterization

The synthetic routes of 2,7-carbazole-based donor monomer (compound **5**) and polymers **P1-P4** are outlined in Figure 2.1. Compound **5** was adequately characterized by ^1H NMR, ^{13}C NMR, MS spectroscopies, and elemental analyses. The thiophene- and bithiophene-based donor monomers (compounds **6** and **7**, respectively) were prepared according to the methods described

elsewhere.⁸⁹ In addition, the synthetic procedures of bithiazole-based acceptor monomers **M1** and **M2** were also reported earlier by our group.⁶⁷ In this study, polymers **P1-P4** consisting of 2,7-carbazole and thiophene (or 2,2'-bithiophene) as electron-donating moieties and bithiazole as electron-accepting moieties were synthesized by Pd(0)-catalyzed Stille coupling polymerization in toluene at 110°C with a feed-in molar ratio of m:n=1:1.

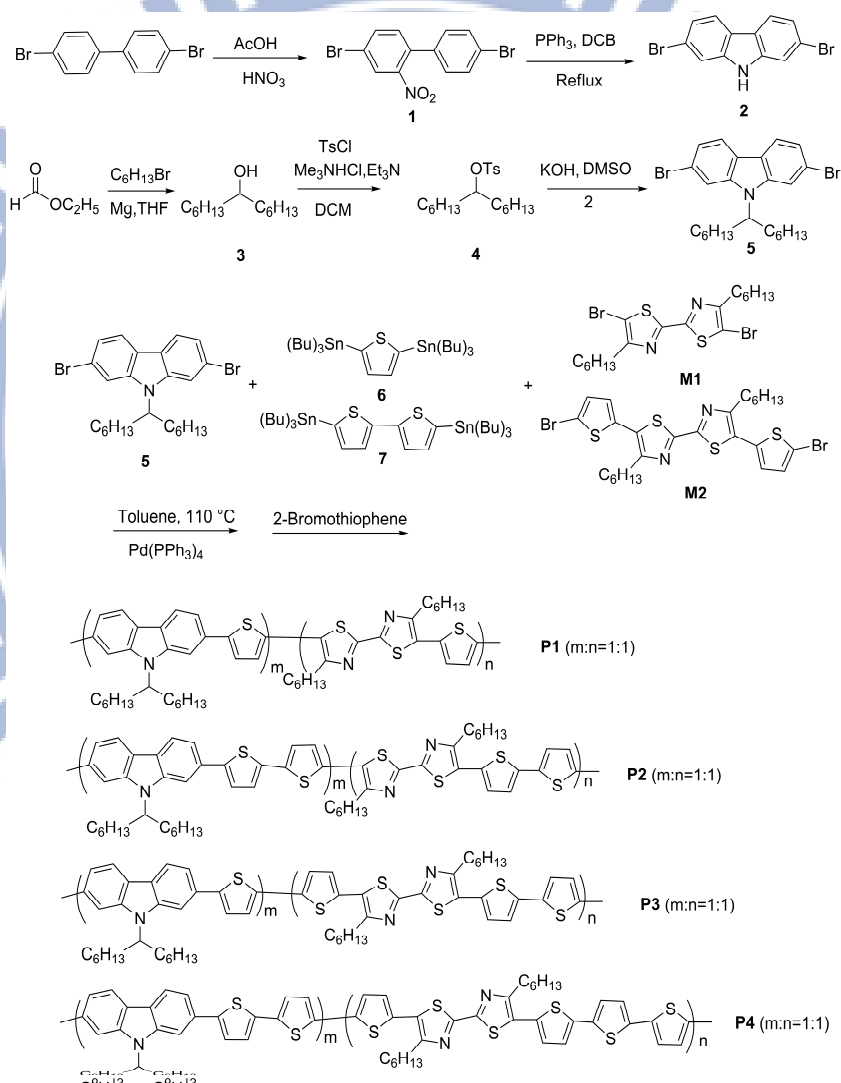


Figure 2.1 Synthetic schemes of compound **5** and polymers **P1-P4**.

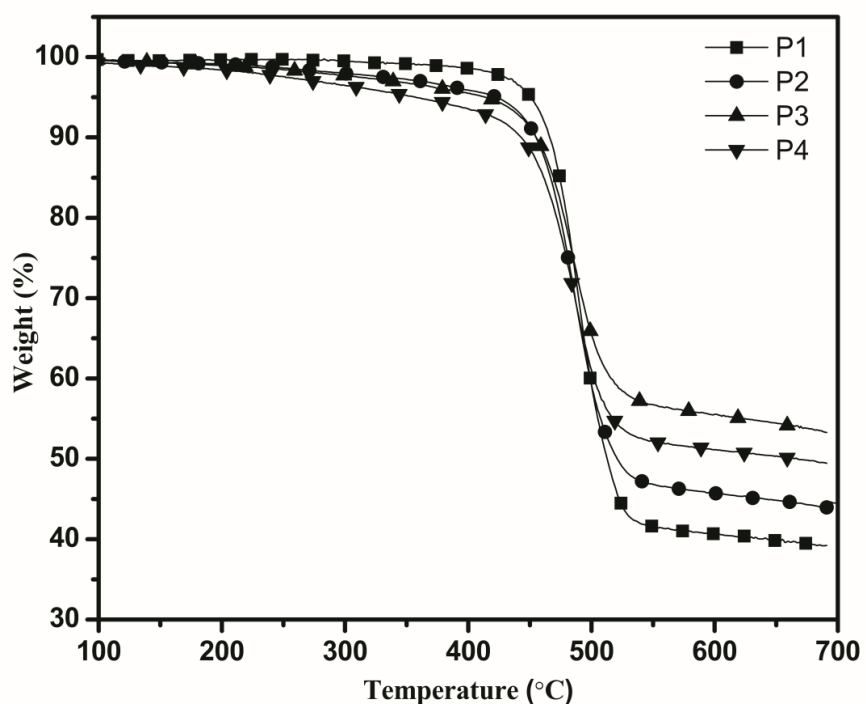


Figure 2.2 TGA measurements of polymers **P1-P4** with a heating rate of 10°C/min.

Table 2.1 Molecular Weights and Thermal Properties of Polymers **P1-P4**.

Polymer	M_w^a	M_n^a	PDI ^a (M_w/M_n)	Yield (%)	T_d^b (°C)
P1	41900	25900	1.62	72	452
P2	25100	18500	1.36	69	423
P3	8900	7400	1.20	66	418
P4	8600	7200	1.19	64	361

^aMolecular weights (M_n and M_w) and polydispersity index (PDI) values were measured by GPC, using THF as an eluent, polystyrene as a standard. M_n , number average molecular weight. M_w , weight average molecular weight. ^bTemperature (°C) at 5% weight loss measured by TGA at a heating rate of 10°C/min under nitrogen.

All these copolymers are readily soluble in common organic solvents such as chloroform, THF, and chlorobenzene at room temperature and completely soluble in high boiling point solvents (e.g., chlorobenzene) at high temperature. The molecular weights of polymers **P1-P4** determined by GPC against polystyrene standards in THF are summarized in Table 2. 1. These results show that considerable molecular weights with high yields (64–72% after Soxhlet extractions) were obtained in these copolymers, where the average molecular weights (M_w) were in the range of 41,900-8,600 with polydispersity index ($PDI=M_w/M_n$) values of 1.62-1.19. The thermal stabilities of conjugated polymers play an important role for optoelectronic applications. TGA measurements of polymers **P1-P4** with a heating rate of 10°C/min As shown in Figure 2.2, the thermal stabilities of polymers **P1-P4** were investigated by thermogravimetric analyses (TGA), and their corresponding results are summarized in Table 2.1. All polymers showed good thermal stabilities and exhibited T_d values (temperatures at 5% weight loss by a heating rate of 10°C/min under nitrogen) between 361 and 452°C, where the T_d value was reduced as the molecular weight decreased.⁷⁸

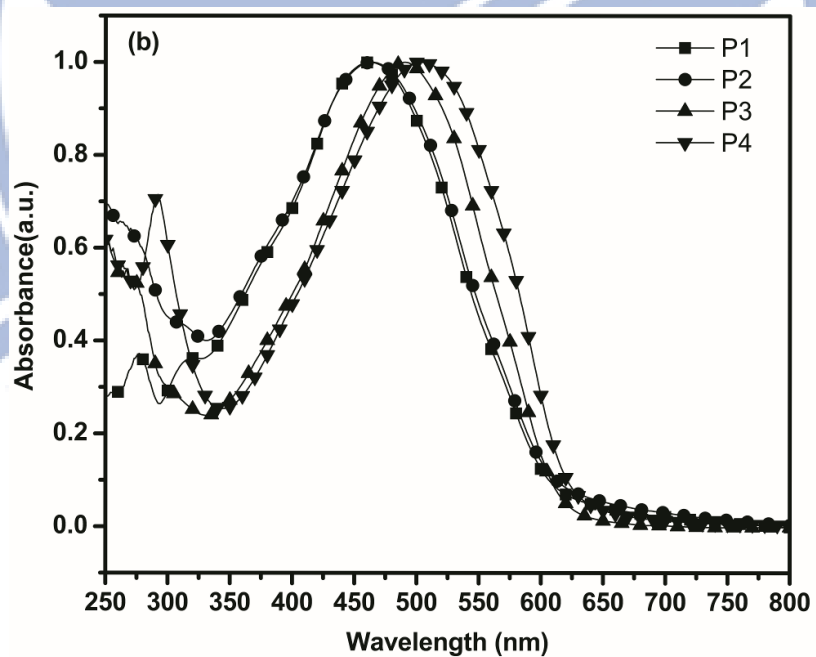
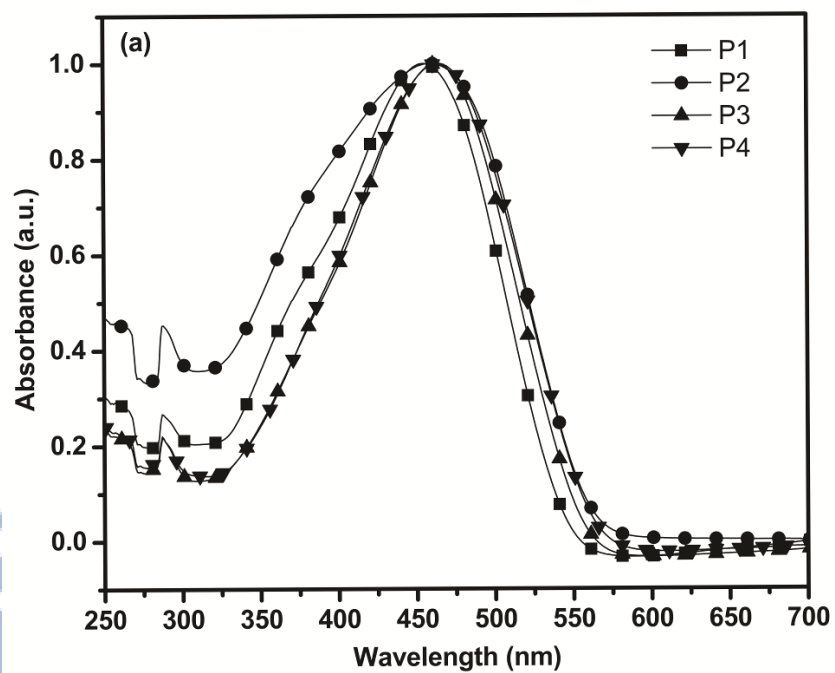


Figure 2.3 Normalized absorption spectra of P1-P4 (a) in dilute chloroform solutions and (b) solid films.

Table 2.2 Optical and Electrochemical Properties of Polymers P1-P4.

Polymer	Solution ^a		Solid film ^b		α_{\max} ($\times 10^4 \text{ M}^{-1} \text{ cm}^{-1}$)		Energy Levels		Band Gaps ^g	
	$\lambda_{\max, \text{abs}}$ (nm)	$\lambda_{\max, \text{abs}}$ (nm)	$\lambda_{\text{onset, abs}}$ (nm)	Solution ^d	Solid Film ^e	$E_{\text{onset}}^{\text{ox}}$ (V)/ HOMO ^f (eV)	$E_{\text{onset}}^{\text{red}}$ (V)/ LUMO ^f (eV)	E_{g}^{ec} (eV)	$E_{\text{g}}^{\text{opt}}$ (eV)	
P1	(314) ^c 455	314, 463	623	4.2	2.0	1.07/-5.42	-0.75/-3.60	1.82	1.99	
P2	(364) ^c 459	464	632	4.5	2.1	1.05/-5.40	-0.76/-3.59	1.81	1.96	
P3	464	490	626	5.2	3.4	1.03/-5.38	-0.77/-3.58	1.80	1.98	
P4	466	290, 504	642	5.7	4.2	0.99/-5.34	-0.80/-3.55	1.79	1.93	

^aIn THF dilute solution and ^b Spin coated from THF solution on glass surface. ^cShoulder peak. ^dAbsorption coefficient determined at λ_{\max} in THF. ^eAbsorption coefficient of the solid film at λ_{\max} . ^f $E_{\text{HOMO}}/E_{\text{LUMO}} = [-(E_{\text{onset}} - E_{\text{onset}}(\text{FC}/\text{FC}^+ \text{ vs. Ag}/\text{Ag}^+)) - 4.8]$ eV where 4.8 eV is the energy level of ferrocene below the vacuum level and $E_{\text{onset}}(\text{FC}/\text{FC}^+ \text{ vs. Ag}/\text{Ag}^+) = 0.45$ eV. ^g Band gaps, electrochemical band gap $E_{\text{g}}^{\text{ec}} = E_{\text{ox/onset}} - E_{\text{red/onset}}$ and optical band gap $E_{\text{g}}^{\text{opt}} = 1240/\lambda_{\text{edge}}$.

2.3.2 Optical Properties

The photophysical features of the copolymers were investigated by UV-vis absorption spectroscopy in dilute THF solutions and spin-coated films on glass substrates, which are presented in Figures 2.3. The normalized absorption spectra of polymers **P1-P4** and their optical data, including the absorption wavelengths ($\lambda_{\max, \text{abs}}$) and the optical band gaps ($E_{\text{g}}^{\text{opt}}$), and absorption coefficients (α_{\max}), are summarized in Table 2.2. All polymers (**P1-P4**) shows relatively high absorption coefficients (α_{\max} , calculated from Beer's law) with the range of 4.2-5.7 and $2.0\text{-}4.2 \times 10^4 \text{ M}^{-1} \text{ cm}^{-1}$ in dilute solutions and solid films, respectively, which assures the copolymers to harvest enough photons. The absorption wavelengths ($\lambda_{\max, \text{abs}}$) of polymers **P1**, **P2**, **P3**, and **P4** in dilute solutions were located at 455, 459, 464, and 466nm, respectively, which can be attributed to $\pi\text{-}\pi^*$ transition of the conjugated copolymer backbones and the $\pi\text{-}\pi$ interaction

between the electron donor (carbazole) and acceptor (bithiazole) units. It is obvious that, by tuning the numbers of thiophene units in the polymer conjugated heterocyclic main-chains, the absorption spectra of carbazole-based copolymers will be effectively influenced (in both solutions and solid films). In contrast to solutions (see Table 2.2), the absorption wavelengths ($\lambda_{\text{max,abs}}$) of polymers **P1-P4** in solid films were found red-shifted to the range of 463-503 nm obviously. These red-shifted wavelengths in solid films are ascribed to the interchain associations and π - π stackings of these copolymers as well as the highly rigid and planar segments of polymer backbones.⁹⁰ Moreover, the red shifts of absorption wavelengths from solutions to solid films are 8, 5, 26, 38 nm for polymers **P1-P4**, respectively. Hence, the larger numbers of thiophene units in **P3** and **P4** with longer conjugation lengths induced stronger π - π stackings in solid films, and thus to have larger red-shifted absorption wavelengths.

As shown in Table 2.2, the optical band gaps (E_g^{opt}) of polymers **P1-P4** in solid films were found in the range of 1.93-1.99 eV, which was determined from the cut-offs of the absorption wavelengths. The optical band gaps of the copolymers were reduced from **P1** to **P2** and from **P3** to **P4** owing to the enhancement of electron donating capabilities, as more thiophene units as well as longer conjugation lengths were introduced in the polymer backbones. These results imply that the light harvesting capabilities along with optical band gaps can be tuned by electron D-A segments in the polymer backbone, which is one of the efficient ways to design the organic photovoltaic materials.

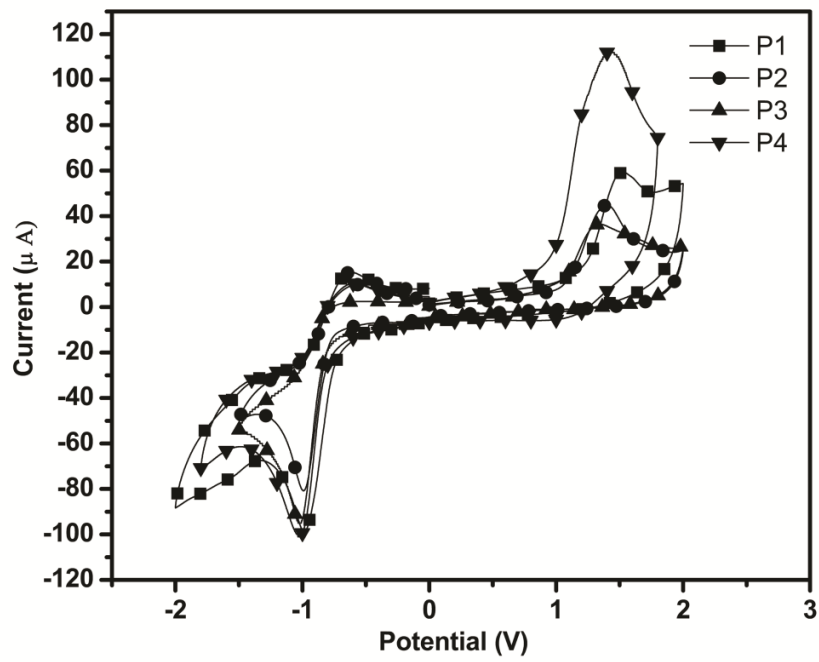


Figure 2.4 Cyclic voltammograms of **P1-P4** in solid films at a scan rate of 100 mV/s.

2.3.3. Electrochemical Properties

To investigate the redox behavior of the random copolymers and determine their electronic states (i.e., HOMO/LUMO levels), the electrochemical properties of polymers **P1-P4** were investigated by cyclic voltammetry. The oxidation and reduction cyclic voltammograms of the copolymers are shown in the Figure 2.4. The electrochemical properties, such as onset potentials of oxidation and reduction, i.e., the estimated positions of the upper edges of the valence band (HOMO) and the lower edges of the conduction band (LUMO), respectively, and electrochemical band gaps are summarized in Table 2.2. The CV measurements were carried out in a 0.1M tetrabutylammonium hexafluorophosphate (TBAPF₆) solution (in acetonitrile) at a scan rate of 100 mV/s under nitrogen. A carbon electrode, which was coated with the polymer film by dip coating, was used as a working electrode and Ag/AgCl was served as a reference electrode, and it was calibrated by ferrocene ($E^{1/2}_{\text{ferrocene}} = 0.45$ mV versus Ag/AgCl). The HOMO and LUMO energy levels were estimated by the oxidation and reduction potentials from the reference energy level of ferrocene (4.8 eV below the vacuum level) according to the following equation: $E_{\text{HOMO}}/E_{\text{LUMO}} = [-(E_{\text{onset}} - E_{\text{onset}}(\text{FC/FC}^+ \text{ vs. Ag/Ag}^+)) - 4.8]$ eV and band gap = $E_{\text{onset/ox}} - E_{\text{onset/red}}$ (where 4.8 eV is the energy level of ferrocene below the vacuum level and $E_{\text{onset}}(\text{FC/FC}^+ \text{ vs. Ag/Ag}^+) = 0.45$ eV).⁶⁷ It can be seen that polymers **P1-P4** possess quasi-reversible p-doping/dedoping (oxidation/rereduction) processes at positive potentials and reversible n-doping/dedoping (reduction/ reoxidation) processes at negative potentials.

The onset oxidation and reduction potentials of polymers **P1-P4** were in the ranges of 1.07-0.99 V and (- 0.75)-(-0.82) V, respectively, from which the estimated HOMO and LUMO levels were found in the range of (-5.34)-(-5.42) eV and (-3.55)-(-3.60) eV, respectively. The

lower HOMO energy levels of the polymers were desirable for high open circuit voltages of PSCs, as the polymers were taken as donor materials.⁴⁵ The noticeably higher oxidation potentials of **P1-P4** can be explained by that the resulting conjugated copolymers were more electron deficient due to the nitrogen atoms in their planar π -conjugated systems. On the other hand, the LUMO energy level of the electron donor (polymer) has to be positioned above the LUMO energy level of the electron acceptor (PCBM) at least 0.3 eV, so the exciton binding energy of polymer could be overcome and result in efficient electron transfer from donor to acceptor. The high reduction potentials of polymers **P1-P4** represent high electron affinities to make these copolymers suitable donors to inject and transport electrons to PCBM acceptor in polymer solar cell devices. The differences between the band gap values directly measured by CV (E_g^{cc} between 1.79 and 1.82 eV) and the optical band gap values obtained from UV-vis spectra (E_g^{opt} between 1.93 and 1.99 eV) lied within an acceptable range of errors.

Table 2.3 Photovoltaic Properties of Polymer Solar Cell (PSC) Devices with a Configuration of ITO/PEDOT:PSS/P1-P4:PC61BM(1:1 w/w)/Ca/Al^a

Active Layer ^b (Polymer:PC ₆₁ BM=1:1)	V_{oc} (V)	J_{sc} (mA/cm ²)	FF (%)	PCE (%)
P1	0.53	1.93	35	0.36
P2	0.56	2.31	36	0.46
P3	0.62	2.52	37	0.57
P4	0.58	2.87	34	0.57

^aMeasured under AM 1.5 irradiation, 100 mW/cm². ^bActive layer of blended polymers with the weight ratio of **P1-P4**:PC₆₁BM=1:1.

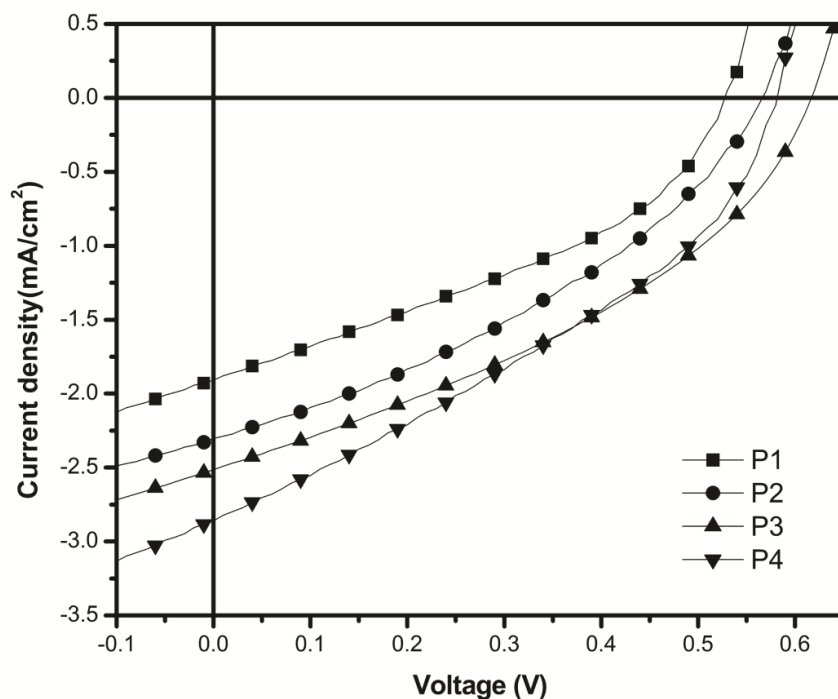


Figure 2. 5 J - V characteristics of ITO/PEDOT:PSS/**P1-P4**:PC₆₁BM(1:1 w/w)/Ca/Al under illumination of AM 1.5 at 100 mW/cm².

2.3.4 Photovoltaic Properties

To investigate the potential applications of copolymers in PSC devices, BHJ solar cells were fabricated by using polymers **P1-P4** as electron donors and fullerene [6,6]-phenyl-C₆₁-butyric acid methyl ester (PC₆₁BM) as an electron acceptor with a device configuration of ITO/PEDOT:PSS(30 nm)/(**P1-P4**):PCBM(1:1 w/w)(~80 nm)/Ca(30 nm)/Al(100 nm). This weight ratio of polymer blends with PCBM (**P1-P4**:PCBM=1:1 w/w) was found to have the optimum power conversion efficiency (PCE) value. Figure 2.5 shows the J - V curves of all polymer solar cells containing **P1-P4** under the condition of AM 1.5 at 100 mW/cm², and the open circuit voltage (V_{oc}), short circuit current density (J_{sc}), fill factor (FF), and PCE values of

the devices are summarized in Table 2.3. In order to have the great performance in PSC devices, DCB was chosen as the solvent to obtain the blended polymer active layers with good film qualities. The obtained PCE values of polymers **P1-P4** were in the range of 0.36-0.57%, where **P3** and **P4** possessed the highest PCE value (0.57%). However, the similar alternating copolymer reported by Li *et al.* which comprised of a planar carbazole unit as an electron donor and a bithiazole unit as an electron acceptor sandwiched between thiophene units, only achieved a lower PCE value of 0.30%.⁶⁴

Table 2.4 Photovoltaic Properties^a of Bulk-Heterojunction PSC Devices Containing Different Weight Ratios of Blended Polymers P4:PC₇₁BM and blend film roughness by AFM measurements.

Weight Ratios of Blended P4 :PC ₇₁ BM	V_{oc} (V)	J_{sc} (mA/cm ²)	FF (%)	R_{rms} (nm) ^b	PCE (%)
1:1	0.60	3.30	39	0.20	0.77
1:1.5	0.60	4.83	35	0.17	1.01
1:2	0.58	3.42	28	0.22	0.55

^aMeasured under AM 1.5 irradiation, 100 mW/cm². ^b R_{rms} : root-mean-square values of roughnesses measured from AFM images.

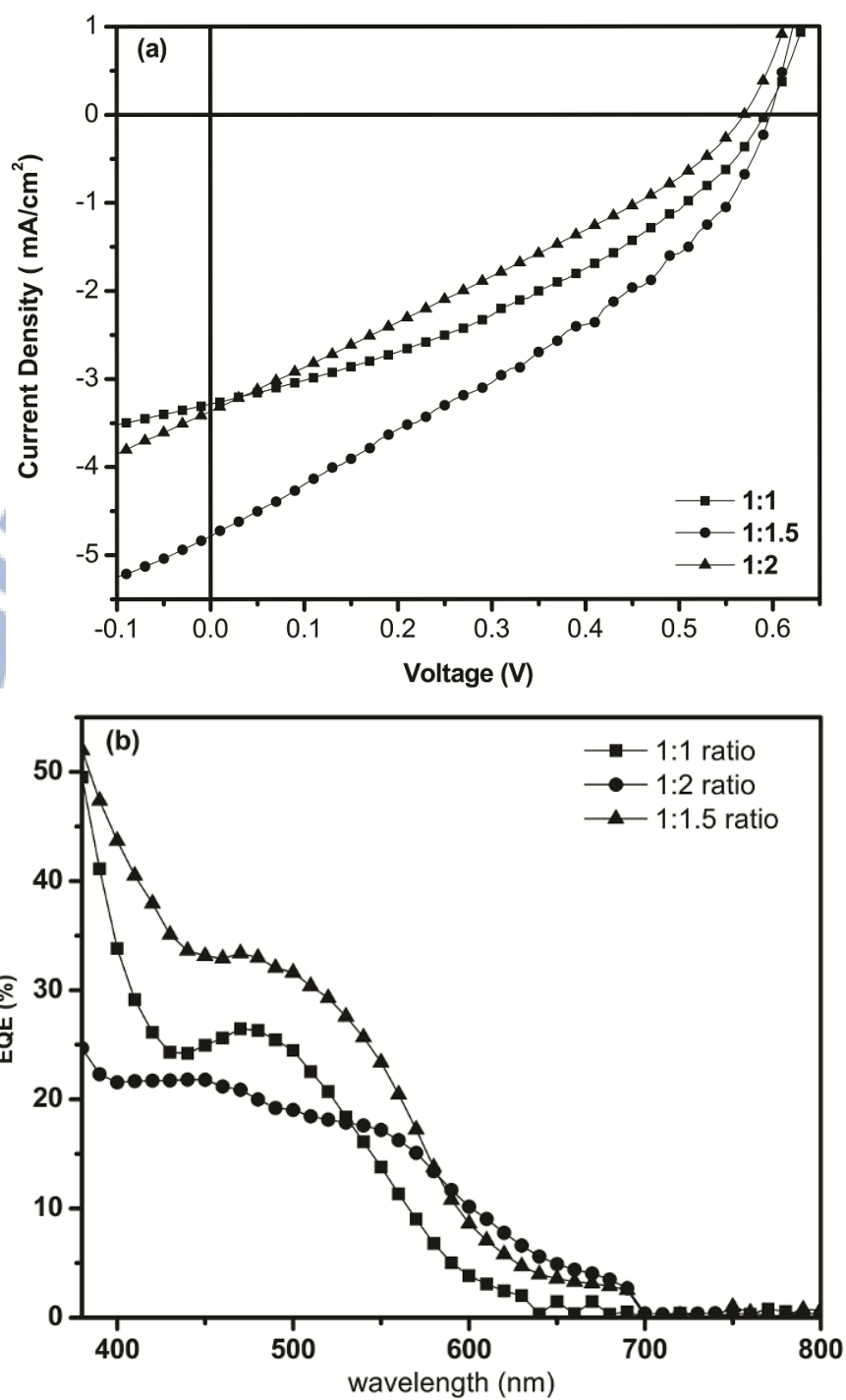


Figure 2.6 (a) J - V characteristics of ITO/PEDOT:PSS/P4:PC₇₁BM/Ca/Al under illumination of AM 1.5 at 100 mW/cm². (b) EQE curves of PSC devices based on polymer blends P4/PC₇₁BM in various weight ratios.

Though both PSC devices containing **P3** and **P4** possessed the highest PCE value (PCE = 0.57%), **P4** generated a higher J_{sc} value, a higher absorption coefficient, and an efficient red shift in UV-vis spectrum compared with those of **P3**. Therefore, the PSC device containing **P4** was chosen to be optimized in further photovoltaic studies. In order to acquire the advantage of a higher absorption coefficient of PC₇₁BM⁹¹ than PC₆₁BM, the bulk heterojunction PSC devices with different weight ratios of **P4** (as an electron donor) and PC₇₁BM (as an electron acceptor) were fabricated, and their J - V characteristics and photovoltaic properties are illustrated in Figure 2.6 and Table 2.4, respectively. The optimum PCE value of 1.01% was obtained in the PSC device having a weight ratio of **P4**:PC₇₁BM = 1:1.5 (with V_{oc} = 0.60 V, J_{sc} = 4.83 mA/cm², and FF = 35%). Using a lower weight ratio of PCBM in blended polymer **P4**:PC₇₁BM (1:1 w/w) led to a reduction in the J_{sc} value, which could be attributed to the inefficient charge separation and electron transporting properties, resulting in the lower PCE value.⁹² However, loading larger weight ratios of PCBM in blended copolymers **P4**:PC₇₁BM (1:2 w/w) also reduced the J_{sc} and PCE values, which could be probably attributed to the increased aggregation of PCBM so as to influence the separation of charges. Hence, both J_{sc} and PCE values decreased with larger PCBM molar ratios of 1:2 (w/w) because of the reasons described here. To investigate the different efficiencies of the PSC devices, the external quantum efficiencies (EQE) for polymer **P4** blended with PC₇₁BM in various weight ratios were further investigated in Figure 2.6, where the PSC devices exhibited a very broad response range covering from 400 to 700 nm with the maximum EQE values of 27%, 34%, and 22% for **P4**:PC₇₁BM = 1:1, 1:1.5, and 1:2 (w/w), respectively. Therefore, the photocurrent generation in the PSC device with **P4**:PC₇₁BM = 1:1.5 (w/w) is higher and leading to the highest PCE value due to more light harvest in the visible region.

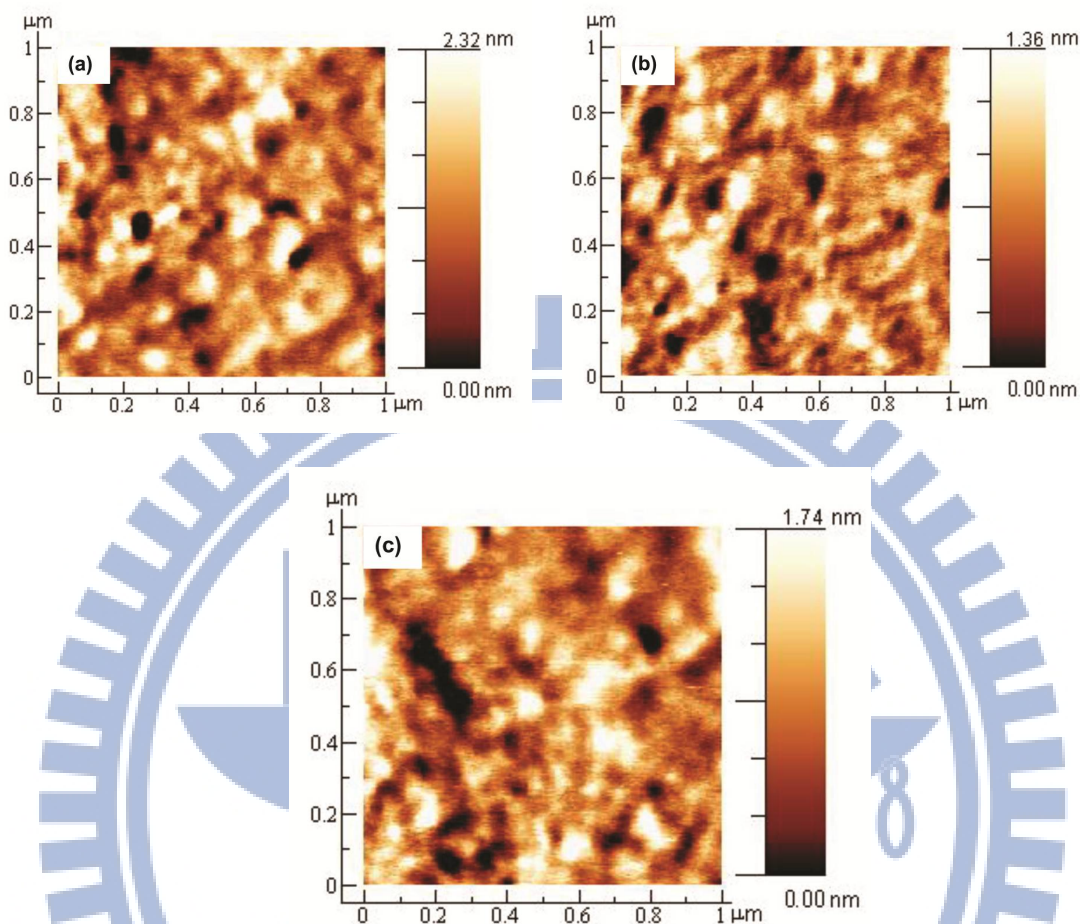


Figure 2.7 AFM images of blended polymer **P4:PC₇₁BM** spin coated from DCB in the ratios of (a) 1:1 (w/w), (b) 1:1.5 (w/w), and (c) 1:2 (w/w) with a size of $1 \times 1 \mu\text{m}^2$.

Surface morphology of the active layer is also the key parameter for device performance in PSC devices.⁹¹ The AFM topographic images of the polymer blends of **P4:PC₇₁BM** in various weight ratios (1:1, 1:1.5, and 1:2) are presented at Figure 2.7 and their root-mean-square values of roughness (R_{rms}) are presented in Table 2.4. It is clearly seen that all the phase images possessed almost similar coarse surfaces, which were attributed to the domains of highly stacked polymer chains in **P4**.⁶⁷ The most coarse surface of $R_{rms} = 0.22 \text{ nm}$ in **P4:PC₇₁BM** = 1:2 (w/w) indicated a large scale phase separation, which might decrease the diffusional escape probability for mobile charge carriers and thus to increase charge recombination. However, the decrease of

PC₇₁BM content in **P4**:PC₇₁BM = 1:1 (w/w) reduced the Rrms value to 0.20 nm, which led to a similar J_{sc} value with that of **P4**:PC₇₁BM = 1:2 (w/w). Compared with the other blending ratios of **P4**:PC₇₁BM, a smoothest surface with Rrms = 0.17 nm was obtained in **P4**:PC₇₁BM = 1:1.5 (w/w), which enhanced the J_{sc} value and yielded the highest efficiency (PCE = 1.01%) in PSCs.⁹⁴

2.4 Conclusions

In conclusion, a series of conjugated main-chain copolymers consisting of 2,7-carbazole electron-donating unit and bithiazole electron-accepting unit were synthesized by Pd(0)-catalyzed Stille coupling polymerization. Carbazole-based polymers exhibited broad absorption bands located in the UV and visible regions from 300 to 600 nm with optical band gaps of 1.93–1.99 eV. The HOMO and LUMO energy levels of the polymers can be finely tuned via the molecular engineering of donor/acceptor moieties and conjugated linkers inside the copolymers, which possessed relatively lower HOMO levels for PSC applications. The BHJ photovoltaic devices utilizing polymers **P1-P4** as electron donors and PC₆₁BM as electron acceptors were fabricated, and the optimization of PSC devices with **P4**:PC₇₁BM in different weight ratios were investigated. Finally, the photovoltaic device bearing an active layer of polymer blend **P4**:PC₇₁BM (1:1.5 w/w) showed the best power conversion efficiency (PCE) value of 1.01%, with a short circuit current density (J_{sc}) of 4.83 mA/cm², a fill factor (FF) of 35%, and V_{oc} = 0.60 V under 100 mW/cm² of AM 1.5 white-light illumination. AFM images revealed that there were a better mixing between polymers and PC₇₁BM to generate a less scale phase separation. Although the PCE values of all PSC devices were not sufficiently high, the tunable optoelectronic properties could be achieved by the structural modifications of electron donor and acceptor units.

Chapter 3

Fine Tuning of HOMO Energy Levels for Low-Band-Gap Photovoltaic Copolymers Containing Cyclopentadithienopyrrole and Bithiazole Units

3.1 Introduction

Solar energy is one of the key alternatives of fossil fuels due to its growing demands for clean, green, and sustainable energy. In the past decade, polymer solar cells used to be an extensive area of research compared with the traditional inorganic silicon counterpart owing to its unique advantages, such as low cost and easy manufacturing of thin films by vacuum deposition, solution cast, and printing technologies.^{11,14,15,81} Moreover, these carbon based materials can be engineered at the molecular level to have tunable electronic and optical properties. Syntheses of new conjugated polymers and small molecules becomes an emerging area after bulk heterojunction (BHJ) polymer solar cell (PSC) concept significantly improved PCE values over 7%^{11a,59,60} by forming a donor-acceptor (D-A) bicontinuous interpenetrated network, which creates large interfacial areas between the electron donor polymers and electron acceptors (such as fullerene derivatives) in the active layer blend and leads to an efficient photo-induced charge transfer in PSC devices.

The efficient BHJ PSC device architectures were obtained by using an active layer of poly (3-hexylthiophene) (P3HT) as an electron donor and [6,6]-phenyl-C₆₁-butyric acid methyl ester (PCBM) as an electron acceptor, which were able to reach power conversion efficiency (PCE) values up to 5%.⁴³ The main disadvantage of P3HT is appreciably wide band gap (1.9 eV) and able to absorb only 22% of influx from solar spectrum because the maximum photon fluxes

from the sun to earth surface is ca. 1.8 eV (i.e., 700 nm). In order to solve this problem, several literatures have been published in last 5 years on low band gap (LBG) D-A conjugated polymers, such materials offer unique advantages, e.g., broad absorption bands, tuning of molecular energy levels (HOMO & LUMO) and high charge carrier mobilities. In BHJ solar cells, where PCBM is used as an acceptor, the ideal band gap (in order to achieve a high V_{oc} value) of donor polymer should be in the range of 1.2-1.9 eV which corresponds to a HOMO energy level between -5.8 and -5.2 eV and a LUMO energy level between -4.0 and -3.8 eV.^{45,81} In such conjugated polymers, electron-donating groups and electron-withdrawing groups are substituted alternatively in the polymer backbones to lower HOMO energy levels. Because V_{oc} values are directly proportional to the difference between the highest occupied molecular orbital (HOMO) levels of polymers to the lowest unoccupied molecular orbital (LUMO) levels of PCBM derivatives.⁸¹ However, the large power conversion efficiency (PCE) value does not only rely upon the high V_{oc} value, but also require an improved current density (J_{sc}) and fill factor (FF). LBG polymers possessing high charge carrier mobilities are required for tuning high light harvesting capabilities and lead to high J_{sc} and PCE values for PSC devices. Moreover, high molecular weights, excellent solubilities and optimal morphologies are necessary to enhance J_{sc} and FF values.^{59,60} Therefore, the molecular design of D-A alternating architectures in polymer backbones have received considerable attention to organic chemists for the developments and applications of new low band gap conjugated polymers in photovoltaic devices.

For competent LBG polymer design, various electron rich and electron deficient building blocks, such as fluorine, carbazole,⁴⁶ cyclopentadithiophene,⁶⁷ dithienopyrrole,⁵²⁻⁵⁴ benzodithiophene,^{59,60} and thiadiazole,⁴⁵ thienopyrazine,^{45,63} and quinoxaline⁴⁵ have been

utilized for optoelectronic applications. Dithieno[3,2-b:2',3'-d]pyrroles (DTPs), i.e., one kind of electron rich building block containing fused thiophene units, offer great processabilities by attaching various alkyl chains to N-substituents of the pyrrole rings without affecting their conjugation lengths.⁵²⁻⁵⁴ However, due to high values of HOMO levels in DTP-based polymers, they showed relatively low V_{oc} values (less than 0.6 V) and thus to induce low PCE values.⁵¹⁻⁵⁴ This problem is expected to be solved by using various electron-deficient units to manipulate their HOMO energy levels. The thiazole unit is one of the five-membered azaheterocycles with electron deficient characteristics, which contains an electron-withdrawing imine ($-C=N$) in place of the carbon atom at the 3-position of thiophene.⁸⁸ Moreover, the thiazole-based polymers showed high oxidative stabilities which minimized the HOMO energy levels and to induce the high V_{oc} values.⁵¹⁻⁵⁵ Our previous approach reached a much higher PCE value of 3.04% by utilizing a copolymer containing bithiazole and cyclopentadithiophene units.⁶⁷ However, Li et al. have newly reported one D-A copolymer containing DTP and bithiazole moieties only possessed a maximum PCE value of 0.06%.⁶⁴ Wang et al. reported that an enhanced PCE value of the PSC device was obtained by decreasing alkyl chain lengths (from eight to five) of N-substituents in the DTP rings of D-A copolymer containing benzothiadiazole units.⁵¹ In addition, McCullough et al. reported DTP- and bithiazole-based polymers possessed field effect mobilities as high as 0.14 cm^2/Vs .⁹⁵

In this report, a series of alternative D-A conjugated DTP-based polymers containing the electron-rich DTP block (with a minimum branched alkyl chain length) and electron-deficient bithiazole block were synthesized via Suzuki coupling polymerization. The manipulation of optical, electrochemical, and photovoltaic properties by copolymerizing with electron-deficient

bithiazole derivatives were discussed. The preliminary PSC performance of these polymers blended with PCBM showed the best PCE value up to 0.69%, with $J_{sc} = 4.0 \text{ mA/cm}^2$, $V_{oc} = 0.40 \text{ V}$, and $FF = 43.0\%$ under AM 1.5 (100 mW/cm^2).

3.2 Experimental Part

3.2.1 Materials

All chemicals and solvents were reagent grades and purchased from Aldrich, ACROS, Fluka, TCI, TEDIA, and Lancaster Chemical Co. Tetrahydrofuran (THF), toluene, and diethyl ether were distilled over sodium/benzophenone. Absolute ethanol was obtained by refluxing with magnesium ethoxide and then distilled. Other reagents were used as received without further purification.

3.2.2 Measurements and Characterization

^1H and ^{13}C NMR spectra were recorded on a Varian Unity 300 MHz spectrometer using CDCl_3 solvent and chemical shifts were reported as δ values (ppm) relative to an internal tetramethylsilane (TMS) standard. Elemental analyses were performed on a HERAEUS CHN-OS RAPID elemental analyzer. Thermogravimetric analyses were conducted with a TA Instruments Q500 at a heating rate of $10^\circ\text{C}/\text{min}$ under nitrogen. Gel permeation chromatography (GPC) analyses were conducted on a Waters 1515 separation module using polystyrene as a standard and THF as an eluant. UV-visible absorption spectra were recorded in dilute chlorobenzene solutions (10^{-6} M) on a HP G1103A spectrophotometer. Thin films of UV-vis measurements were spin-coated on glass substrates from chlorobenzene solutions with a concentration of 5 mg/ml . Cyclic voltammetry (CV) measurements were performed by a

scanning rate of 100 mV/s at room temperature using a BAS 100 electrochemical analyzer with a standard three-electrode electrochemical cell in a 0.1 M tetrabutylammonium hexafluorophosphate (TBAPF₆) solution (in acetonitrile). During the CV measurements, the solutions were purged with nitrogen for 30 s. In each case, a carbon rod coated with a thin layer of polymers as the working electrode, a platinum wire as the counter electrode, and a silver wire as the quasi-reference electrode were used, and Ag/AgCl (3M KCl) electrode was served as a reference electrode for all potentials quoted herein. The redox couple of ferrocene/ferrocenium ion (Fc/Fc⁺) was used as an external standard. The HOMO and LUMO energy levels were estimated by the onset oxidation and reduction potentials from the reference energy level of ferrocene (4.8 eV below the vacuum level) according to the following equation: $E_{\text{HOMO/LUMO}} = [-(E_{\text{onset}} - E_{\text{onset}}(\text{Fc/Fc}^+ \text{ vs. Ag/Ag}^+)) - 4.8]$ eV and band gap = $E_{\text{onset/ox}} - E_{\text{onset/red}}$ (where 4.8 eV is the energy level of ferrocene below the vacuum level and $E_{\text{onset}}(\text{Fc/Fc}^+ \text{ vs. Ag/Ag}^+) = 0.45$ eV).⁶⁷ For CV experiments in solid films of polymers, which were performed by drop-casting films with the similar thickness from THF solutions (ca. 5 mg/ml). The LUMO level of PCBM employed was in accordance with the literature datum. The onset potentials were determined from the intersections of two tangents drawn at the rising currents and background currents of the CV measurements. Surface morphology images of thin films (on glass substrates) were obtained using atomic force microscopy (AFM, Digital instrument NS3a controller with D3100 stage).

3.2.3 Fabrication of Polymer Solar Cells

The polymer photovoltaic (PV) cells in this study contained an active layer of copolymers (**P1-P5**) blended with [6,6]-phenyl-C₆₁-butyric acid methyl ester (PCBM) in solid films, which was sandwiched between a transparent indium tin oxide (ITO) anode and a metal

cathode (Ca). Prior to the device fabrication, ITO-coated glass substrates ($1.5 \times 1.5 \text{ cm}^2$) were ultrasonically cleaned in detergent, deionized water, acetone, and isopropyl alcohol. After routine solvent cleaning, the substrates were treated with UV ozone for 15 min. Then, a modified ITO surface was obtained by spin-coating a layer of poly(ethylene dioxythiophene):polystyrenesulfonate (PEDOT:PSS) ($\sim 30 \text{ nm}$). After baking at 130°C for one hour, the substrates were transferred to a nitrogen-filled glove box. Subsequently, on the top of PEDOT:PSS layer, the active layer was prepared by spin coating from blended solutions of polymers **P1-P5**:PCBM (with 1:1 w/w) with a spin rate ca. 1500 rpm, and the thickness of the active layer was typically ca. 80 nm. Initially, the blended solutions were prepared by dissolving both polymers and PCBM in 1,2 dichlorobenzene (DCB)(20 mg/1 ml), followed by continuous stirring for 12 h at 50°C . In the slow-growth approach, blended polymers in solid films were kept in the liquid phase after spin-coating by using the solvent with a high boiling point (such as a glass petri dish) and allowed to dry the solvent slowly. Finally, a calcium layer (30 nm) and a subsequent aluminum layer (100 nm) were thermally evaporated through a shadow mask at a pressure below 6×10^{-6} Torr to have the active device area of 0.12 cm^2 . The solar cell testing was done inside a glove box under simulated AM 1.5G irradiation (100 mW/cm^2) using a Xenon lamp based solar simulator (Thermal Oriel 1000W). The light intensity was calibrated by a mono-silicon photodiode with KG-5 color filter (Hamamatsu). The external quantum efficiency (EQE) action spectra were obtained at short-circuit condition. The light source was a 450 W Xe lamp (Oriel Instrument, model 6266) equipped with a water-based IR filter (Oriel Instrument, model 6123NS). The light output from the monochromator (Oriel Instrument, model 74100) was focused on the photovoltaic cell under test.

3.2.4 Fabrication of Hole- and Electron-Only Devices

The hole- and electron-only devices in this study contain polymer blend films of **P1-P5**:PCBM (1:1 wt.) sandwiched between transparent ITO anode and cathode (MoO₃ and Ca, respectively). The devices have been prepared following the same procedure as fabrication of BHJ devices, except that Ca was replaced with MoO₃ ($\Phi = 5.3$ eV) in the hole-only devices, and the PEDOT:PSS layer was replaced with Cs₂CO₃ ($\Phi = 2.9$ eV) in the electron-only devices. The MoO₃ was thermally evaporated to a thickness of 20 nm and then capped with 50 nm of Al on the top of the active layer in the hole-only devices and Cs₂CO₃ was thermally evaporated with a thickness of approximately 2 nm on the transparent ITO in the electron-only devices. For both devices, annealing of the active layer was performed at 130°C for 20 min.

3.2.5 Synthesis of Monomers and Polymers

4-(Nonan-5-yl)-4*H*-dithieno[3,2-*b*:2',3'-*d*]pyrrole (**1**)

3,3'-Dibromo-2,2'-bithiophene (1 g, 3.08 mmol), *t*-BuONa (0.71 g, 7.40 mmol), Pd₂dba₃ (0.071 g, 0.007 mmol), and BINAP (0.288 g, 0.046 mmol) were dissolved in dry toluene (15 ml). The solution was purged with N₂ for 30 min. Nonan-5-amine (0.88 g, 6.17 mmol) was added via a syringe, and the mixture was stirred at 110°C under N₂ for 12 h. After cooling, water was added to quench the reaction, and the solution was extracted twice with diethyl ether. The combined organic layer was dried over MgSO₄, and the solvent was removed by rotary evaporation. The crude product was purified by column chromatography using silica, hexane as an eluent to give a white solid (0.69 g, 73.3 %). ¹H NMR (300 MHz, CDCl₃, δ): 7.10 (d, $J = 5.4$

Hz, 2H), 7.02 (d, $J = 5.4$ Hz, 2H), 4.26-4.16 (m, 1H), 1.96-1.82 (m, 2H), 1.81-1.32 (m, 2H), 1.14-1.05 (m, 8H), 0.88 (t, $J = 7.2$ Hz, 6H).

4-(Heptadecan-9-yl)-2,6-bis(4,4,5,5-tetramethyl-1,3,2-dioxaborolan-2-yl)-4*H*-dithieno[3,2-*b*:2',3'-*d*]pyrrole (2)

Compound **1** (0.5 g, 1.63 mmol) was dissolved in 50 ml of dry THF, and the solution was cooled down to -78°C under nitrogen protection. Then, 0.65 ml of *n*-BuLi (2.5M in Hexane, 3.26 mmol) was added, and the solution was warmed up to room temperature for 30 min and cooled again to -78°C . 2-Isopropoxy-4,4,5,5-tetramethyl-1,3,2-dioxaborolane (1.0 ml, 4.90 mmol) was rapidly injected into the solution by a syringe, and the resulting mixture was stirred at -78°C for 1 h and left to stir overnight at room temperature. The resulting mixture was quenched with H_2O and extracted with DCM. The DCM extracts were washed with saturated brine and dried with MgSO_4 . The solvent was removed by rotary evaporator and the product was further purified by column chromatography on silica using a mixture of hexane and DCM (4:1) as an eluent to yield a white solid (0.49 g, 53.8%). ^1H NMR (300 MHz, CDCl_3 , δ): 7.50 (s, 2H), 4.20 (m, 1H), 2.05-1.97 (m, 2H), 1.86-1.78 (m, 2H), 1.37 (s, 24H), 0.84 (t, $J = 6.0$ Hz, 6H). ^{13}C NMR (75 MHz, CDCl_3 , δ): 147.78, 121.51, 120.68, 84.31, 60.26, 34.93, 29.07, 25.02, 22.60, 14.13. MS (EI): m/z [M^+] 557.42 calcd m/z [M^+] 557.0. Anal. calcd. for $\text{C}_{29}\text{H}_{45}\text{B}_2\text{NO}_4\text{S}_2$: C, 62.49, H, 8.14, N, 2.51; Found: C 62.22, H 8.01, N 2.54.

4,4'-dihexyl-5,5'-bis(4-hexylthiophen-2-yl)-2,2'-bithiazole (3)

To a solution of monomer **M2** (1 g, 2.02 mmol) in THF (30 ml), 2-(4-hexylthiophen-2-yl)-4,4,5,5-tetramethyl-1,3,2-dioxaborolane (1.78 g, 6.06 mmol), Pd(PPh₃)₄ (35 mg) and 10 mL of 2 M aqueous K₂CO₃ solution were added. The reaction mixture was purged with N₂ and refluxed for 24 h. The reaction mixture was cooled to room temperature and extracted with DCM followed by washing with water and brine, and dried by anhydrous MgSO₄. The organic fraction was concentrated by rotary evaporation and pure product was obtained by recrystallization from methanol as a yellow solid (1.09 g, 80.7%). ¹H NMR (300 MHz, CDCl₃, δ): 7.02 (s, 2H), 6.95 (s, 2H), 2.92 (t, *J* = 6.0 Hz, 4H), 2.61 (t, *J* = 6.0 Hz, 4H), 1.36-1.25 (m, 32H), 0.88 (t, *J* = 6.0 Hz, 12H).

5,5'-bis(5-bromo-4-hexylthiophen-2-yl)-4,4'-dihexyl-2,2'-bithiazole (M5)

At room temperature, NBS (0.80 g, 4.48 mmol) was added portion wise to a solution of compound **3** (1.0 g, 1.49 mmol) in 25 ml THF. After 30 min, water was added and the crude compound was extracted with DCM. The organic layer was washed by water and brine, and dried by anhydrous MgSO₄. The organic fraction was concentrated by rotary evaporation and pure product was obtained by recrystallization from methanol as an orange solid (0.98 g, 79.7%). ¹H NMR (300 MHz, CDCl₃, δ): 6.87 (s, 2H), 2.87 (t, *J* = 6.0 Hz, 4H), 2.57 (t, *J* = 6.0 Hz, 4H), 1.36-1.25 (m, 32H), 0.89 (t, *J* = 6.0 Hz, 12H). ¹³C NMR (75 MHz, CDCl₃, δ): 157.97, 154.98, 143.09, 132.62, 128.52, 122.52, 110.23, 31.82, 30.56, 29.80, 29.35, 22.80, 14.30. MS (EI): *m/z* [M⁺] 658.60 calcd. *m/z* [M⁺] 659.0. Anal. calcd. for C₃₈H₅₄Br₂N₂S₄: C, 55.19; H, 6.58; N, 3.39. Found: C, 55.12; H, 6.50; N, 3.30.

General Polymerization Procedure

The synthetic routes of polymers are shown in Figure 3.1. All polymerization steps were carried out through the palladium(0)-catalyzed Suzuki coupling reactions. In a 25 ml flame dried two-neck flask, compound **2**, dibromo monomers (**M1-M5**), and $(\text{PPh}_3)_4 \text{Pd}(0)$ (1.5-0.5 mol %) were dissolved in a mixture of toluene (10 ml) and aqueous 2 M K_2CO_3 (5 ml). The reaction mixture was vigorously stirred at 90°C for 3-4 days. After reaction, an excess of iodobenzene was added to the reaction then one hour later, an excess of phenylboronic acid was added and the reaction was refluxed overnight to complete the end-capping reaction. The polymer was purified by precipitation in methanol/water (10:1), filtered and washed on Soxhlet apparatus using hexane, acetone, and chloroform. The chloroform fraction was reduced to 40-50 ml under reduced pressure, precipitated in methanol/water (10:1, 500 ml), filtered through $0.45 \mu\text{m}$ nylon filters, and finally air-dried overnight.

P1

Following the general polymerization procedure, compound **2** (0.5 equiv.) and **M1** (0.5 equiv.) were used in this polymerization, and the polymer was obtained as a black powder. Yield: 50%. ^1H NMR (300 MHz, CDCl_3 , δ): 7.95 (s, 2H), 7.12 (s, 2H), 4.21 (m, 1H), 2.81 (br, 2H), 1.79-1.33 (br, 2H), 1.15-1.03 (br, 8H), 0.86 (m, 6H). Anal. calcd. for $\text{C}_{23}\text{H}_{25}\text{N}_3\text{S}_4$: C, 58.56; H, 5.34; N, 8.91; S, 27.19; Found: C, 58.06; H, 5.13; N, 8.22.

P2

Following the general polymerization procedure, compound **2** (0.5 equiv.) and **M2** (0.5 equiv.) were used in this polymerization, and the polymer was obtained as a black powder. Yield:

66%. ¹H NMR (300 MHz, CDCl₃, δ): 7.20 (s, 2H), 4.21 (m, 1H), 3.03 (m, 4H), 2.95-1.74 (br, m, 6H), 1.60-1.15 (br, m, 22H), 0.90-0.83 (m, 12H). Anal. calcd. for C₃₅H₄₉N₃S₄: C, 65.68; H, 7.72; N, 6.57; S, 20.04; Found: C, 65.23; H, 7.52; N, 6.14.

P3

Following the general polymerization procedure, compound **2** (0.5 equiv.) and **M3** (0.5 equiv.) were used in this polymerization, and the polymer was obtained as a black powder. Yield: 62%. ¹H NMR (300 MHz, CDCl₃, δ): 7.95 (s, 2H), 7.20 (s, 4H), 4.21 (m, 1H), 2.93 (m, 4H), 2.95-1.70 (br, m, 6H), 1.61-1.11 (br, m, 22H), 0.90-0.83 (m, 12H). Anal. calcd. for C₄₃H₅₃N₃S₆: C, 64.21; H, 6.64; N, 5.22; S, 23.92; Found: C, 63.71; H, 6.64; N, 5.05.

P4

Following the general polymerization procedure, compound **2** (0.5 equiv.) and **M4** (0.5 equiv.) were used in this polymerization, and the polymer was obtained as a black powder. Yield: 59 %. ¹H NMR (300 MHz, CDCl₃, δ):7.30-7.13 (s, 6H), 4.23 (m, 1H), 3.03 (m, 4H), 2.95- 1.74 (br, m, 6H),1.61-1.13 (br, m, 22H), 0.90-0.83 (m, 12H). Anal. calcd. for C₄₃H₅₃N₃S₆: C, 64.21; H, 6.64; N, 5.22; S, 23.92; Found: C, 65.11; H, 6.34; N, 5.41.

P5

Following the general polymerization procedure, compound **2** (0.5 equiv.) and **M5** (0.5 equiv.) were used in this polymerization, and the polymer was obtained as a dark red powder. Yield: 61%. ¹H NMR (300 MHz, CDCl₃, δ):7.20-6.91 (br, 4H), 4.21 (m, 1H), 3.03 (m, 10H),

2.95-1.74 (br, m, 10H), 1.81-1.15 (br, m, 32H), 0.90-0.83 (m, 18H). Anal. calcd. for $C_{55}H_{77}N_3S_6$: C, 67.92; H, 7.98; N, 4.32; S, 19.78; Found: C, 67.22; H, 7.46; N, 4.01.

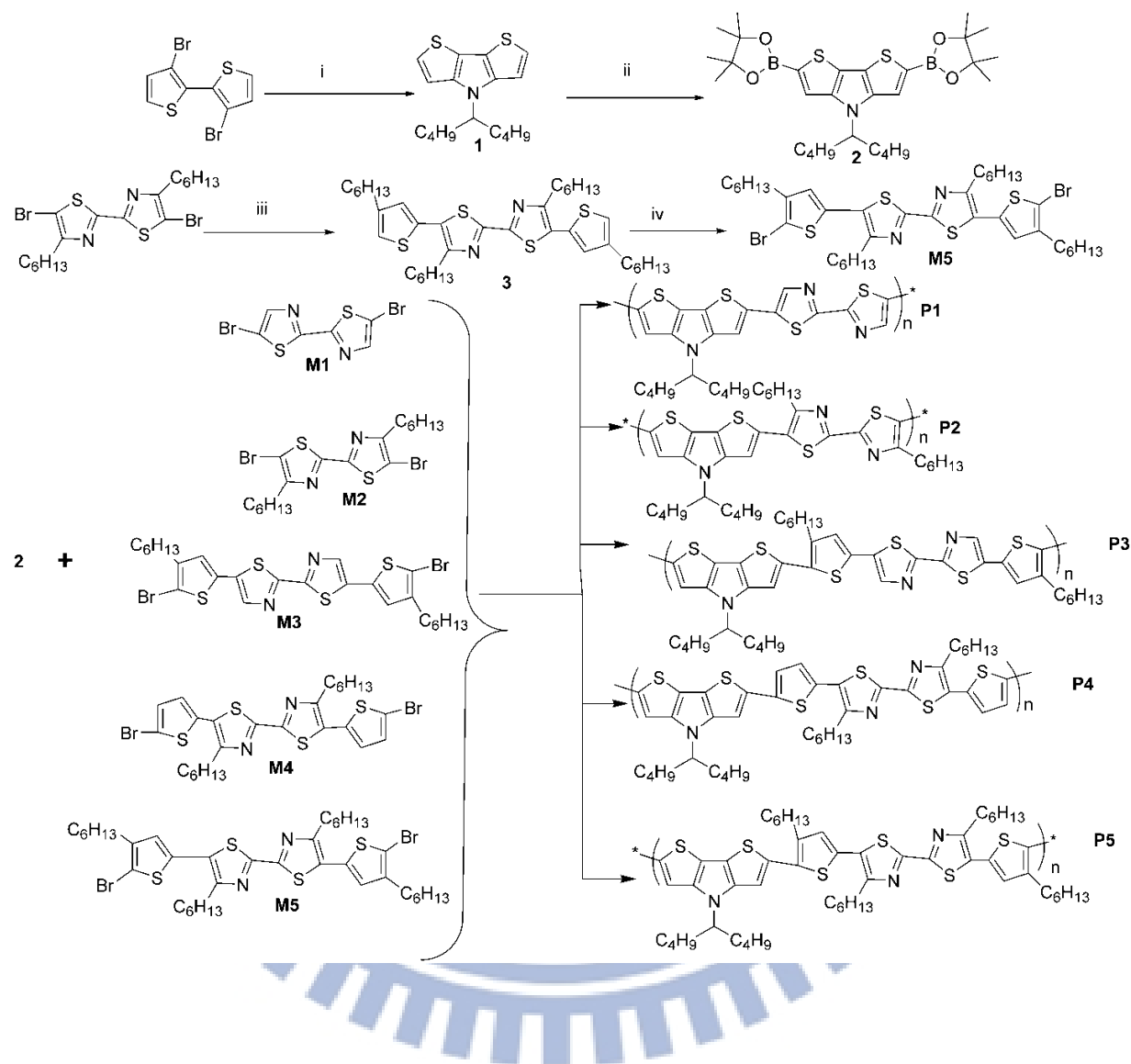


Figure 3.1 Synthesis of **M5** and polymers (**P1-P5**)^a.

^aReagents and conditions: (ii) Toluene, *t*-BuONa, Pd₂dba₃, BINAP, Nonan-5-amine (ii) THF, *n*-BuLi, 2-isopropoxy-4,4,5,5-tetramethyl-1,3,2-dioxaborolane, -78°C (iii) THF, 2-(4-hexylthiophen-2-yl)-4,4,5,5-tetramethyl-1,3,2-dioxaborolane, Pd(PPh₃)₄, 24 h (vi) NBS, THF, 30 min (v) Toluene, 2M K₂CO₃, Pd(PPh₃)₄, 90°C, 3-4 days.

3.3 Results and discussion

3.3.1 Synthesis and characterization

The synthetic routes of monomer (**M5**) and polymers are shown in Figure 3.1. Synthesis of monomers **M2** and **M4** were reported previously,⁹⁶ and monomer **M1**^{90b} and **M3**⁹⁷ were prepared by modified methods according to the literature. **M2** was converted to compound **3** by Suzuki coupling with 2-(4-hexylthiophen-2-yl)-4,4,5,5-tetramethyl-1,3,2-dioxaborolane and finally brominated by NBS to form **M5**. Donor moiety (**1**), i.e., dithieno[3,2-b:2',3'-d]pyrrole (DTP), was synthesized via Buchwald-Hartwig reaction of 3,3'-dibromo-2,2'-bithiophene⁵¹ and nonan-5-amine.⁹⁸ Compound **1** was converted to compound **2** by deprotonation with n-BuLi followed by addition of 2-isopropoxy-4,4,5,5-tetramethyl-1,3,2-dioxaborolane with a yield of 54%. Monomers **M5**, and compound **2** were satisfactorily characterized by ¹H NMR, ¹³C NMR, MS spectroscopy, and elemental analyses.

All polymers (**P1-P5**) were synthesized by Suzuki coupling polymerization in toluene between one electron sufficient moiety (**2**) and five electron deficient moieties (**M1-M5**). All these polymers (except polymer **P1**) are readily soluble in organic solvents, such as chloroform, THF, and chlorobenzene at room temperature and completely soluble in high boiling point solvents (e.g., chlorobenzene) at high temperature. The average molecular weights (M_n and M_w) of polymers **P1-P5** determined by GPC against polystyrene standards in THF are summarized in Table 3.1. These results show that considerable molecular weights with moderate yields (50-66% after Soxhlet extractions) were obtained in these polymers, where the average molecular weights (M_w) ranged 11200-91,000 with polydispersity indices ($PDI=M_w/M_n$) of 1.04-2.02. The thermal stabilities of conjugated polymers play a key role for optoelectronic applications. The thermal

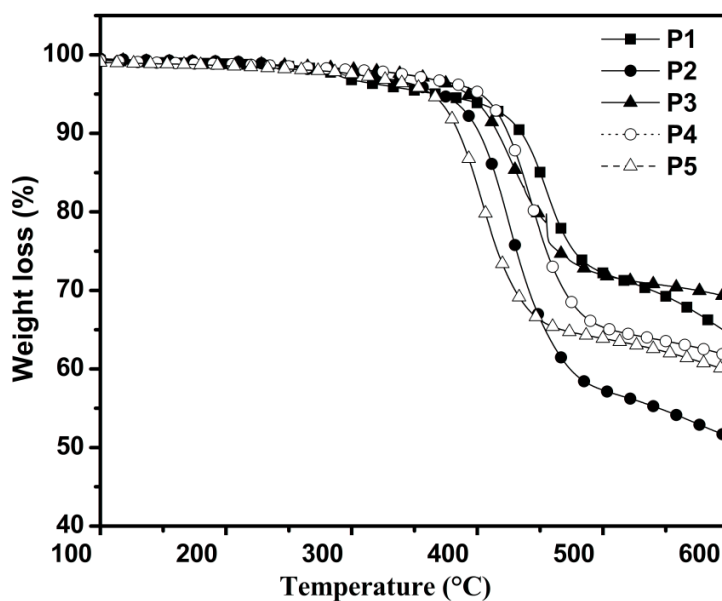


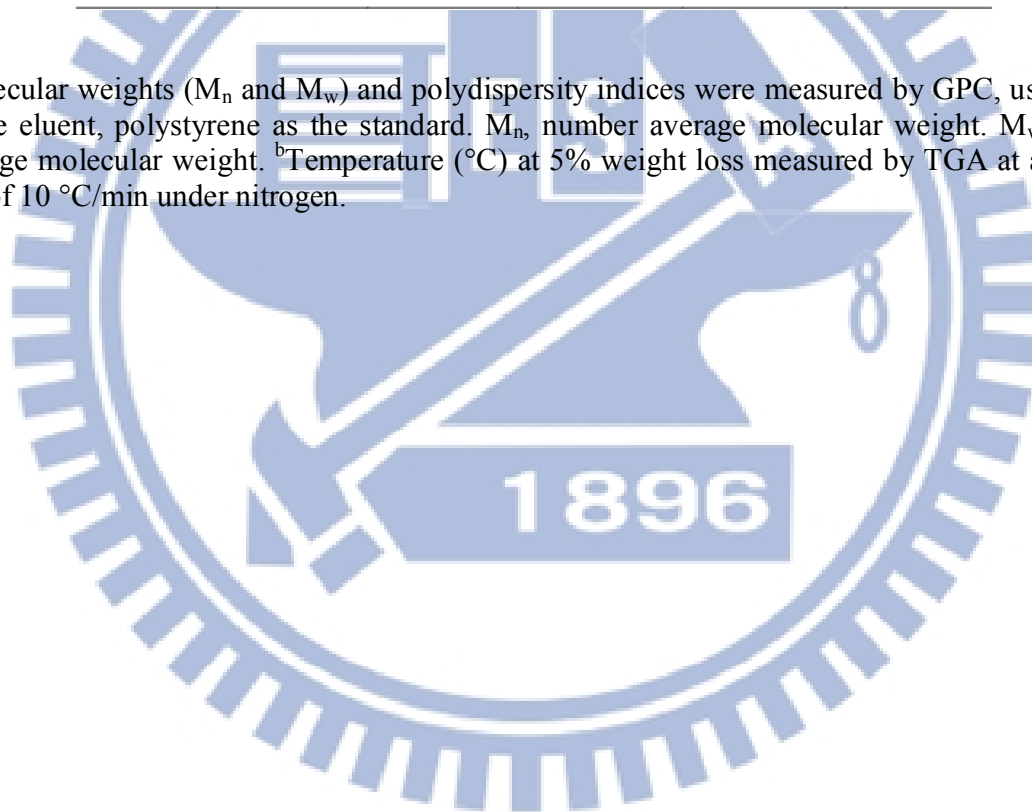
Figure 3.2 TGA measurements of polymers **P1-P5** with a heating rate of $10^{\circ}\text{C}/\text{min}$.

stabilities of polymers **P1-P5** were investigated by thermogravimetric analyses (TGA), and their corresponding results are summarized in Figure 3.2 and Table 3.1. It is apparent that all polymers exhibited good thermal stabilities as their weight losses less than 5% (under nitrogen) found to be $403\text{-}369^{\circ}\text{C}$, which are adequate for their applications in polymer solar cells and other optoelectronic devices.

Table 3.1 Molecular Weights and Thermal Properties of Polymers (P1-P5).

Polymer	M_w^a	M_n^a	PDI ^a (M_w/M_n)	Yield (%)	T_d^b (°C)
P1	11133	10681	1.04	50	389
P2	65575	34062	1.93	66	376
P3	91059	44987	2.02	62	370
P4	28864	22646	1.27	59	403
P5	12560	10884	1.15	61	369

^aMolecular weights (M_n and M_w) and polydispersity indices were measured by GPC, using THF as the eluent, polystyrene as the standard. M_n , number average molecular weight. M_w , weight average molecular weight. ^bTemperature (°C) at 5% weight loss measured by TGA at a heating rate of 10 °C/min under nitrogen.



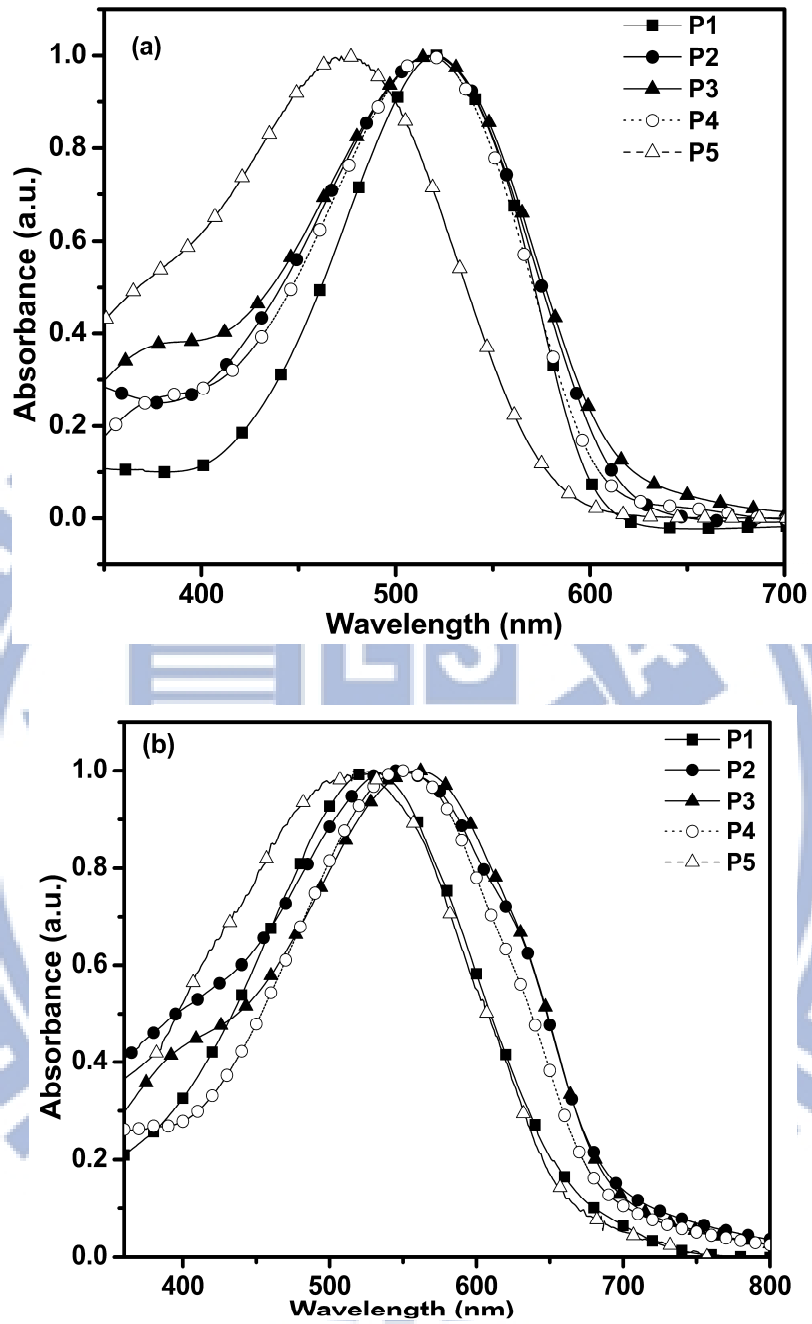


Figure 3.3 Normalized UV-vis spectra of polymers (P1-P5) in (a) in dilute chlorobenzene solutions and (b) as solid films on glass surfaces, respectively.

3.3.2 Optical Properties

The photophysical characteristics of polymers were investigated by UV-vis absorption spectra in chlorobenzene solutions as well as in solid films presented in Figure 3.3, and the absorption maxima (both solutions and solid films) and optical band gaps (E_g^{opt}) are listed in Table 3.2. As expected, all electron donor-acceptor polymers demonstrated red-shifted absorption from solutions to solid films. In addition, the absorption maxima of polymers **P1-P5** were in the range of 480-522 nm and 508-558 nm for solutions and solid films, respectively. As shown in Figure 3.3, similar intramolecular charge transfer (ICT) interactions between electron donor DTP and acceptor bithazole derivatives were found in the UV-vis spectra of rigid π -conjugated D-A polymers.^{67,79} Due to the presence of various electron donating moieties in polymers (**P2-P5**), such as alkyl chains (e.g. hexyl groups) on thiophene and bithazole units, different extents of red-shifted absorption occurred from the solutions to solid films. Due to the worst solubility of **P1** in the chlorobenzene solution, Polymer **P1** possessed the least (3 nm) red-shifted absorption maxima from the solution to the solid film. Compared with polymers **P3-P4**, polymer **P5** possessed blue-shifted absorption maxima in both solution and solid film, which might be due to the twist of polymer backbones induced by the alkyl side-chains on both bithiazole and thiophene units.⁶⁷ Compared with polymers **P1** and **P2** in solid films, the corresponding **P3** and **P4** possesses 33 and 6 nm red-shifted absorption maxima, respectively, which implied that the electron donating hexyl thiophene units had more contribution to broaden the conjugation lengths in the copolymers than the thiophene units.⁵⁶ The optical band gaps (E_g^{opt}) of the polymers in solid films determined by the cut off wavelengths of the optical absorptions are in the range of 1.68-1.79 eV (see Table 3.2). Moreover, the optical band gaps of

the polymers could be lowered to the narrowest value of $E_g^{\text{opt}} = 1.68$ eV (or $E_g^{\text{ec}} = 1.33$ eV) for **P4**. These results implies that it is an efficient way to design the DTP-based photovoltaic polymers to have higher light harvesting capabilities by tuning various electron donating moieties in the electron deficient bithiazole derivatives.

Table 3.2 Optical and Electrochemical Data of Polymers (P1-P5).

Polymer	<u>Solution^a</u>		<u>Solid film^b</u>		<u>Energy levels</u>		<u>Band gaps^g</u>	
	$\lambda_{\text{max,abs}}$ (nm)	$\lambda_{\text{max,abs}}$ (nm)	$\lambda_{\text{onset,abs}}$ (nm)	$E_{\text{onset}}^{\text{ox}}$ (V)/ HOMO ^f (eV)	$E_{\text{onset}}^{\text{red}}$ (V)/ LUMO ^f (eV)	E_g^{ec} (eV)	E_g^{opt} (eV)	
P1	522	525	704	0.93/-5.28	-0.62/-3.76	1.52	1.76	
P2	518	543	712	0.82/-5.17	-0.81/-3.54	1.63	1.74	
P3	519	558	725	0.63/-4.99	-0.77/-3.55	1.40	1.71	
P4	517	549	734	0.49/-4.81	-0.84/-3.59	1.33	1.68	
P5	480	508	691	0.71/-5.06	-0.64/-3.71	1.35	1.79	

^aChlorobenzene solutions (10^{-6} M). ^bSpin-coated from Chlorobenzene solution on glass surface. ^c $E_{\text{HOMO}}/E_{\text{LUMO}} = [-(E_{\text{onset}} - E_{\text{onset}}(\text{FC}/\text{FC}^+ \text{ vs. } \text{Ag}/\text{Ag}^+)) - 4.8]$ eV where 4.8 eV is the energy level of ferrocene below the vacuum level and $E_{\text{onset}}(\text{FC}/\text{FC}^+ \text{ vs. } \text{Ag}/\text{Ag}^+) = 0.45\text{eV}$. ^dBand gaps: electrochemical band gap $E_g^{\text{ec}} = E_{\text{onset}}^{\text{ox}} - E_{\text{onset}}^{\text{red}}$ and optical band gap $E_g^{\text{opt}} = 1240/\lambda_{\text{edge}}$.

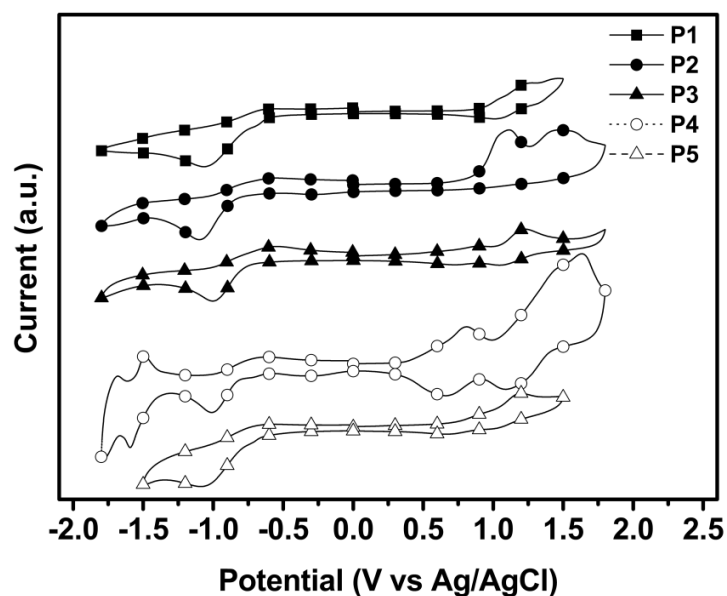


Figure 3.4 Cyclic voltammograms of **P1-P5** in solid films at a scan rate of 100 mV/s.

3.3.3 Electrochemical Properties

To investigate the redox behavior of the random copolymers and their electronic states (i.e., HOMO/LUMO levels), the electrochemical properties of polymers **P1-P5** were investigated by cyclic voltammetry (CV). The oxidation and reduction cyclic voltammograms of the polymers are shown in Figure 3.4. The electrochemical properties, such as the onset potentials of oxidation and reduction, i.e., the estimated positions of the upper edges of the valence bands (HOMO) and the lower edges of the conduction bands (LUMO), respectively, and electrochemical band gaps of all polymers are summarized in Table 3.2. It can be seen that polymers **P1-P2** possess one and **P3-P5** possess two quasi-reversible or reversible p-doping/dedoping (oxidation/reduction) processes at positive potential ranges and one reversible n-doping/dedoping (reduction/reoxidation) processes at negative potential ranges. All these

polymers exhibited oxidation (p-doping) due to the electron-rich DTP units and reduction (n-doping) because of electron deficient bithiazole derivatives.

The moderate onset oxidation and reduction potentials of polymers **P1-P5** occurred between 0.49-0.93 V and (-0.62)-(-0.84) V, respectively. The estimated HOMO and LUMO levels for polymers **P1-P5** are found to be (-4.81)-(-5.26) eV and (-3.54)-(-3.76) eV, respectively, which are in good agreements with the previous reported results. The electrochemical band gaps calculated from the differences between oxidation and reduction potentials were found to be in the range of 1.33-1.63 eV for polymers **P1-P5**. Polymers **P1-P1** possessed relatively lower HOMO energy levels compared with polymers **P3-P5** due to high onset oxidation potentials. By adding two alkyl chains at bithiazole rings of **P1**, the rigidity and oxidation potential of **P2** is reduced, so the HOMO energy level of **P1** is lower than **P2**.^{90b} The presence of electron rich species (thiophene or hexyl thiophene) maximizes the HOMO energy levels of polymers **P3-P5** compared with polymers **P1-P2**.⁹⁹ Hence, increasing electron donating moieties in the polymer backbones lowers the band gaps and also their oxidation potentials.¹⁰⁰ DTP-based polymers possessing similar LUMO energy levels suggest that electron deficient bithiazole derivatives have similar accepting capabilities. The electrochemical band gaps of all polymers are smaller than the corresponding optical band gaps which might be due to interface energy barriers present between the polymer films and the electrode surfaces.¹⁰¹ The LUMO energy levels of the donor polymers should be positioned above the LUMO energy levels of the acceptor PCBM by at least 0.3 eV, so the exciton binding energies of polymers could be overcome and result in efficient electron transfers from electron donors to acceptors. The high reduction potentials of polymers

P1-P5 represent high electron affinities to make these polymers suitable donors to inject and transport electrons to acceptor PCBM for polymer solar cell devices.

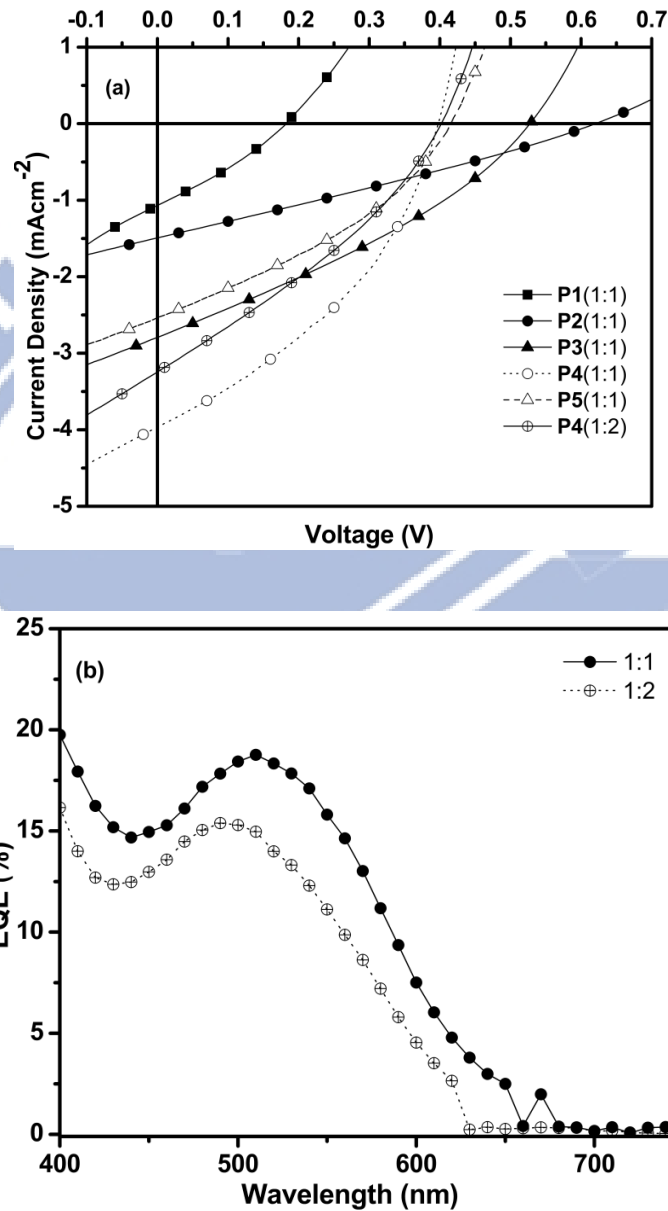


Figure 3.5 (a) J - V characteristics of ITO/PEDOT:PSS/ **P1-P5**:PCBM (1:1 or 1:2 by wt.)/Ca/Al under illumination of AM 1.5 at 100 mW/cm^2 . (b) EQE curves of PSC devices based on polymer blends **P4**:PCBM at various weight ratios (1:1 or 1:2).

3.3.4 Photovoltaic Cell Properties

The motivation to design and synthesize these DTP-based copolymers is to look for new LBG polymers for the application of PSCs. BHJ photovoltaic devices were fabricated with a configuration of ITO/PEDOT:PSS(30 nm)/(**P1-P5**):PCBM(~80 nm)(1:1 w/w)/Ca(30 nm)/Al(100 nm). Figure 3.5 presents the current-voltage (J - V) curves of the copolymers under the condition of AM 1.5 at 100 mW/cm²; and their photovoltaic properties, including the open circuit voltage (V_{oc}), short circuit current density (J_{sc}), fill factor (FF), and power conversion efficiency (PCE) values, of the PSC devices are summarized in Table 3.3.

The solar cells devices based on polymers **P1-P5** showed different V_{oc} values in the range of 0.18-0.62 V, which were related to the differences between the HOMO energy levels of the polymers and the LUMO energy levels of the acceptors. However a low V_{oc} (0.28 V) value obtained from DTP and bithiazole based polymer reported by Li. et al.⁶⁴ shows a low PCE value. The oxidation potential of polymer **P1** incorporated with the electron-withdrawing bithiazole unit showed a higher value, so polymer **P1** showed the deepest HOMO level among all polymers. It is clear that electron deficient bithiazole unit has a strong tendency to enhance the oxidation strength (high oxidation state) of the polymer. On the other hand, the addition of electron donating moieties to bithiazole derivatives caused the reduction of oxidation potentials in polymers **P1-P5** and increased their HOMO values. Unfortunately, polymer **P1** showed the lowest PCE value of 0.06% which is attributed to the poor solubility and film forming quality. Polymer **P2** achieved much higher V_{oc} value in DTP and bithiazole based polymers owing to its lower HOMO level. The V_{oc} values gradually decreased among polymers **P2-P4** due to the enhancement of HOMO values in the polymers.

Table 3.3 Electron and Hole Mobilities, Photovoltaic Properties, and Roughnesses (R_{rms}) of Polymers (P1-P5).

Polymer: PCBM (w/w ratio)	Electron mobility ($\mu_e, \text{cm}^2/\text{Vs}$)	Hole mobility ($\mu_h, \text{cm}^2/\text{Vs}$)	μ_e/μ_h	J_{sc} (mA/cm^2)	V_{oc} (V)	FF (%)	PCE (%)	R _{rms} (nm)
P1 (1:1)	2.97×10^{-6}	9.64×10^{-8}	30.8	1.1	0.18	0.34	0.06	0.39
P2 (1:1)	1.23×10^{-6}	3.22×10^{-8}	23.5	1.5	0.62	0.29	0.27	0.36
P3 (1:1)	9.63×10^{-7}	5.30×10^{-8}	18.2	2.8	0.53	0.32	0.47	0.25
P4 (1:1)	1.21×10^{-6}	2.17×10^{-7}	5.6	4.0	0.40	0.43	0.69	0.22
P5 (1:1)	8.29×10^{-6}	4.16×10^{-8}	19.9	2.5	0.41	0.35	0.36	0.25
P4 (1:2)	-	-	-	3.2	0.40	0.43	0.55	0.32

Charge transporting properties, including hole- and electron-mobilities, are the key parameters for both material design and device fabrication.¹⁰² The hole- and electron- mobilities were determined precisely by fitting the plot of the dark current versus the voltage (J - V) curves for single carrier devices to the SCLC model. The dark current is given by $J = 9\varepsilon_0\varepsilon_r\mu V^2/8L^3$, where $\varepsilon_0\varepsilon_r$ is the permittivity of the polymer, μ is the carrier mobility, and L is the device thickness. As shown in Table 3.3, the hole- and electron-mobilities of polymers **P1-P5** are found to be in the ranges of 10^{-8} - 10^{-7} cm^2/Vs and 10^{-7} - 10^{-6} cm^2/Vs , respectively. The electron mobilities are much higher (i.e., ca. 1 order of magnitude) than hole mobilities resulting in the imbalance transport of holes and electrons in the polymer active layer. The highest hole-mobility was found to be 2.17×10^{-7} cm^2/Vs for polymer **P4**, which is the key parameter for higher J_{sc} value among all polymers. Furthermore, the balanced ratio of 5.6 for both charge transports ($\mu_e/\mu_h = 5.6$) is found to be the lowest value in polymer **P4**, which is also another reason to explain the highest

PCE value of **P4** in all polymers (**P1-P5**).¹⁰³ All polymers showed poor mobilities may be attribute to molecular weight¹⁰⁴ and the low FF values and this could be due to the imbalance of the hole and electron transports in the polymer active layer.¹⁰⁵ By increasing the weight ratios of polymer **P4**:PCBM from 1:1 to 1:2, a lower J_{sc} and PCE values were observed. In order to further explain the lower efficiency (0.55%) of **P4**, the EQE spectra of PSC devices containing polymer **P4** with various ratios of PCBM (1:1 and 1:2 by weight) are presented in Figure 3.5. The maximum EQE values of PSC devices containing **P4** in the ratios of 1:1 and 1:2 are found to be 20% and 15% (at 500-520 nm), respectively.

Surface morphology of the active layer in PSC devices is also a key parameter for the device performance.⁹¹ The AFM topographic images of polymer blends **P1-P5**:PCBM (1:1 by weight) and **P4**:PCBM (1:2 by weight) are presented in Figure 3.6 and their root-mean-square values of roughness (R_{rms}) are demonstrated in Table 3.3. It is clear that the phase images of all surfaces possessed almost similar roughnesses, which were attributed to the domains of highly stacked polymer chains.⁶⁷ The most and least rough surfaces were found to be $R_{rms} = 0.39$ and 0.22 nm in polymer blends **P1** and **P4** (with PCBM = 1:1 by weight), respectively, where polymer blend **P1**:PCBM (1:1 w/w) possessed a larger scale phase separation and thus to induce the lowest PCE value (0.06%). This low PCE value of polymer blend **P1**:PCBM (1:1 w/w) might be originated from the reduced diffusional escape probability for mobile charge carriers and consequently to increase the charge recombination.¹⁰⁶ As a result, polymer blends **P1** and **P4** possessed the least and highest J_{sc} values, correspondingly. However, polymer **P4** blended with higher weight ratios of PCBM (**P4**:PCBM = 1:2 by weight) possessed a lower J_{sc} value, due to a larger phase separation indicated by a larger roughness ($R_{rms} = 0.32$ nm). However, Li et al.⁶⁴

reported one D-A copolymer containing DTP and bithiazole moieties as electron-donor and electron-acceptor

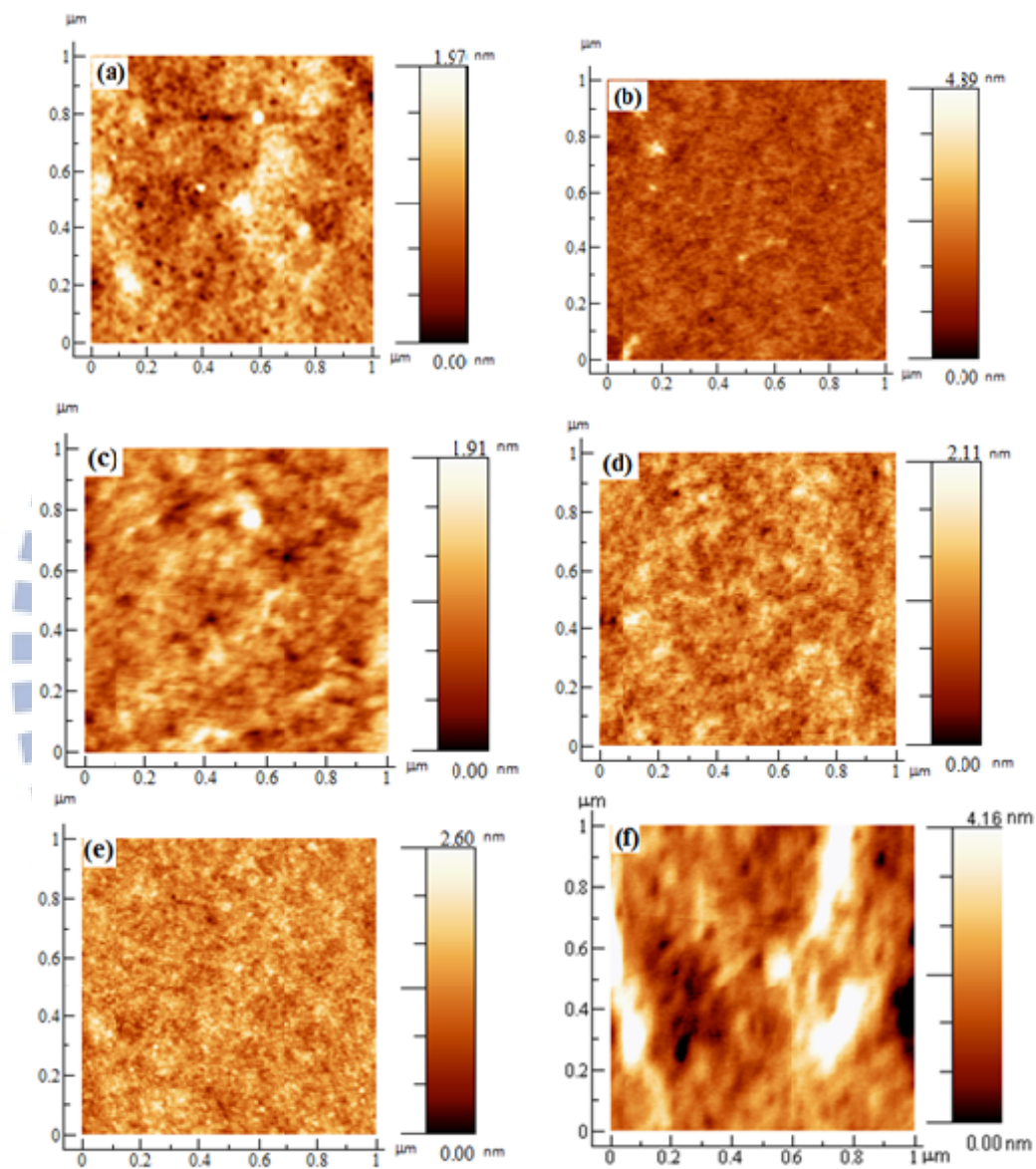


Figure 3. 6. AFM images of blended polymers (a) **P1**, (b) **P2**, (c) **P3**, (d) **P4**, and (e) **P5**, respectively, blended with PCBM in the ratio of **P1-P5**:PCBM=1:1 (w/w) and (f) in another ratio of **P4**:PCBM=1:2 (w/w) spin-coated from DCB with a size of $1 \times 1 \mu\text{m}^2$.

segments, respectively, possessed a maximum PCE value of 0.06%, with V_{oc} = 0.28 V, J_{sc} = 0.51 mA/cm², and FF = 0.34. The most efficient PSC device with the maximum PCE value of 0.69% was established by the polymer blend of **P4** and PCBM (with a weight ratio of 1:1) in this report.

3.4 Conclusion

Five DTP based low-band-gap photovoltaic polymers (**P1-P5**) containing an electron-donor dithienopyrrole (DTP) unit and various electron-acceptor bithiazole derivatives were designed and synthesized via palladium-catalyzed Suzuki coupling polymerization. Optical properties revealed that these new copolymers exhibit strong π - π stacking and enhanced absorption maximum band in solid films due to strong ICT in the polymer backbone. HOMO and LUMO energy levels of DTP-based polymers can be finely tuned to the ranges of -(5.26-4.99) and -(3.7-3.54) eV by copolymerization with electron-deficient bithiazole derivatives. Among the photovoltaic devices fabricated from the active layer of polymer blends **P1-P5**:PCBM in a weight ratio of 1:1, **P4** offered the best performance of PCE = 0.69%, with V_{oc} = 0.40 V, J_{sc} = 4.0 mA/cm², and FF = 43% under air mass 1.5 global illumination conditions. Therefore, tunable optical, electrochemical, and photovoltaic properties could be obtained by attaching lateral segments (such as hexyl chains) and conjugated linkers (such as thiophene and hexyl-thiophene units) to the bithiazole moieties in the polymer backbones.

Chapter 4

Synthesis and Applications of a Novel Supramolecular Polymer Network with Multiple H-bonded Melamine Pendants and Uracil Cross-linkers

4.1 Introduction

During the past decade, semi-conducting polymers containing supramolecular structures, including hydrogen-bonds (H-bonds), are one of the key targets for sensors and optoelectronic devices.⁶⁸ Owing to the self-assembly behavior, high specificity, and directionality of H-bonds, well-defined nanostructures and mesoscopic assemblies are generated by utilizing complementary hydrogen-bonding concept. Due to self-assembly between complementary molecular components, various kinds of non-covalent interactions, such as hydrogen-bonds (H-bonds),⁷³ ionic forces,⁷⁰ and metal-coordinations,⁷² can give rise to unique properties, which are not possessed by their individual components. Extensive researches devoted towards engineering of polymeric materials as well as devices in electron donor-acceptor (D-A) bulk heterojunction (BHJ) solar cells due to the substantial future prospects of low-cost photovoltaic technologies.⁵⁸⁻⁶⁰ Recently, power conversion efficiency (PCE) values have reached over 7% by an active layer of low-band-gap (LBG) electron-donating polymers and electron-accepting fullerene derivatives, such as [6,6]-phenyl-C₆₁-butyric acid methyl ester (PC₆₁BM) or [6,6]-phenyl-C₇₁-butyric acid methyl ester (PC₇₁BM).^{11a,58,59} A numerous advantages of LBG polymers, such as broad absorption spectra, fine controls of molecular energy levels, high mobilities, and favorable morphologies, were utilized for organic solar cells. A solution processable dithieno[3,2-b:2',3'-d]pyrroles (DTP) unit, as an efficient electron-donating unit, can be co-polymerized with various

electron-deficient moieties to form LBG polymers possessing PCE values up to ~3%.⁵²⁻⁵⁴ However, due to high values of highest occupied molecular orbital (HOMO) levels in DTP-based polymers, they showed relatively low V_{oc} values and thus to result in low PCE values for organic solar cells. This problem can be solved by either using different electron-deficient units⁵⁷ or introducing supramolecular architectures to manipulate their HOMO energy levels and thus to get higher V_{oc} values. The introduction of electron-deficient units, e.g., bithiazole, could be one of the best choices as it showed high oxidative stabilities by lowering the HOMO level.⁶²⁻⁶⁷ Lately, we have introduced organic dyes (as proton donors) to be H-bonded with side-chain pyridyl polymers (as proton acceptors) for the application of BHJ solar cell devices, where the PCE values were mainly contributed from the organic dyes rather than the side-chain polymers.⁷⁶

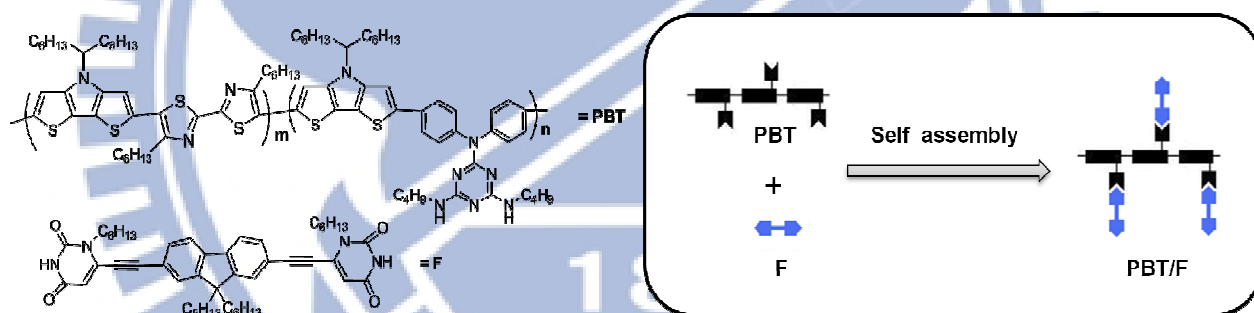


Figure 4.1 Schematic representation of **PBT/F** after complexation with **PBT** and **F**.

Herein, we synthesized a conjugated main-chain copolymer (**PBT**) by introducing bithiazole, DTP, and pendent melamine units, and the supramolecular polymer network could be formed by mixing with stoichiometric amounts of **PBT** and bi-functional π -conjugated cross-linker (**F**), i.e., **PBT:F** = 2:1 in molar ratio. As shown in Figure 4.1, two uracil motifs of **F** (as H-bonded cross-linking sites) attached to a fluorene core via triple bonds can be H-bonded with

the complementary melamine pendants of the main-chain copolymer (**PBT**). To the best of our knowledge, the supramolecular polymer network (**PBT/F**) is firstly developed by H-bonded complexation of LBG main-chain copolymer **PBT** containing melamine pendants and π -conjugated cross-linker **F**. The unique features of this multiple H-bonding approach to optimizing light harvesting and manipulating HOMO level of polymer **PBT** by incorporating H-bonded cross-linker **F** through supramolecular architecture are investigated.

4.2 Experimental Section

4.2.1 Materials

All chemicals and solvents were reagent grades and purchased from Aldrich, ACROS, Fluka, TCI, TEDIA, and Lancaster Chemical Co. Tetrahydrofuran (THF) and toluene, were distilled over sodium/benzophenone. Other reagents were used as received without further purification. Monomers **M2**, **M3**, and 2,7-diethynyl-9,9-dihexyl-9*H*-fluorene were synthesized by our previously reported synthetic procedures.

4.2.2 Measurements and Characterization

^1H and ^{13}C NMR spectra were recorded on a Varian Unity 300 MHz spectrometer using CDCl_3 solvent and chemical shifts were reported as δ values (ppm) relative to an internal tetramethylsilane (TMS) standard. Elemental analyses were performed on a HERAEUS CHN-OS RAPID elemental analyzer. Thermogravimetric analyses were conducted with a TA Instruments Q500 at a heating rate of $10^\circ\text{C}/\text{min}$ under nitrogen. Gel permeation chromatography (GPC) analyses were conducted on a Waters 1515 separation module using polystyrene as a standard and THF as an eluant. Fourier transform infrared (FTIR) spectra of samples (dispersed

in KBr disks) were recorded on a Perkin-Elmer Spectrum 100 Series. UV-visible absorption spectra were recorded in dilute dichlorobenzene solutions on a HP G1103A spectrophotometer. Thin films of UV-vis measurements were spin-coated on glass substrates from dichlorobenzene solutions with a concentration of 5 mg/ml. Cyclic voltammetry (CV) measurements were performed by a scanning rate of 100 mV/s at room temperature using a BAS 100 electrochemical analyzer with a standard three-electrode electrochemical cell in a 0.1 M tetrabutylammonium hexafluorophosphate (TBAPF₆) solution in acetonitrile. During the CV measurements, the solutions were purged with nitrogen for 30 s. In each case, a carbon rod coated with a thin layer of polymers as the working electrode, a platinum wire as the counter electrode, and a silver wire as the quasi-reference electrode were used, and Ag/AgCl (3M KCl) electrode was served as a reference electrode for all potentials quoted herein. The redox couple of ferrocene/ferrocenium ion (Fc/Fc⁺) was used as an external standard. The corresponding highest occupied molecular orbital (HOMO) and lowest unoccupied molecular orbital (LUMO) levels were calculated using $E_{\text{onset}}^{\text{ox}}$ and $E_{\text{onset}}^{\text{red}}$ for experiments in solid films of polymers, which were performed by drop-casting films with the similar thickness from THF solutions (ca. 5 mg/ml). The LUMO level of PCBM employed was in accordance with the literature datum. The onset potentials were determined from the intersections of two tangents drawn at the rising currents and background currents of the CV measurements. Topographic images of the copolymer: PC₆₁BM or PC₇₁BM films (surface area: 2 × 2 μm²) were obtained through atomic force microscopy (AFM) in the tapping mode under ambient conditions using (AFM, Digital instrument NS 3a controller with D3100 stage). The small-angle X-ray diffraction (SAXD) measurements were performed at the beamline BL17A of the National Synchrotron Radiation Research Center (NSRRC), Taiwan.

4.2.3 Fabrication and Testing of Polymer Solar Cell Devices

The polymer photovoltaic (PV) cells in this study contained an active layer of [6,6]-phenyl-C₆₁-butyric acid methyl ester (PC₆₁BM) or [6,6]-phenyl-C₇₁-butyric acid methyl ester (PC₇₁BM) blended with polymer **PBT** and H-bonded polymer network **PBT/F**, respectively, in solid film, which was sandwiched between a transparent indium tin oxide (ITO) anode and a metal cathode (Ca). Prior to the device fabrication, ITO-coated glass substrates (1.5×1.5 cm²) were ultrasonically cleaned in detergent, deionized water, acetone, and isopropyl alcohol. After routine solvent cleaning, the substrates were treated with UV ozone for 20 min. Then, a modified ITO surface was obtained by spin-coating a layer of poly(ethylene dioxythiophene):polystyrenesulfonate (PEDOT:PSS) (~30 nm). After baking at 130°C for 1 hr, the substrates were transferred to a nitrogen-filled glove box. Subsequently, on the top of PEDOT:PSS layer, the active layer was prepared by spin-coating from blended solutions of polymers: PC₆₁BM or PC₇₁BM (1:1 w/w) with a spin rate ca. 1000 rpm, and the thickness of the active layer was typically ca. 90 nm. Initially, the blended solutions were prepared by dissolving both polymers and PC₆₁BM or PC₇₁BM in 1,2 dichlorobenzene (DCB)(10 mg/1 ml), followed by continuous stirring for 12 h at 50°C. In the slow-growth approach, blended polymers in solid films were kept in the liquid phase after spin-coating by using the solvent DCB with a high boiling point. Finally, a calcium layer (30 nm) and a subsequent aluminum layer (100 nm) were thermally evaporated through a shadow mask at a pressure below 6×10⁻⁶ torr to have the active device area of 0.12 cm². All polymer solar cell (PSC) devices were annealed at 70°C for 30 min. before measurements. The solar cell testing was done at room temperature inside a glove box under simulated AM 1.5G irradiation (100 mW/cm²) using a Xenon lamp based solar simulator

(Thermal Oriel 1000W). The light intensity was calibrated by a mono-silicon photodiode with KG-5 color filter (Hamamatsu). The external quantum efficiency (EQE) action spectra were obtained at short-circuit conditions. The light source was a 450 W Xe lamp (Oriel Instrument, model 6266) equipped with a water-based IR filter (Oriel Instrument, model 6123NS). The light output from the monochromator (Oriel Instrument, model 74100) was focused on the photovoltaic cell under test.

4.2.4 Fabrication of Hole Only Devices

The hole devices in this study containing polymers **PBT** or **PBT/F:PC₆₁BM** (1:1) blend film sandwiched between transparent ITO anode and cathode. The devices were prepared following the same procedure as fabrication of bulk-heterojunction (BHJ) devices, except that in the hole-only devices, Ca was replaced with MoO₃ ($\Phi = 5.3$ eV). The MoO₃ was thermally evaporated to a thickness of 20 nm and then capped with 50 nm of Al on the top of active layer. The devices, annealing of the active layer was performed at 130 °C for 20 min. The hole-mobilities were determined precisely by fitting the plot of the dark current versus the voltage (J - V) curves for single carrier devices to the SCLC model. The dark current is given by $J = 9\varepsilon_0\varepsilon_r\mu V^2/8L^3$, where $\varepsilon_0\varepsilon_r$ is the permittivity of the polymer, μ is the carrier mobility, and L is the device thickness.

4.2.5 Synthesis of Monomers and Polymers

4,6-Dichloro-*N,N*-diphenyl-1,3,5-triazin-2-amine (1)

Under N₂, a solution of diphenylamine (9.16 g, 54.22mmol) in THF (50 mL) was added dropwise to a mixture of diisopropylethylamine (9.5 ml, 54.22 mmol) and 2,4,6-trichloro-1,3,5-triazine (10.0 g, 52.22 mmol) in THF(150 mL) at 20°C. After stirring for 3 hr, the solvent was removed by rotatory evaporation and the residue was purified by column chromatography over silica gel (hexane: ethyl acetate = 4:1) to give a white color solid. (12.9 g, yield 75%). ¹H NMR (300 MHz, CDCl₃, δ):7.45-7.41 (m, 4H), 7.35-7.33 (m, 2H), 7.30-7.27 (m, 4H).

*N*²,*N*⁴-Dibutyl-*N*⁶,*N*⁶-diphenyl-1,3,5-triazine-2,4,6-triamine (2)

Sodium bicarbonate (8.0 g, 84.01 mmol) was added to a solution of compound 1 (10.0 g, 31.52 mmol) in 1,4-dioxane (100 ml). After that, butyl amine (9.4 ml, 94.58 mmol) was added and the resulting mixture was refluxed for overnight. The reaction mixtures was cooled to room temperature and pour into cold water and extracted three times with ethyl acetate. The combined organic fractions were washed with brine, dried over MgSO₄, and concentrated by rotary evaporation and purified by column chromatography using silica, (hexane: ethyl acetate = 7:3) to give a white solid. (10.70 g, yield 87%). ¹H NMR (300 MHz, CDCl₃, δ):7.45-7.41 (m, 4H), 7.35-7.33 (m, 2H), 7.30-7.27 (m, 4H),4.84 (br, 2H), 3.34-3.11(br, 4H), 1.43-1.25 (m, 8H), 0.88 (t, *J*= 6.2Hz, 6H).

***N*²,*N*²-Bis(4-bromophenyl)-*N*⁴,*N*⁶-dibutyl-1,3,5-triazine-2,4,6-triamine (M1)**

NBS (6.9 g, 38.40 mmol) was added portion-wise to a solution of compound **2** (5.0 g, 12.80 mmol) in DMF (50 ml) at 0°C. The reaction mixture was stirred for 6 hr at the same temperature and water was added to quench the reaction. The organic layer was extracted with three times by ethyl acetate followed by brine and water washing and dried by anhydrous MgSO₄. The solvent was removed by rotary evaporator and the product was further purified by column chromatography on silica (hexane: ethyl acetate = 4:1) to yield a white solid. (5.7 g, 80%). ¹H NMR (300 MHz, CDCl₃, δ): 7.47-7.38 (m, 4H), 7.43-7.28 (m, 4H), 4.84 (br, 2H), 3.34-3.31 (br, 4H), 1.43-1.25 (m, 8H), 0.88 (t, *J* = 6.2 Hz, 6H). ¹³C NMR (75 MHz, CDCl₃, δ): 166.48, 166.11, 143.25, 131.81, 129.77, 118.79, 40.60, 32.09, 20.24, 14.01; EIMS [M⁺] calcd. *m/z* = 548.32, found 548.0. Anal. Calcd. for C₂₃H₂₈Br₂N₆: C, 50.38; H, 5.15; Br, 29.15; N, 15.33; found: C, 50.78; H, 5.48; N, 15.04.

1-Hexyluracil (3)

K₂CO₃ (14.80 g, 107.05 mmol) was added to a suspension of uracil (10.0 g, 89.21 mmol) in DMSO (150 mL), and stirred for 15-20 min at 45°C. 1-Bromo-hexane (3.5 mL, 25 mmol) was added and the reaction mixture was stirred for 48 hr. The reaction was cooled to room temperature and poured into cold water. The product was extracted three times with DCM, and washed with dilute HCl, water, brine, and dried over MgSO₄. The organic layer was concentrated and poured into cold hexane with vigorous stirring. The resulting precipitate was filtered and washed with cold hexane to afford compound **3** (12.40 g, 70.9%) as a white solid. ¹H NMR (300 MHz, CDCl₃, δ): 9.12 (br, 1H), 7.14 (d, *J* = 9.0 Hz, 1H), 5.70 (d, *J* = 6.0 Hz, 1H), 3.71 (t, *J* = 7.5 Hz, 2H), 1.74-1.65 (m, 2H), 1.34-1.27 (m, 6H), 0.88 (t, *J* = 6.6 Hz, 3H).

1-Hexyl-6-iodouracil (4)

At -78°C, LDA (20.4 mL of a 2.5 M solution, 51.0 mmol) was added drop-wise to a solution of 1-hexyluracil (2.0 g, 10.2 mmol) in THF (55 mL), and the resulting solution was stirred under N₂ for 2 hr. I₂ (12.9 g, 51.0 mmol) was added and the reaction mixture was stirred for another 2 hr at the same temperature. Acetic acid (2.0 mL) was added to react with stirring at room temperature for overnight. The organic phase was extracted with ethyl acetate washed with saturated NaHCO₃ (3×30.0 mL) and Na₂SO₃ (3×30 mL) solutions. Finally, the product was washed with brine (30 mL), and dried over Mg₂SO₄. The solvent was removed by rotary evaporator and the crude product was purified by column chromatography silica (hexane: ethyl acetate = 5:5) to afford compound **4** (2.2 g, 67%). ¹H NMR (300 MHz, CDCl₃, δ): 9.48 (br, 1H), 6.41 (s, 1H), 4.0 (t, *J* = 8.1 Hz, 2H), 1.74-1.65 (m, 2H), 1.34-1.27 (m, 6H), 0.88 (t, *J* = 6.9 Hz, 3H).

6,6'-(9,9-Dihexyl-9H-fluorene-2,7-diyl)bis(ethyne-2,1-diyl)bis(1-hexylpyrimidine-2,4(1H,3H)-dione) (F)

To a mixture of compound **4** (1.26 g, 3.9 mmol) in THF (15 mL), 2,7-diethynyl-9,9-dihexyl-9H-fluorene³ (0.5 g, 1.3 mmol), triphenylphosphine (10 mg, 0.05), CuI (10 mg, 0.05 mmol), and NEt₃ (15 mL) were added. Then, [Pd(PPh₂)Cl₂] (4 mg, 0.034 mmol) was added under N₂ and the reaction mixture was heated to 50 °C for 36 hr. The crude product was extracted with DCM followed by brine wash and dried over MgSO₄. The resulting solution was concentrated by rotary evaporator, and purified by column chromatography using silica, (hexane: ethyl acetate 7:3) to give a yellow solid. (0.58 g, yield 58%). ¹H NMR (300 MHz, CDCl₃, δ): 9.60 (br, 2H), 7.77 (d, *J* = 8.1 Hz, 2H), 7.53 (m, 4H), 6.04 (m, 2H), 4.01 (t, *J* = 7.8 Hz, 4H), 2.0 (t, *J* = 8.1 Hz,

4H), 1.82 (t, $J = 7.2$ Hz, 4H), 1.44-1.34 (m, 12H), 1.36-1.08 (m, 12H), 1.15-1.08 (m, 12H), 0.88 (t, $J = 6.9$ Hz, 6H), 0.77 (t, $J = 7.2$, 6H), 0.59 (m, 4H). ^{13}C NMR (75 MHz, CDCl_3 , δ): 162.96, 151.95, 151.08, 142.41, 138.89, 131.72, 126.58, 121.05, 119.76, 106.89, 101.28, 81.30, 55.84, 46.94, 40.31, 31.67, 29.77, 29.02, 26.65, 23.97, 22.77, 22.75, 14.19; EIMS [M^+] calcd. $m/z = 771.04$, found 772.0. Anal. Calcd. For $\text{C}_{49}\text{H}_{62}\text{N}_4\text{O}_4$: C, 76.33; H, 8.10; N, 7.27; O, 8.30; found: C, 76.00; H, 7.97; N, 7.17.

Synthesis of PBT via Stille Coupling Polymerization

Into 25 mL of two-neck flask, 1 equiv of dibromo monomers (**M1** and **M3**) and 2 equiv of 2,6-bis(tributylstannyl)-4-(tridecan-7-yl)-4*H*-dithieno[3,2-*b*:2',3'-*d*]pyrrole (**M2**) were added in anhydrous toluene and deoxygenated with nitrogen for 30 min. The Pd(0) complex, i.e., tetrakis(triphenylphosphine)palladium (1 mol %), was transferred into the mixture in a dry environment. The reaction mixture was stirred at 110 °C for 48 hr, and then an excess amount of 2-bromothiophene was added to end-cap the trimethylstannyl groups for 4 hr. After cooling to room temperature, the solution was added dropwise into MeOH (200 mL). The crude polymer was collected, dissolved in hot CHCl_3 , filtered through a 0.5- μm poly(tetrafluoroethylene) (PTFE) filter, and reprecipitated in MeOH. The solid was washed with acetone, hexane, and CHCl_3 in a Soxhlet apparatus. The CHCl_3 solution was concentrated and then added dropwise into MeOH. Finally, the polymer was collected and dried under vacuum to give **PBT**. Yield: 59 %. ^1H NMR (300 MHz, CDCl_3 , δ): 7.53 (br), 7.45-7.04 (br), 4.90-4.65 (br), 4.15 (br), 3.36-2.97 (br), 2.10-1.60 (m), 1.55-0.90 (m), 0.87-0.65 (m). Anal. Calcd. For $\text{C}_{83}\text{H}_{114}\text{N}_{10}\text{S}_6$: C, 69.02; H, 7.96; N, 9.70; S, 13.32; Found: C, 68.31; H, 6.94; N, 10.41.

4.2.6 Preparation of Supramolecular Polymer Network (PBT/F)

Supramolecular polymer (**PBT/F**) was prepared by dissolving 2 molar of polymer **PBT** and 1 molar bi-functional H-bonded π -conjugated cross-linker (**F**) in a minimum amount of CHCl_3 and then the solvent was evaporated under ambient temperature.

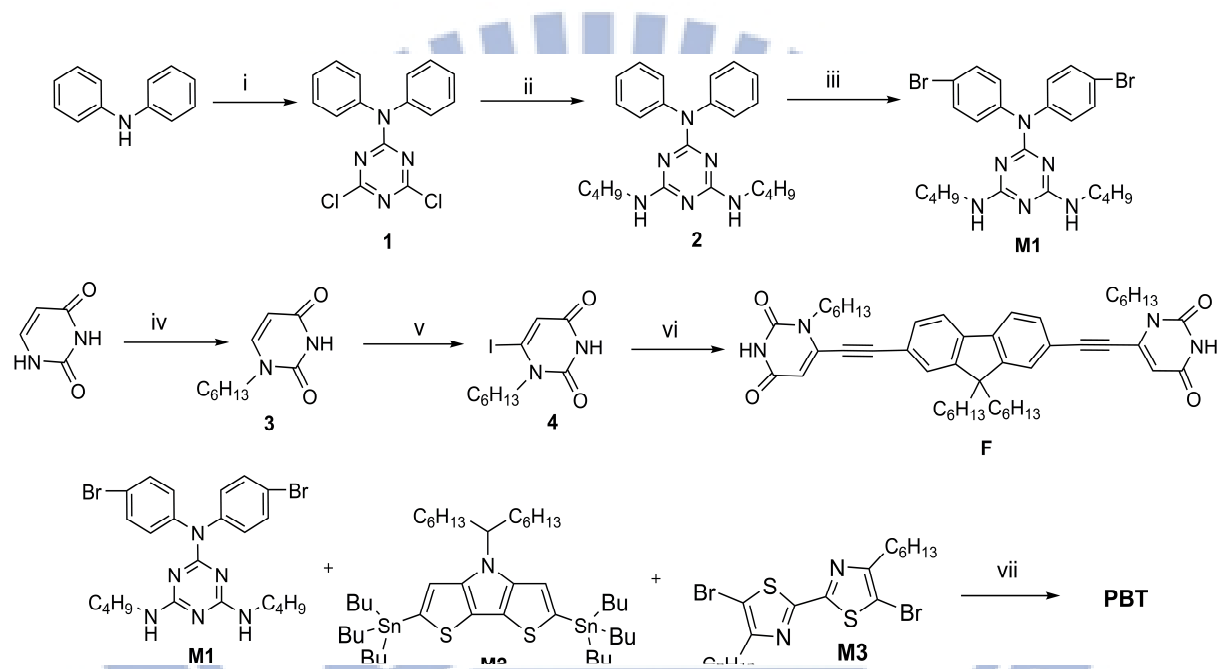


Figure 4.2 Synthetic Routes of **M1**, **F**, and Polymer **PBT**^a

^aReagents and conditions: (i) diisopropylethylamine, 2,4,6-trichloro-[1,3,5]triazine, THF, 20°C, 3 hr; (ii) sodium bicarbonate, bromo butane, 1,4-dioxane, reflux, overnight; (iii) NBS, 0-5°C, THF; (iv) K_2CO_3 , DMSO, 45°C, overnight; (v) -78°C, LDA, THF, 5 hr, I_2 ; $\text{Pd}(\text{PPh}_3)_4$, toluene, 110°C, 48 h; (vi) 2,7-diethynyl-9,9-dihexyl-9H-fluorene, Ph_3P , CuI, THF, Et_3N , $\text{Pd}(\text{PPh}_2)\text{Cl}_2$, 50°C, overnight; (vii) Toluene, $\text{Pd}(\text{PPh}_3)_4$, 110°C, 48 hr.

4.3 Results and Discussion

4.3.1 Syntheses and Characterization

The synthetic details of monomers **M1**, H-bonded π -conjugated cross-linker **F**, and polymer **PBT** are depicted in Figure 4.2. **PBT** was synthesized by Stille copolymerization of three monomers **M1**, **M2**, and **M3** (1:2:1 in mol ratio), and **F** was synthesized by sonogashira coupling of 2,7-diethynyl-9,9-dihexyl-9*H*-fluorene^{72a} and 1-hexyl-6-iodopyrimidine-2,4(1*H*,3*H*)-dione. According to the GPC result, **PBT** showed a number-average molecular weight (M_n) of 20.1 kg/mol with a polydisperse index (PDI) value of 1.43. The thermal stabilities of polymer **PBT** and H-bonded polymer network **PBT/F** were investigated by thermogravimetric analyses (TGA), and demonstrated in Figure 4.3.

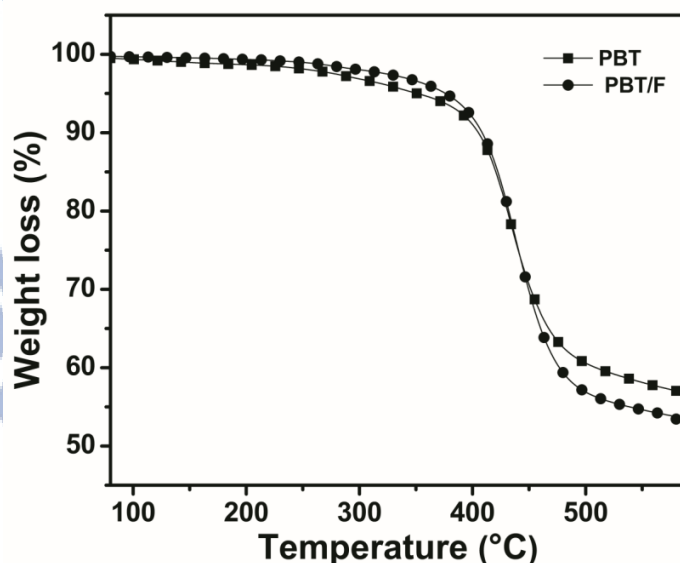


Figure 4.3 TGA thermogram of **PBT** and **PBT/F**, recorded at a heating rate of $10\text{ }^{\circ}\text{C min}^{-1}$ under N_2 atmosphere.

Both polymer **PBT** and H-bonded polymer network **PBT/F** showed good thermal stabilities and exhibited T_d values (temperatures at 5% weight loss by a heating rate of 10°C/min under nitrogen) at 361 and 381°C, which indicates that due to H-bonded effects the T_d value of H-bonded polymer network **PBT/F** is higher than that of polymer **PBT**. However, the crosslinker **F** in H-bonded polymer network **PBT/F** will be decomposed more completely at the final stage, so the final weight loss of H-bonded polymer network **PBT/F** (with a lower weight ratio of **PBT** to be sustained at the high temperature end) is larger than that of polymer **PBT**.

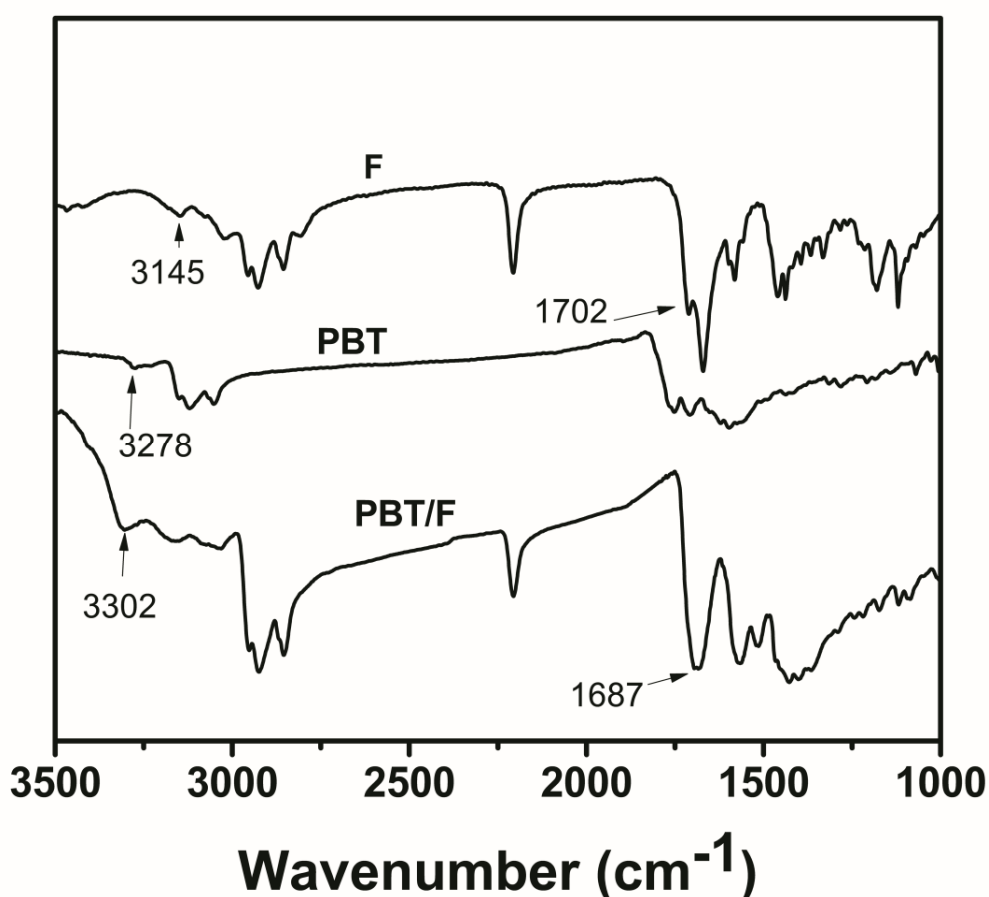


Figure 4.4 FT-IR spectra of π -conjugated cross-linker **F**, polymer **PBT**, and supramolecular polymer network **PBT/F** at room temperature.

As shown in Figure 4.4, **F** demonstrates free C=O and N–H stretching bands located at 1702 and 3145 cm^{-1} and **PBT** demonstrates a N–H stretching band located at 3278 cm^{-1} in their IR spectra.^{107,108} After the formation of triple hydrogen bonds in H-bonded polymer network **PBT/F**, the C=O stretching band shifted to a lower wave number 1687 cm^{-1} due to uracilic (C=O) vibrations with major contributions from N–H in plane bending modes¹⁰⁷ and NH–N stretching to a higher wave number at 3302 cm^{-1} .¹⁰⁸ To gain insight into the structural orders of both polymers, powder X-ray diffraction (XRD) patterns of **PBT** and **PBT/F** were performed and demonstrated in Figure 4.5. It can be seen that **PBT/F** showed two more obvious XRD peaks than **PBT**, which indicates the higher crystallinity in H-bonded polymer network **PBT/F**. In contrast to **PBT**, the higher crystallinities in both small- and wide-angle regions of **PBT/F** are assumed to be increased by the presence of multiple hydrogen-bonds, which enhances chain-reorganization and self-assembled behavior and also induce a higher power conversion efficiency of H-bonded polymer network **PBT/F**.^{68a}

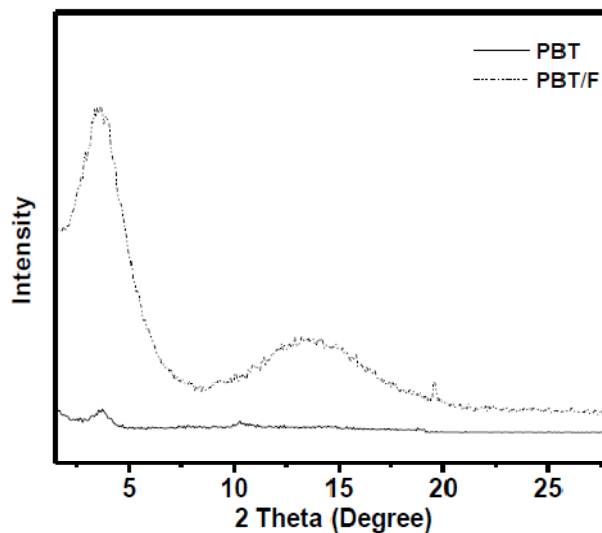


Figure 4.5 X-ray diffraction patterns of **PBT** and **PBT/F**.

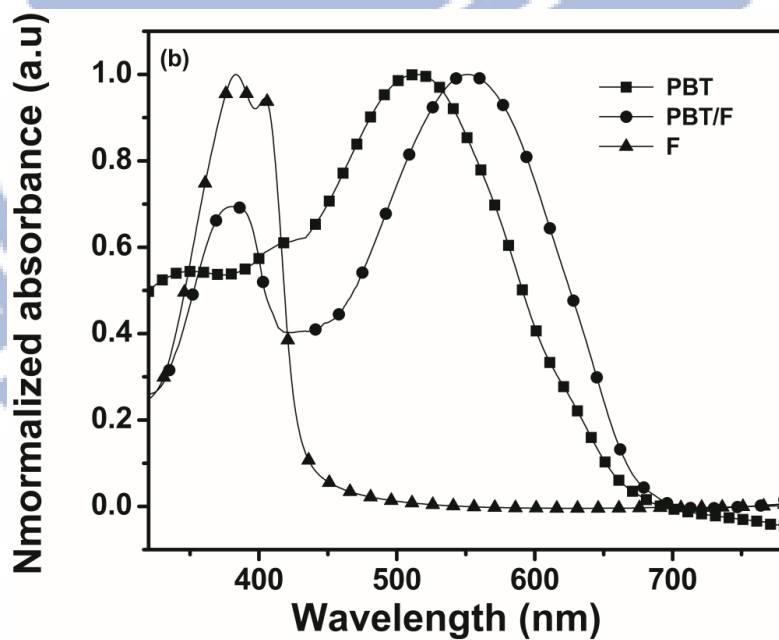
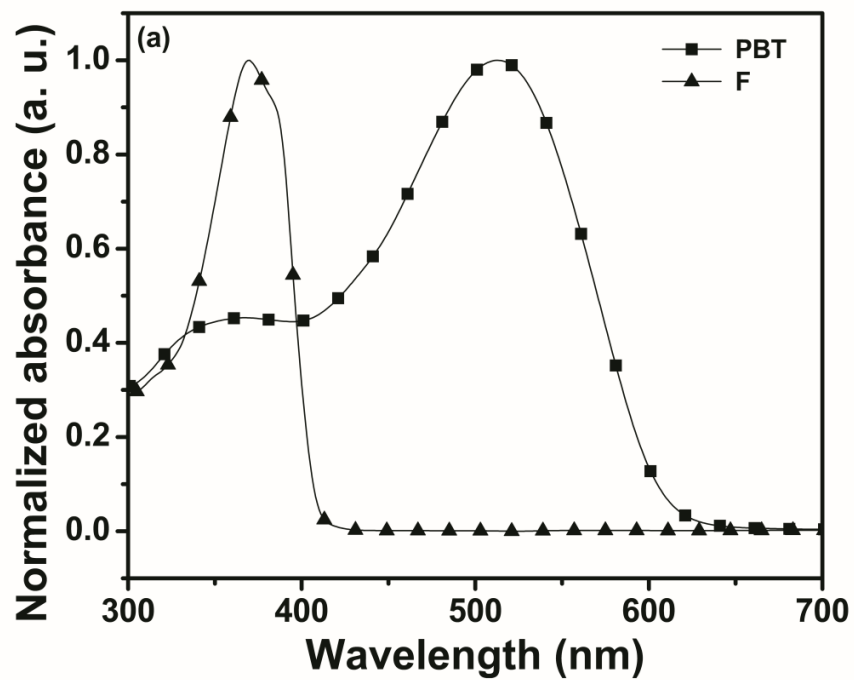


Figure 4.6 Normalized UV-Vis absorption spectra of (a) **PBT** and H-bonded π -conjugated cross-linker **F** in dilute dichlorobenzene solutions; and (b) **PBT**, **PBT/F**, and **F** in solid films.

Table 4.1 Optical and Electrochemical Properties of Polymer PBT, Cross-Linker F, and H-Bonded Polymer Network PBT/F.

Polymer	Solution ^a	Solid film ^b	$E_{\text{onset}}^{\text{ox}}$ (V)/	$E_{\text{onset}}^{\text{red}}$ (V)/	$E_g^{\text{opt}}/E_g^{\text{ec}}$ (eV)
	λ_{abs} (nm)	λ_{abs} (nm)	HOMO ^c (eV)	LUMO ^c (eV)	
PBT	505	520	0.77/-5.12	-0.84/-3.51	1.80/1.61
F	369	409	1.49/-5.84	-1.11/-3.24	2.66/2.60
PBT/F	-	385, 548	0.89/-5.24	-0.91/-3.44	1.77/1.80

^aIn dilute dichlorobenzene solution and ^bSpin coated from dilute dichlorobenzene solution on glass surface. ^cHOMO/LUMO = $[-(E_{\text{onset}} - E_{\text{onset}}(\text{FC}/\text{FC}^+ \text{ vs. Ag/Ag}^+)) - 4.8]$ eV where 4.8 eV is the energy level of ferrocene below the vacuum level and $E_{\text{onset}}(\text{FC}/\text{FC}^+ \text{ vs. Ag/Ag}^+) = 0.45\text{eV}$.

4.3.2 Optical Properties

Figure 4.6 displays the absorption spectra of **PBT**, **PBT/F**, and **F**, measured from dichlorobenzene solutions (**PBT** and **F**) and solid films (**PBT**, **PBT/F**, and **F**), and their photophysical data are summarized in Table 4.1. The absorption maximum of **PBT** solution (in dichlorobenzene) was found to be 505 nm which can be attributed to intramolecular charge transfer between the electron donor (DTP) and acceptor (bithiazole) units.⁵²⁻⁵⁴ Relative to the solution absorption, the absorption maximum is located at 520 nm in the solid film which is slightly red-shifted, indicating intermolecular interactions and aggregations occurred in solid films.^{64,109} The absorption maximum of π -conjugated cross-linker **F** was found to be 369 nm (in the dichlorobenzene solution) and found to be 409 nm (in the solid film), respectively, where the red-shift of 40 nm in the solid film is due to the inter-chain association and π - π stacking of π -conjugated cross-linker **F**.¹¹⁰ Compared with **PBT** (in solid films), a new peak appeared at 385 nm in the UV region of H-bonded polymer network **PBT/F** by the introduction of **F**, and a red-

shifted (ca. 28 nm, from 520 to 548 nm) absorption peak occurred due to the multiple H-bonded effect.^{108b} The optical band-gaps (E_g^{opt}) of **PBT** and **PBT/F** were found from the cut-offs of the absorption wavelengths to be 1.80 and 1.77 eV, respectively. This result implies that it is an efficient way to tune optical properties of the side-chain polymer through supramolecular interactions to absorb maximum photons from visible regions for enhanced photovoltaic applications. Moreover, the homogeneous incorporation of the organic dye (a small molecule) to the polymer with a complimentary absorption band through multi-H-bonds so as to broaden the total light absorption (as shown in Figure 4.6) and thus to induce enhanced photovoltaic properties, which can be further proven by PCE values and EQE measurements in later discussion.

4.3.3 Electrochemical Properties

Cyclic voltammetry (CV) measurements were employed to estimate the highest occupied molecular orbital (HOMO) and lowest unoccupied molecular orbital (LUMO) levels of polymers **PBT** and **PBT/F** and their CV curves are provided in Figure 4.7. The CV measurements were carried out in a 0.1M tetrabutylammonium hexafluorophosphate (TBAPF6) solution (in acetonitrile) at a scan rate of 100 mV/s under nitrogen. A carbon electrode, which was coated with the polymer film by dip coating, was used as a working electrode and Ag/AgCl was served as a reference electrode, and it was calibrated by ferrocene ($E_{ferrocene}^{1/2} = 0.45$ mV versus Ag/AgCl). The HOMO and LUMO energy levels were estimated by the oxidation and reduction potentials from the reference energy level of ferrocene (4.8 eV below the vacuum level) according to the following equation¹¹¹: $E_{HOMO/ELUMO} = [-(E_{onset} - E_{onset}^{(FC/FC^+ \text{ vs. Ag/Ag}^+)}) - 4.8]$ eV and band gap = $E_{onset}^{ox} - E_{onset}^{red}$ (where 4.8 eV is the energy level of ferrocene below the

vacuum level and $E_{\text{onset}}(\text{FC}/\text{FC}^+ \text{ vs. Ag}/\text{Ag}^+) = 0.45 \text{ eV}$). The HOMO and LUMO levels as well as the electrochemical band-gap (E_g^{ec}) were determined from oxidation and reduction potentials ($E_{\text{onset}}^{\text{ox}}$ and $E_{\text{onset}}^{\text{red}}$) of both polymers and their values are summarized in Table 4.1. It can be seen that polymer **PBT**, cross-linker **F**, and H-bonded polymer network **PBT/F** possess both quasi-irreversible p-doping/dedoping (oxidation/reduction) processes at positive potentials and n-doping/dedoping (reduction/reoxidation) processes at negative potentials.

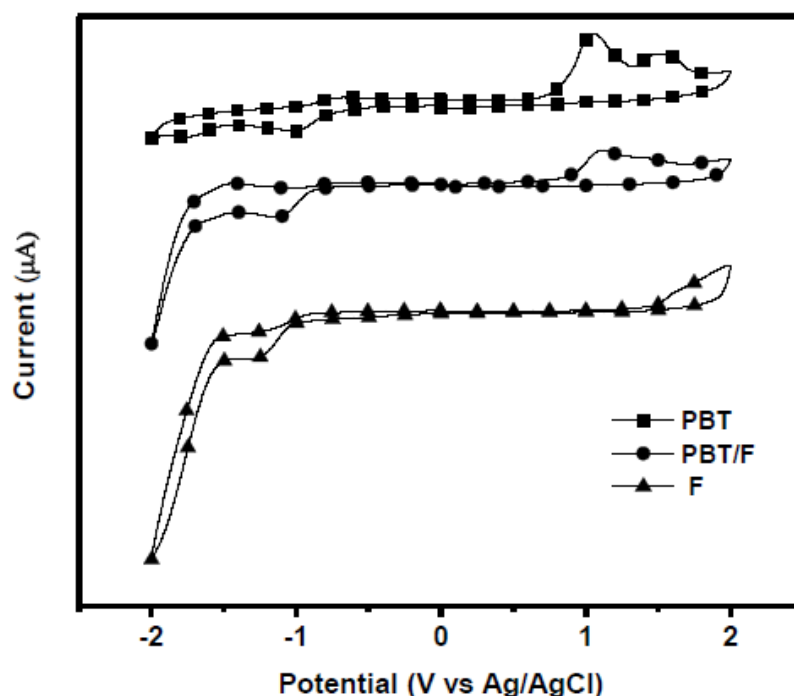


Figure 4.7 Cyclic voltammograms of polymer **PBT** and supramolecular polymer network **PBT/F** and cross-linker **F**.

The onset potentials of (oxidation; reduction) of polymer **PBT**, cross-linker **F**, and those of H-bonded polymer network **PBT/F**, were found to be (0.77; -0.84) V, and (1.49; -1.11), and (0.89; -0.91) V, respectively. The estimated values of (HOMO; LUMO) levels for polymer **PBT**,

cross-linker **F**, and those of H-bonded polymer network **PBT/F** were found to be (-5.12; -3.51) eV, (-5.84) and (-3.84), and (-5.24; -3.44) eV, respectively. Compared with polymer **PBT**, the lower HOMO level of H-bonded polymer network **PBT/F** (induced by the H-bonded structure) indicates that it could be more stable against oxidation due to the incorporation of highly oxidative stable fluorene in cross-linker **F**.¹¹² Compared with polymer **PBT**, the lower HOMO energy level of H-bonded polymer network **PBT/F** (as a donor material) is desirable for the high open circuit voltage of PSC.¹¹³ The LUMO energy levels of the electron donors (**PBT** and **PBT/F**) have to be positioned above the LUMO energy levels of the acceptors (e.g., PCBM) at least 0.3 eV, so the exciton binding energy of polymer could be overcome and result in efficient electron transfer from donors to acceptors.

Table 4.2 Photovoltaic Properties^a and Film Roughnesses^b (R_{rms} Measured by AFM) of Bulk-Heterojunction PSC Devices Containing PBT and PBT/F with PC₆₁BM and PC₇₁BM in a Blending Wt. Ratio of 1:1.

Active layer (1:1 by wt.)	V_{oc} (V)	J_{sc} (mA/cm ²)	FF (%)	PCE (%)	R_{rms} (nm)
PBT:PC₆₁BM	0.50	2.07	33.0	0.34	1.46
PBT/F:PC₆₁BM	0.55	3.60	35.4	0.70	0.52
PBT:PC₇₁BM	0.50	2.90	39.3	0.57	0.50
PBT/F:PC₇₁BM	0.55	4.97	31.5	0.86	0.42

4.3.4 Photovoltaic Properties

PBT and **PBT/F** were utilized as electron donors to investigate the photovoltaic properties of BHJ photovoltaic devices with a device structure of ITO/PEDOT-PSS/polymers:acceptors/Ca/Al, where PC₆₁BM (or PC₇₁BM) was an electron acceptors. Table 4.2 and Figure 4.8 demonstrate current density-voltage (*J-V*) curves of **PBT** and **PBT/F** blended with PC₆₁BM (or PC₇₁BM) with a wt. ratio of 1:1. (The photovoltaic devices with thicknesses ca. 90 nm were annealed at 70°C and tested under 100mWcm⁻² AM 1.5G solar illumination condition.) It can be clearly seen that H-bonded polymer network **PBT/F** possessed higher PCE values than polymer **PBT**. However, Li et al. have reported an analogous D-A copolymer containing DTP and bithiazole moieties only possessed $V_{oc} = 0.28$ V, $J_{sc} = 0.51$ mA/cm², and a maximum PCE value of 0.06%.⁶⁴ In addition, recently we reported a similar polymer with a PCE of 0.27%.¹¹⁴ The most efficient solar cell device exhibited a PCE of 0.86% with V_{oc} , J_{sc} , and FF (fill factor) values 0.55 V, 4.97 mA/cm², and 31.5%, respectively. Compared with **PBT**, the higher PCE value of 0.86% in H-bonded polymer network **PBT/F** was improved by larger V_{oc} and J_{sc} values were due to a lower value of HOMO energy level (to induce a larger V_{oc} value), a higher light harvesting amount (by introducing **F** to induce a larger J_{sc} value) in visible regions, and an improved crystallinity (by introducing **F** to have a higher crystallinity). For effective charge carrier transport, hole-mobility is a key parameter and also equally affects FF values of the solar cell devices.¹⁰⁵ We employed hole-only devices to characterize the hole mobilities of **PBT** and **PBT/F** films blended with PC₆₁BM and found to be 1.72×10^{-7} and 2.32×10^{-6} cm²/Vs, respectively, and thus the low hole-mobilities of both polymers induced low FF values (< 40%, see Table 2).¹⁰⁵

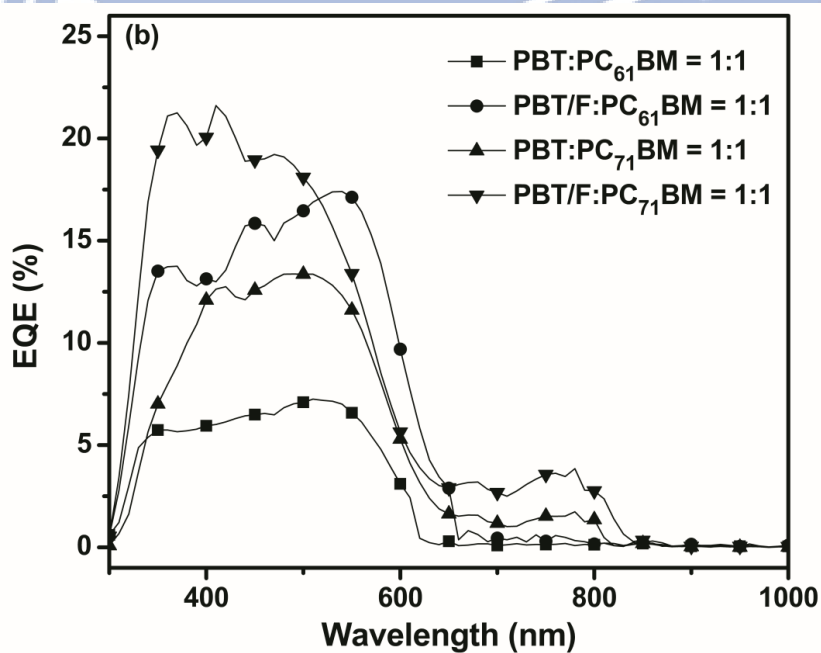
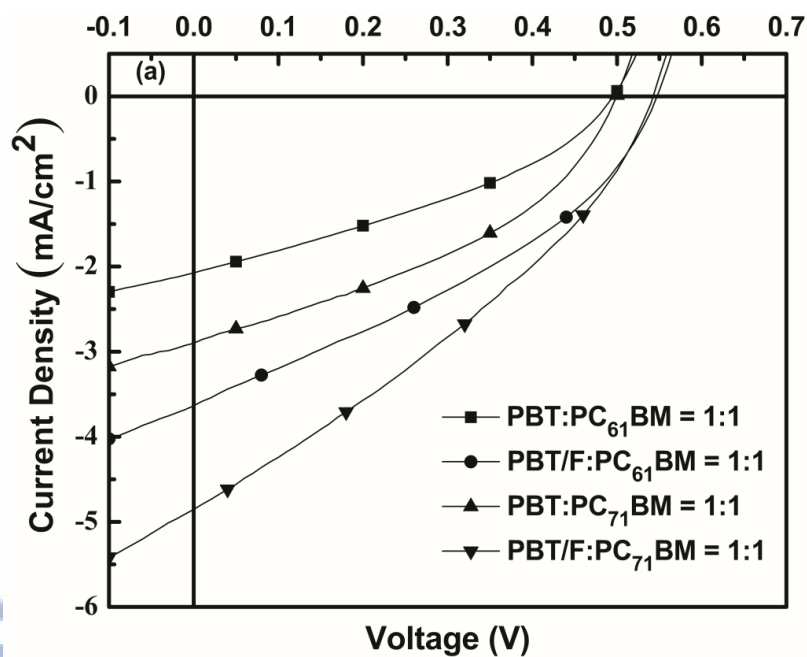


Figure 4.8 (a) J - V and (b) EQE characteristic curves of polymer **PBT** and H-bonded polymer network **PBT/F** blended with PC₆₁BM (or PC₇₁BM) in a wt. ratio of 1:1.

In order to understand the origins of low current densities, we carried out external quantum efficiency (EQE) measurements for solar cell devices by mixing either PC₆₁BM or PC₇₁BM with polymers **PBT** and **PBT/F** (1:1 by wt.), respectively (Figure 4.8). The results illustrate the solar cell devices containing H-bonded polymer network **PBT/F** are able to have higher absorptions of visible lights, which demonstrates enhancements of EQE values with a maximum of ~20% (ca. 350-550 nm) after incorporation of **F** with **PBT** through supramolecular interactions. Hence, the lower current densities of solar cell devices containing **PBT** (without **F**) might be induced by their smaller EQE values and lower hole-mobilities.¹⁰⁴

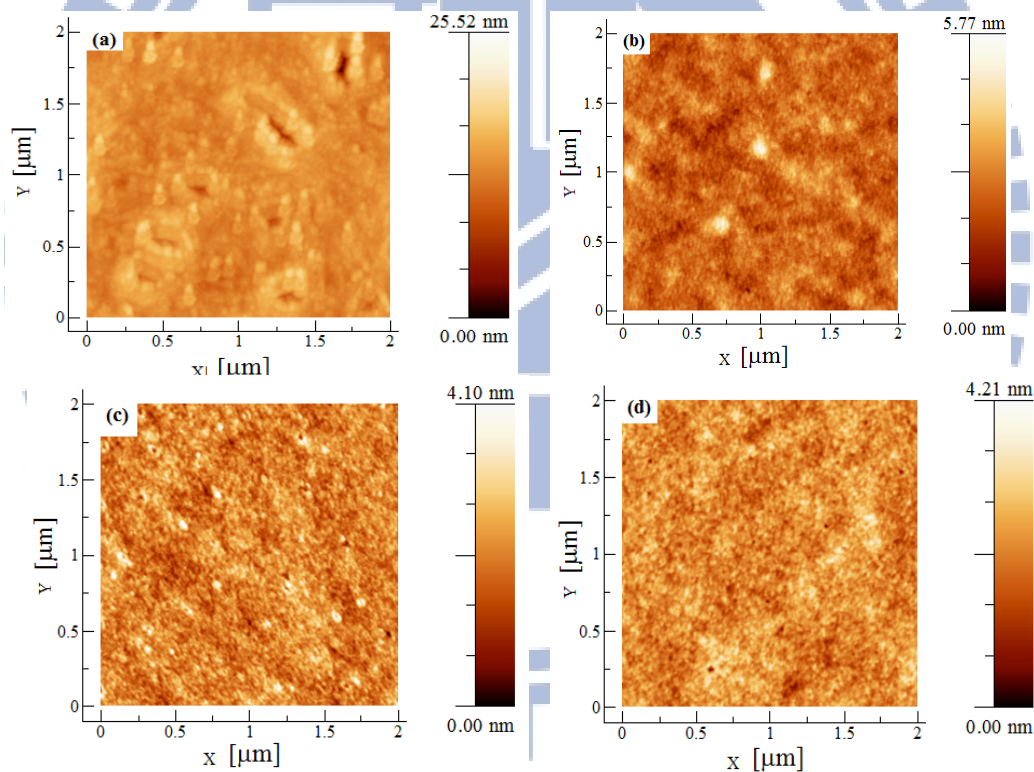


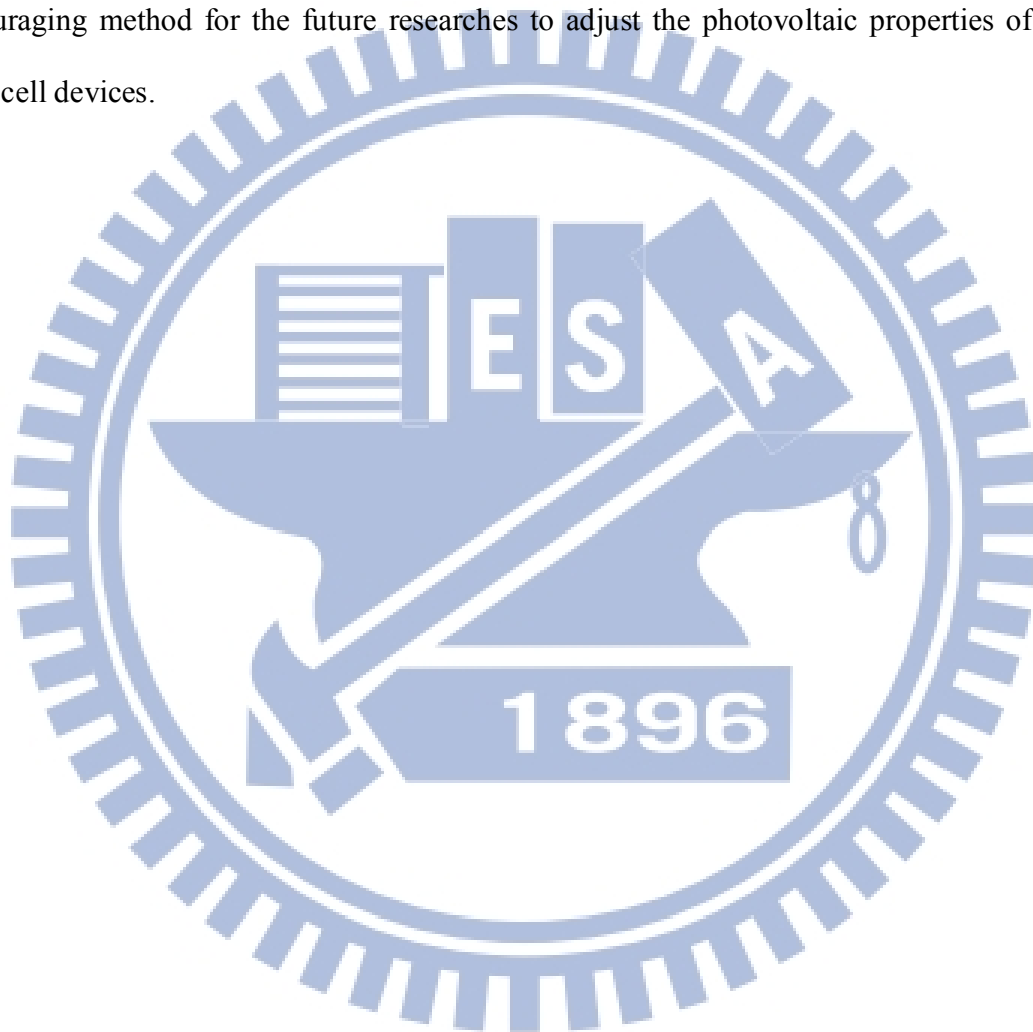
Figure 4.9 AFM images of blended polymers (a) **PBT** and (b) **PBT/F** mixed with PC₆₁BM, respectively; (c) **PBT** and (d) **PBT/F** mixed with PC₇₁BM, respectively (in a wt. ratio of 1:1 by spin-coating from dichlorobenzene and annealing at 70°C for 30 min.)

Surface morphologies of the active layer in solar cell devices are also a key parameter for the device performance.¹¹⁵ AFM images of of blended polymers **PBT** and **PBT/F** mixed with either PC₆₁BM or PC₇₁BM (1:1 by wt. and annealed at 70°C for 30 min.) are presented in Figure 4.9 and their root-mean-square roughness (R_{rms}) values are demonstrated in Table 4.2. The active layers of **PBT** and **PBT/F** showed good film formation to have smooth surfaces with no obvious aggregations (only nano-scale phase separations) between polymers and PC₆₁BM (or PC₇₁BM).¹¹³ Mixed with PC₆₁BM (or PC₇₁BM) in a wt. ratio of 1:1, **PBT** (without **F**) showed larger R_{rms} values than H-bonded polymer network **PBT/F** in the blended polymers. This larger R_{rms} value resulted in the decreased diffusional escape probabilities for mobile charge carriers, and hence increased their recombinations.¹¹⁵ It is evident from AFM images that lesser aggregation between electron-donor polymer and electron-acceptor PCBM molecules and higher π - π stacking allows for better photogenerated charges and inducing higher J_{sc} values via supramolecular engineering of solar cell devices.

4.4 Conclusion

In conclusion, we could tune molecular energy levels, morphologies, and device preferemances by a new and straight-forward approach to introducing multiple H-bonded supramolecular structures. The broader light absorption (an extra blue absorption from H-bonded crosslinker **F** and the red-shifted absorption from H-bonded main-chain polymer **PBT**), lower HOMO level (to have a higher V_{oc} value), higher hole mobility, larger crystallinity, and better morphorlogy in H-bonded polymer network **PBT/F** induces better photovoltaic properties than that containing polymer **PBT**. The preliminary photovoltaic performance showed the solar cell device containing 1:1 wt. ratio of **PBT/F** and [6,6]-phenyl C₇₁ butyric acid methyl ester

(PC₇₁BM) offers the best power conversion efficiency (PCE) value of 0.86% with a short-circuit current density (J_{sc}) of 4.97 mA/cm², an open circuit voltage (V_{oc}) of 0.55 V, and a fill factor (FF) of 31.5%. The highly directional multiple H-bonded strategy between melamine and uracil motifs significantly increased self-assembled behavior as well as π - π stackings, which is an encouraging method for the future researches to adjust the photovoltaic properties of polymer solar cell devices.



Chapter 5

Enhancement of Photovoltaic Properties in Supramolecular Polymer Networks Featuring a Solar Cell Main-Chain Polymer H-Bonded with Conjugated Cross-Linkers

5.1 Introduction

Over the past decade, exploiting and tailoring novel materials with promoted properties by utilizing supramolecular approaches in conjunction with π -conjugated structures is one of the key way to design optoelectronic devices.^{68,107a} Control of hierarchical self-assembled behaviors of various π -conjugated molecules through multiple hydrogen bonds can generate nano-structural materials with long-range orders intrinsically, in which defect-free structures are feasible to be the bottom-up approach via supramolecular chemistry.¹¹⁶ Due to self-assembly between complementary molecular components, a variety of non-covalent interactions, for instance hydrogen-bonds (H-bonds),⁷³ ionic forces,⁷⁰ and metal-coordinations,⁷² can produce unique properties, which are not possessed by the individual components. Among these supramolecular interactions, H-bonds are ideal non-covalent interactions to form self-assembled architectures due to their selectivity and directionality.^{107a} Tremendous research efforts have been devoted towards engineering of polymeric materials as well as donor-acceptor (D-A) bulk heterojunction (BHJ) solar cell devices due to substantial future prospects as low-cost 3rd generation photovoltaic technology.^{11,117} Remarkable achievements in the field of conjugated polymers and dramatic increase in device performance, reaching a power conversion efficiencies (PCE) over 7% by

utilizing low-band-gap (LBG) polymers as electron donors and fullerene derivatives, such as [6,6]-phenyl-C₆₁-butyric acid methyl ester (PC₆₁BM) or [6,6]-phenyl-C₇₁-butyric acid methyl ester (PC₇₁BM), as electron acceptors.^{11a,58-60}

An enhanced intermolecular π -stacking, long-range order, and solution processable electron donating dithieno[3,2-b:2',3'-d]pyrroles (DTP) unit can be co-polymerized with various electron-deficient units to generate LBG polymers and showed PCE values up to ~3%.⁵²⁻⁵⁴ However, due to high values of the highest occupied molecular orbital (HOMO) levels in DTP-based polymers, they showed relatively low V_{oc} values and thus to result in low PCE values for organic solar cells.^{55,56} This problem can be solved either by using various electron-deficient units⁵⁷ or introducing supramolecular architectures to manipulate their HOMO energy levels and thus to get higher V_{oc} values. As an electron deficient unit, the bithiazole unit containing two electron-withdrawing imine ($-C=N$) could show high oxidative stabilities and minimize the HOMO energy levels to induce the high V_{oc} values.^{52-57,88} However, Li et al. have reported one D-A copolymer containing DTP and bithiazole sandwiched between two thiophene units only possessed a maximum PCE value of 0.06%,⁶⁴ but our later report demonstrated that one of the analogous D-A copolymers containing DTP, thiophene, and bithiazole units could reach a maximum PCE value of 0.69%.¹¹⁴

The design of supramolecular D-A systems was recognized as a promising strategy via the charge-transfer processes between donor and acceptor units.¹¹⁸ Würthner, Schenning, and Meijer et al. reported well-defined mesoscopic assemblies by using complementary H-bonded moieties of perylene bisimide and melamine derivatives.^{118,119} Moreover, Bonifazi and Samori et al. constructed several discrete and multi-component nano-scale supramolecular assemblies from triple H-bonded D-A complexes consisting of diamino-

pyridine and uracil derivatives.^{107a} In addition, Meijer et al. reported a PCE value of 0.25% for the polymer solar cell (PSC) device by utilizing a main-chain H-bonded polymer containing oligo(p-phenylene vinylene) and ureido-pyrimidinone units (as H-bonded groups).⁷⁴ Small molecules and their polymer analogues have attracted exceptional attentions in the recent days owing to their corresponding advantages, including high purities and (hole and electron) mobilities for small molecules, and easy processing capabilities and low costs for polymers.⁷⁵ Consequently, one of the attractive approaches is to achieve advanced π -conjugated materials by the combination of both small molecular and polymeric designs through supramolecular architectures, so the H-bonded polymer networks are explored in this report. Our previous studies focus on solar cell dyes H-bonded to conjugated side-chain polymers to form either supramolecular side-chain polymers by single H-bonds attached to one side of (asymmetric) single carboxylic acid dyes^{76a} or supramolecular polymer networks by single H-bonds attached to both sides of (symmetric) double carboxylic acid dyes.^{76b} However, these proton acceptor polymers contain pyridyl pendants to form weak single H-bonds, and have shorter conjugation to exhibit worse solar cell properties than the conjugated main-chain polymers. Therefore, a conjugated main-chain polymer (with better PSC properties) containing multiple H-bonded pendants (with stronger H-bonds to the π -conjugated small molecules) is applied to our molecular design of supramolecular architectures in this study.

To the best of our knowledge, it is the first time to disclose the supramolecular polymer networks containing multiple functionalized melamine pendants and complementary H-bonded uracil motifs for the PSC applications. To accomplish this goal, we choose DTP, bithiazole, and thiophene units as the backbone of a conjugated main-chain polymer **PBTH**,

in which the melamine pendants can be H-bonded with complementary uracil-based conjugated cross-linkers **C** and **F** (in proper molar amounts), i.e., the symmetrical uracils of cross-linkers **C** and **F** are linked to central carbazole and fluorene units, respectively, through triple bonds (see Figure 5.1), to generate supramolecular polymer networks **PBTH/C** and

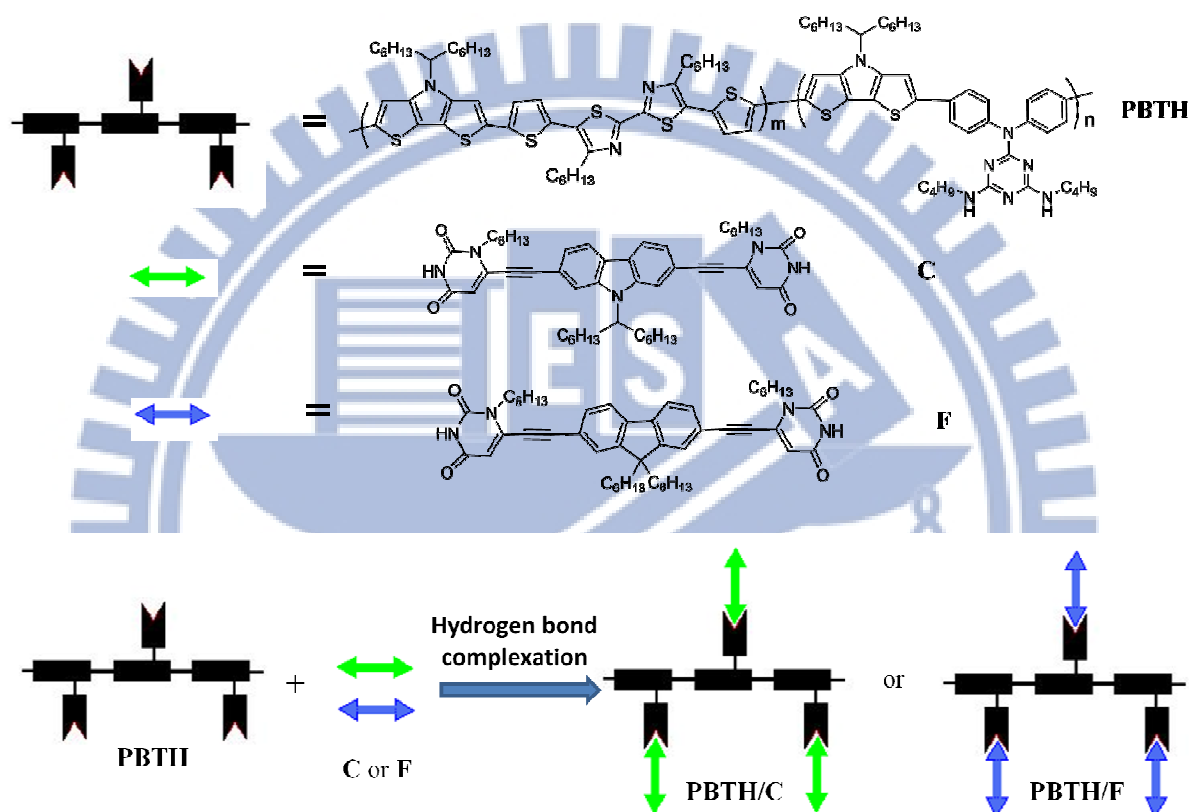


Figure 5.1 Schematic illustration of conjugated main-chain polymer (**PBTH**) and supramolecular polymer networks (**PBTH/C**, and **PBTH/F**).

PBTH/F. The unique features of this triple H-bonded approach are to tune light harvesting capabilities, manipulation of HOMO energy levels, and power conversion efficiencies of supramolecular polymer networks **PBTH/C** and **PBTH/F**. Moreover, the functionalized supramolecular polymer networks are developed to possess better solubilities as well as processabilities in solvents and enhance photovoltaic properties in this study.

5.2 Experimental

5.2.1 Materials

All chemicals and solvents were reagent grades and purchased from Aldrich, ACROS, Fluka, and Lancaster Chemical Co. Tetrahydrofuran (THF), toluene, and diethyl ether were distilled over sodium/benzophenone. Absolute ethanol was obtained by refluxing with magnesium ethoxide and then distilled. The other reagents were used as received without further purification.

5.2.2 Measurements and Characterization

^1H and ^{13}C NMR spectra were recorded on a Varian Unity 300 MHz spectrometer using CDCl_3 solvent and chemical shifts were reported as δ values (ppm) relative to an internal tetramethylsilane (TMS) standard. Elemental analyses were performed on a HERAEUS CHN-OS RAPID elemental analyzer. Thermogravimetric analyses were conducted with a TA Instruments Q500 at a heating rate of $10^\circ\text{C}/\text{min}$ under nitrogen. Gel permeation chromatography (GPC) analyses were conducted on a Waters 1515 separation module using polystyrene as a standard and THF as an eluant. UV-visible absorption spectra were recorded in dilute dichlorobenzene solutions and solid films (spin-coated on glass

substrates from dichlorobenzene solutions) on a HP G1103A spectrophotometer. Cyclic voltammetry (CV) measurements were performed at a scanning rate of 100 mV/s at room temperature using a BAS 100 electrochemical analyzer with a standard three-electrode electrochemical cell in 0.1 M tetrabutylammonium hexafluorophosphate (TBAPF₆) solution in acetonitrile. During the CV measurements, the solutions were purged with nitrogen for 30 s. In each case, a carbon rod coated with a thin layer of polymers as the working electrode, a platinum wire as the counter electrode, and a silver wire as the quasi-reference electrode were used, and Ag/AgCl (3M KCl) electrode was served as a reference electrode for all potentials quoted herein. The redox couple of ferrocene/ferrocenium ion (Fc/Fc⁺) was used as an external standard. The corresponding highest occupied molecular orbital (HOMO) was calculated using $E_{\text{ox/onset}}$ for experiment in solid film of polymer, which were performed by drop-casting film with the similar thickness from THF solutions (ca. 5 mg/ml). The LUMO level of PCBM employed was in accordance with the literature datum.⁷⁶ The onset potentials were determined from the intersections of two tangents drawn at the rising currents and background currents of the CV measurements.

5.2.3 Fabrication and Testing of Polymer Solar Cells

The polymer photovoltaic cells in this study contained an active layer of polymer **PBTH**, supramolecular polymer networks **PBTH/C** and **PBTH/F** blended with [6,6]-phenyl-C₇₁-butyric acid methyl ester (PC₇₁BM) in solid films, which was sandwiched between a transparent indium tin oxide (ITO) anode and a metal cathode (Ca). Prior to the device fabrication, ITO-coated glass substrates (1.5×1.5 cm²) were ultrasonically cleaned in detergent, deionized water, acetone, and isopropyl alcohol. After routine solvent cleaning,

the substrates were treated with UV ozone for 20 min. Then, a modified ITO surface was obtained by spin-coating a layer of poly(ethylene dioxythiophene):polystyrenesulfonate (PEDOT:PSS) (~30 nm). After baking at 130°C for 1 hr, the substrates were transferred to a nitrogen-filled glove box. Subsequently, on the top of PEDOT:PSS layer, the active layer was prepared by spin coating from blended solutions of **PBTH**, **PBTH/C** and **PBTH/F**: PC₇₁BM (with 1:1 w/w) with a spin rate ca. 1000 rpm, and the thickness of the active layer was typically ca. 90 nm. Initially, the blended solutions were prepared by dissolving both polymers and PC₇₁BM in chlorobenzene (10 mg/1 ml), followed by continuous stirring for 12 hr at 50°C. In the slow-growth approach, blended polymers in solid films were kept in the liquid phase after spin-coating by using the solvent with a high boiling point (such as chlorobenzene) and allowed to dry the solvent slowly. Finally, a calcium layer (30 nm) and a subsequent aluminum layer (100 nm) were thermally evaporated through a shadow mask at a pressure below 6×10^{-6} Torr to have the active device area of 0.12 cm². All PSC devices were prepared and measured under ambient conditions. The solar cell testing was done inside a glove box under simulated AM 1.5G irradiation (100 mW/cm²) using a Xenon lamp based solar simulator (Thermal Oriel 1000W). The light intensity was calibrated by a mono-silicon photodiode with KG-5 color filter (Hamamatsu).

5.2.4 Synthesis of Monomer M1, Conjugated Cross-Linkers (C and F), and Conjugated Main-Chain Polymer PBTH

4,6-Dichloro-*N,N*-diphenyl-1,3,5-triazin-2-amine (1)

Under N₂, a solution of diphenylamine (9.16 g, 54.22 mmol) in THF (50 ml) was added dropwise to a mixture of diisopropylethylamine (9.5 ml, 54.22 mmol) and 2,4,6-

trichloro-1,3,5-triazine (10.0 g, 52.22 mmol) in THF(150 ml) at 20°C. After stirring for 3 hr, the solvent was removed by rotatory evaporation and the residue was purified by column chromatography over silica gel (hexane: ethyl acetate = 4:1) to give a white color solid. (12.9 g, yield 75%). ¹H NMR (300 MHz, CDCl₃, δ):7.45-7.41 (m, 4H), 7.35-7.33 (m, 2H), 7.30-7.27 (m, 4H).

***N*²,*N*⁴-dibutyl-*N*⁶,*N*⁶-diphenyl-1,3,5-triazine-2,4,6-triamine (2)**

Sodium bicarbonate (8.0 g, 84.01 mmol) was added to a solution of compound **1** (10.0 g, 31.52 mmol) in 1,4-dioxane (100 ml). After that, butyl amine (9.4 ml, 94.58 mmol) was added and the resulting mixture was refluxed for overnight. The reaction mixtures was cooled to room temperature and pour into cold water and extracted three times with ethyl acetate. The combined organic fractions were washed with brine, dried over MgSO₄, and concentrated by rotary evaporation and purified by column chromatography using silica, (hexane: ethyl acetate = 7:3) to give a white solid. (10.70 g, yield 87%). ¹H NMR (300 MHz, CDCl₃, δ):7.45-7.41 (m, 4H), 7.35-7.33 (m, 2H), 7.30-7.27 (m, 4H), 4.84 (br, 2H), 3.34-3.11(br, 4H), 1.43-1.25 (m, 8H), 0.88 (t, *J* = 6.2Hz, 6H).

***N*²,*N*²-bis(4-bromophenyl)-*N*⁴,*N*⁶-dibutyl-1,3,5-triazine-2,4,6-triamine (M1)**

NBS (6.9 g, 38.40 mmol) was added portion-wise to a solution of compound **2** (5.0 g, 12.80 mmol) in DMF (50 ml) at 0°C. The reaction mixture was stirred for 6 hr at the same temperature and water was added to quench the reaction. The organic layer was extracted with three times by ethyl acetate followed by brine and water washing and dried by anhydrous MgSO₄. The solvent was removed by rotary evaporator and the product was

further purified by column chromatography on silica (hexane: ethyl acetate = 4:1) to yield a white solid. (5.7 g, 80%). ¹H NMR (300 MHz, CDCl₃, δ):7.47-7.38 (m, 4H), 7.43-7.28 (m, 4H), 4.84 (br, 2H), 3.34-3.31(br, 4H), 1.43-1.25 (m, 8H), 0.88 (t, *J* = 6.2 Hz, 6H). ¹³C NMR (75 MHz, CDCl₃, δ):166.48, 166.11, 143.25, 131.81, 129.77, 118.79, 40.60, 32.09, 20.24, 14.01; EIMS [M⁺] calcd. *m/z* = 548.32, found 548.0. Anal. Calcd. for C₂₃H₂₈Br₂N₆: C, 50.38; H, 5.15; Br, 29.15; N, 15.33; found: C, 50.78; H, 5.48; N, 15

1-Hexyluracil (3)

K₂CO₃ (14.80 g, 107.05 mmol) was added to a suspension of uracil (10.0 g, 89.21 mmol) in DMSO (150 ml), and stirred for 15-20 min at 45°C. 1-Bromohexane (3.5 mL, 25 mmol) was added and the reaction mixture was stirred for 48 hr. The reaction was cooled to room temperature and poured into cold water. The product was extracted three times with DCM, and washed with dilute HCl, water, brine, and dried over MgSO₄. The organic layer was concentrated and poured into cold hexane with vigorous stirring. The resulting precipitate was filtered and washed with cold hexane to afford compound **3** (12.40 g, 70.9%) as a white solid. ¹H NMR (300 MHz, CDCl₃, δ):9.12 (br, 1H), 7.14 (d, *J* = 9.0 Hz, 1H), 5.70 (d, *J* = 6.0 Hz, 1H), 3.71(t, *J* = 7.5 Hz, 2H), 1.74-1.65 (m, 2H), 1.34-1.27 (m, 6H), 0.88 (t, *J* = 6.6 Hz, 3H).

1-Hexyl-6-iodouracil (4)

At -78°C, LDA (20.4 ml of a 2.5 M solution, 51.0 mmol) was added drop-wise to a solution of 1-hexyluracil (2.0 g, 10.2 mmol) in THF (55 ml), and the resulting solution was stirred under N₂ for 2 hr. I₂ (12.9 g, 51.0 mmol) was added and the reaction mixture was

stirred for another 2 hr at the same temperature. Acetic acid (2.0 ml) was added to react with stirring at room temperature for overnight. The organic phase was extracted with ethyl acetate washed with saturated NaHCO₃ (3×30.0 ml) and Na₂SO₃ (3×30 ml) solutions. Finally, the product was washed with brine (30 ml), and dried over Mg₂SO₄. The solvent was removed by rotary evaporator and the crude product was purified by column chromatography silica (hexane: ethyl acetate = 5:5) to afford compound **4** (2.2 g, 67%). ¹H NMR (300 MHz, CDCl₃, δ): 9.48 (br, 1H), 6.41 (s, 1H), 4.0 (t, *J* = 8.1 Hz, 2H), 1.74-1.65 (m, 2H), 1.34-1.27 (m, 6H), 0.88 (t, *J* = 6.9 Hz, 3H).

4,4'-(9-(Tridecan-7-yl)-9H-carbazole-2,7-diyl)bis(2-methylbut-3-yn-2-ol) (6)

To a solution of 2,7-dibromo-9-(tridecan-7-yl)-9H-carbazole (**5**) (5.0 g, 9.84 mmol) in 50 ml of THF/Et₃N (1/1), 3-methyl-1-butyn-3-ol (3.85 ml, 39.37 mmol), Pd(PPh₃)₂Cl₂ (0.13 g, 0.28 mol), PPh₃ (0.1 g, 0.39 mol), and CuI (0.07 g, 0.39 mmol) were added. The reaction mixture was degassed with nitrogen for 30 min, and refluxed at 70°C under N₂ for 12 hr. The solvent was removed under reduced pressure and resulting solid was extracted with CH₂Cl₂ then dried over MgSO₄. The crude product was purified by column chromatograph silica (hexane: ethyl acetate = 4:1) to afford a white solid (3.9 g, 77%). ¹H NMR (300 MHz, CDCl₃, δ): 7.97 (t, *J* = 9.0, 2H), 7.65 (s, 1H), 7.47 (s, 1H), 7.30 (m, 2H), 4.48 (m, 1H), 2.29-2.17 (m, 2H), 1.95-1.87 (m, 2H), 1.67 (s, 12H), 1.28-1.08 (m, 16H), 0.80 (t, *J* = 6.6 Hz, 6H).

2,7-Diethynyl-9-(tridecan-7-yl)-9H-carbazole (7)

A mixture of compound **6** (3.5 g, 6.81 mmol) and KOH (2.70 mg, 47.68 mmol) in 60 ml of 2-propanol was heated to reflux under N₂ with a vigorous stirring for 4 hr. Solvent was

removed and then the crude product was purified by column chromatography silica (hexane) to afford a white solid (1.90 g, 70%). ¹H NMR (300 MHz, CDCl₃, δ): 8.01 (t, *J* = 9.0, 2H), 7.72 (s, 1H), 7.56 (s, 1H), 7.35 (d, 2H), 4.48 (m, 1H), 3.15 (s, 1H), 2.30-2.17 (m, 2H), 1.97-1.87 (m, 2H), 1.25-1.04 (m, 16H), 0.80 (t, *J* = 6.6 Hz, 6H).

6,6'-(9-(Tridecan-7-yl)-9H-carbazole-2,7-diyl)bis(ethyne-2,1-diyl)bis(1-hexylpyrimidine-2,4(1H,3H)-dione) (C)

To a mixture of compound 7 (0.5 g, 1.26 mmol) in 20ml THF/NEt₃ (1:1), compound 4 (1.22 g, 3.77 mmol), triphenylphosphine (13 mg, 0.05), and CuI (10 mg, 0.05 mmol) were added. [Pd(PPh₂)Cl₂] (36 mg, 0.05 mmol) was added under N₂ and then the reaction mixture was heated at 50 °C for 36 hr. The crude product was extracted with DCM followed by brine wash and dried over MgSO₄. The resulting solutions were concentrated by rotary evaporator, and purified by column chromatography using silica, (hexane:ethyl acetate 7:3) to give a light yellow solid. (0.60 g, yield 60%). ¹H NMR (300 MHz, CDCl₃, δ): 9.04 (br, 2H), 8.04 (m, 2H), 7.69 (s, 1H), 7.54 (s, 1H), 7.32 (m, 2H), 6.0 (s, 2H), 4.48 (m, 1H), 4.06 (t, *J* = 6.0 Hz, 4H), 2.20 (m, 2H), 1.97 (m, 2H), 1.77 (m, 4H), 1.64 (m, 4H), 1.36-1.52 (m, 10H), 1.42-0.92 (m, 14H), 0.80 (t, *J* = 6.9 Hz, 6H), 0.71 (t, *J* = 6.2, 6H). ¹³C NMR (75 MHz, CDCl₃, δ): 161.50, 156.79, 149.67, 137.77, 122.65, 121.97, 120.45, 114.39, 111.98, 105.50, 100.79, 79.45, 56.26, 45.75, 32.75, 30.50, 30.45, 29.27, 28.67, 27.96, 27.82, 25.78, 25.49, 21.57, 21.44, 12.96; EIMS [M⁺] calcd. *m/z* = 786.06, found 787.0. Anal. Calcd. For C₄₉H₆₂N₄O₄: C, 74.87; H, 8.08; N, 8.91; O, 8.14; found: C, 74.68; H, 7.97; N, 8.77.

6,6'-(9,9-Dihexyl-9H-fluorene-2,7-diyl)bis(ethyne-2,1-diyl)bis(1-hexylpyrimidine-2,4(1H,3H)-dione) (F)

The synthesis procedure for **F** was followed using the same procedure as that of **C**. After purification by silica (hexane:ethyl acetate 7:3) afforded a light yellow solid. (0.58 g, yield 58%). ¹H NMR (300 MHz, CDCl₃, δ): 9.60 (br, 2H), 7.77 (d, *J* = 8.1 Hz, 2H), 7.53 (m, 4H), 6.04 (m, 2H) 4.01 (t, *J* = 7.8 Hz, 4H), 2.0 (t, *J* = 8.1 Hz, 4H), 1.82 (t, *J* = 7.2 Hz, 4H), 1.44-1.34 (m, 12H), 1.36-1.08 (m, 12H), 1.15-1.08 (m, 12H), 0.88 (t, *J* = 6.9 Hz, 6H), 0.77 (t, *J* = 7.2, 6H), 0.59 (m, 4H). ¹³C NMR (75 MHz, CDCl₃, δ): 162.96, 151.95, 151.08, 142.41, 138.89, 131.72, 126.58, 121.05, 119.76, 106.89, 101.28, 81.30, 55.84, 46.94, 40.31, 31.67, 29.77, 29.02, 26.65, 23.97, 22.77, 22.75, 14.19; EIMS [M⁺] calcd. *m/z* = 771.04, found 772.0. Anal. Calcd. For C₄₉H₆₂N₄O₄: C, 76.33; H, 8.10; N, 7.27; O, 8.30; found: C, 76.00; H, 7.97; N, 7.17.

Synthesis of PBTH via Stille Coupling Polymerization

Into 25 ml of two-neck flask, 1 equiv. of dibromo monomers (**M1** and **M3**) and 2 equiv. of 2,6-bis(tributylstannyl)-4-(tridecan-7-yl)-4*H*-dithieno[3,2-*b*:2',3'-*d*]pyrrole (**M2**) were added in anhydrous toluene and deoxygenated with nitrogen for 30 min. The Pd(0) complex, i.e., tetrakis(triphenylphosphine)palladium (1 mol %), was transferred into the mixture in a dry environment. The reaction mixture was stirred at 110°C for 48 hr, and then an excess amount of 2-bromothiophene was added to end-cap the trimethylstannyl groups for 4 hr. After cooling to room temperature, the solution was added dropwise into MeOH (200 ml). The crude polymer was collected, dissolved in hot CHCl₃, filtered through a 0.5-μm poly(tetrafluoroethylene) (PTFE) filter, and reprecipitated in MeOH. The solid was washed

with acetone, hexane, and CHCl_3 in a Soxhlet apparatus. The CHCl_3 solution was concentrated and then added dropwise into MeOH. Finally, the product was collected and dried under vacuum to give polymer **PBTH** (140 mg, 77%) with $M_w = 21,100$ g/mol and polydispersity index (PDI) = 1.65. ^1H NMR (300 MHz, CDCl_3): δ 7.17 (m), 7.21-7.15 (m), 4.91 (br), 4.21 (m), 3.56 (br, 2H), 2.99 (m), 2.11–1.74 (m), 1.27–1.49 (m), 1.66–1.11 (m), 0.91–0.81 (m). Anal. Calcd For: $\text{C}_{91}\text{H}_{118}\text{N}_{10}\text{S}_8$: C, 67.95; H, 7.39; N, 8.71; S, 15.95; Found: C, 66.38; H, 7.85; N, 8.12.

Preparation of Supramolecular Polymer Networks (PBTH/C and PBTH/F)

Supramolecular polymer networks (**PBTH/C** and **PBTH/F**) were prepared by dissolving 2 moles of polymer (**PBTH**) and 1 mole of bi-functional conjugated cross-linker (**C** and **F**) in minimum amounts of CHCl_3 and then the solvent was evaporated under ambient temperature.

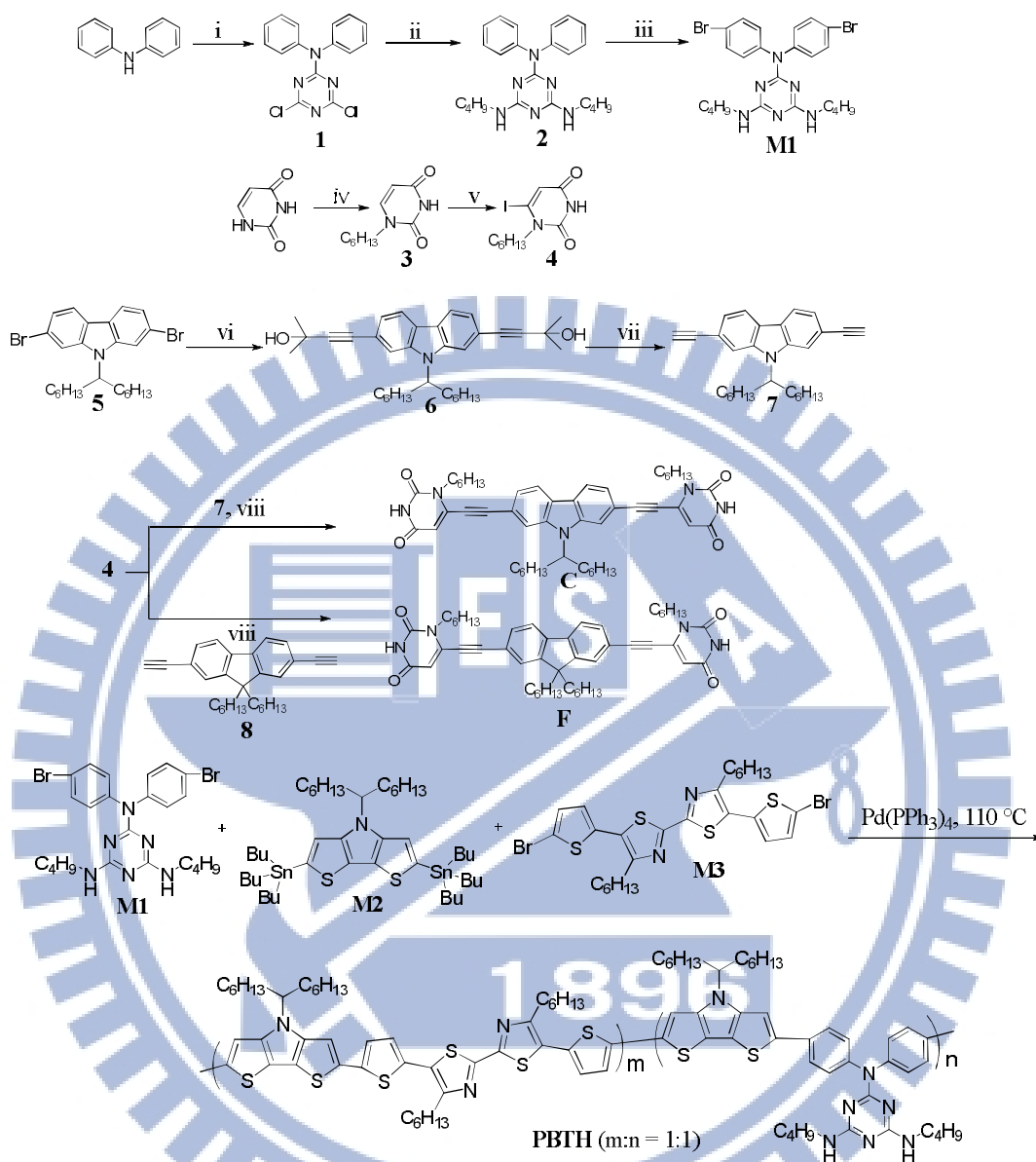


Figure 5.2 Synthesis routes of monomer **M1**, **C**, **F**, and polymer **PBTH**^a

^aReagents and conditions: (i) diisopropylethylamine, 2,4,6-trichloro-[1,3,5]triazine, THF, 20°C, 3 hr; (ii) sodium bicarbonate, bromo butane, 1,4-dioxane, reflux, overnight; (iii) NBS, 0-5°C, THF; (iv) K₂CO₃, DMSO, 45°C, overnight; (v) -78°C, LDA, THF, 5 hr, I₂; (vi) THF/Et₃N (1/1), 3-methyl-1-butyn-3-ol, Pd(PPh₃)₂Cl₂, PPh₃, CuI, 12 hr; (vii) KOH, 2-propanol, 4 hr; (viii) Ph₃P, CuI, THF, Et₃N, Pd(PPh₂)Cl₂, 50°C, overnight; (ix) Toluene, Pd(PPh₃)₄, 110°C, 48 hr.

5.3 Results and Discussion

5.3.1 Synthesis and Characterization

The synthetic details of monomer **M1**, π -conjugated cross-linkers (**C** and **F**), and conjugated main-chain polymer **PBTH** are outlined in Scheme 1. 4,6-Dichloro-*N,N*-diphenyl-1,3,5-triazin-2-amine (**1**) was prepared by reacting of diphenylamine and 2,4,6-trichloro-1,3,5-triazine, and subsequently converted to *N*²,*N*⁴-dibutyl-*N*⁶,*N*⁶-diphenyl- and finally brominated to **M1** by *N*-bromosuccinimide (NBS) at 0-5°C. 1-Hexyluracil (**3**) was prepared by reaction of unsubstituted uracil with 1-bromohexane in the presence of K₂CO₃ and dimethyl sulfoxide (DMSO). Deprotonation of compound **3** with lithium diisopropylamide (LDA) and addition of I₂ could yield 1-hexyl-6-iodouracil (**4**). Then, 2,7-dibromo-9-(tridecan-7-yl)-9*H*-carbazole (**5**) was reacted with 3-methyl-1-butyn-3-ol via the Sonogashira coupling reaction to form 4,4'-(9-(tridecan-7-yl)-9*H*-carbazole-2,7-diyl)bis(2-methylbut-3-yn-2-ol) (**6**) and further deprotected by refluxing 2-propanol in a basic condition to obtain 2,7-diethynyl-9-(tridecan-7-yl)-9*H*-carbazole (**7**). The H-bonded cross-linkers **C** and **F** were synthesized via palladium catalyzed Sonogashira cross-coupling reactions of compound **4** with compound **7** and 2,7-diethynyl-9,9-dihexyl-9*H*-fluorene (**8**)^{72a}, respectively. In addition, compounds **8**, **M2**,¹⁷ and **M3**⁹⁶ were prepared by similar procedures reported earlier. In this study, a conjugated main-chain polymer (**PBTH**) consisting of DTP and **M1** units as the electron-donating moieties and bithiazole unit as the electron-accepting moiety (sandwiched between two thiophene units) were synthesized by Pd(0)-catalyzed Stille coupling polymerization in toluene at 110°C with an input molar ratio of m:n=1:1 (output molar ratio of m:n=1.32:1 determined by NMR characterization). The chemical structures of **PBTH**, **M1**, **C** and **F** were satisfactorily characterized by ¹H NMR, MS spectroscopy, and

elemental analyses. The weight average molecular weight (M_w) of **PBTH** was determined by gel permeation chromatography (GPC) with THF as the eluting solvent and polystyrene as a standard. The M_w and polydispersity index (PDI) of **PBTH** were found to be 21,100 g/mol and 1.65, respectively. The decomposition temperatures (T_d) of polymer **PBTH** and supramolecular polymer networks **PBTH/C** and **PBTH/F** were measured by thermogravimetric analysis (TGA) (see Figure 5.3) and found to be 380, 402, and 391°C, respectively, indicating supramolecular polymer networks **PBTH/C** and **PBTH/F** have better thermal stabilities than polymer **PBTH**. These thermal stabilities are adequate for their applications in polymer solar cells and other optoelectronic devices.

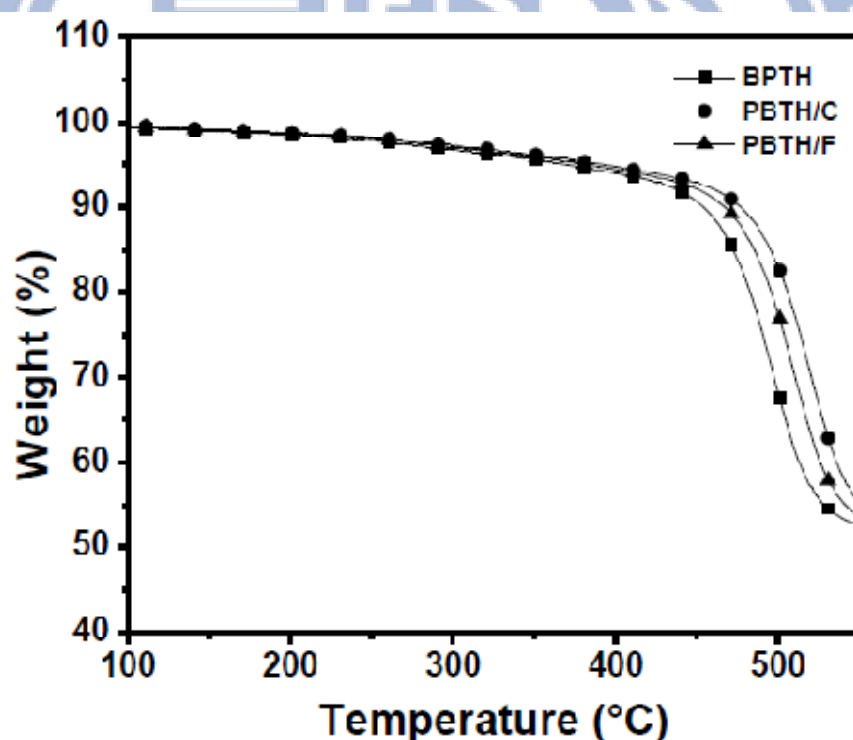


Figure 5.3 TGA plots of polymer **PBTH** and supramolecular polymer networks (**PBTH/C**, and **PBTH/F**) with a heating rate of 10°C / min under N_2 .

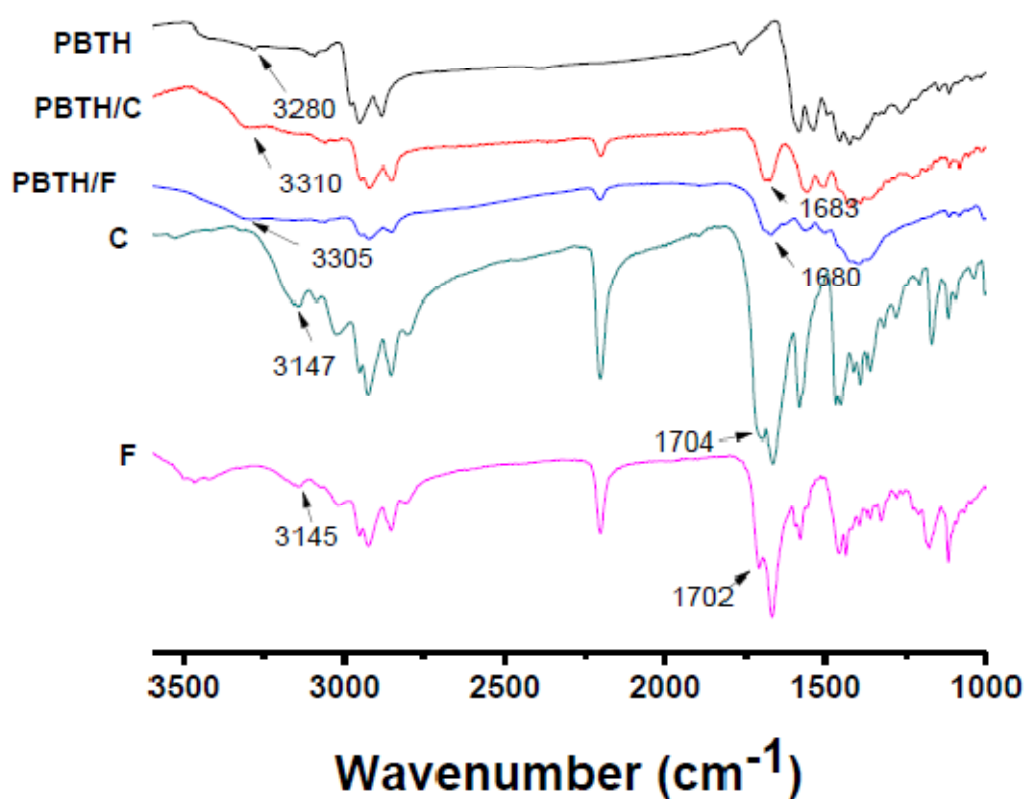


Figure 5.4 FT-IR spectra of polymer **PBTH**, cross-linkers (**C** and **F**), and supramolecular polymer networks (**PBTH/C** and **PBTH/F**).

5.3.2 IR Measurements

The existence of multiple H-bonds in the H-bonded complexes can be confirmed by FT-IR spectroscopy. Therefore, IR spectra of π -conjugated cross-linkers **C** and **F**, conjugated main-chain polymer **PBTH**, and supramolecular polymer networks **PBTH/C** and **PBTH/F** are shown in Figure 5.4. Both IR spectra of cross-linkers **C** and **F** are located likewise at 1702-1704 cm^{-1} and 3145-3147 cm^{-1} for free C=O and N-H stretching bands, respectively.^{107,108} The peak at 3280 cm^{-1} can be assigned to stretching frequency of amine groups (-NH-) present in **PBTH**.¹⁰⁷ Therefore, the C=O stretching bands of supramolecular

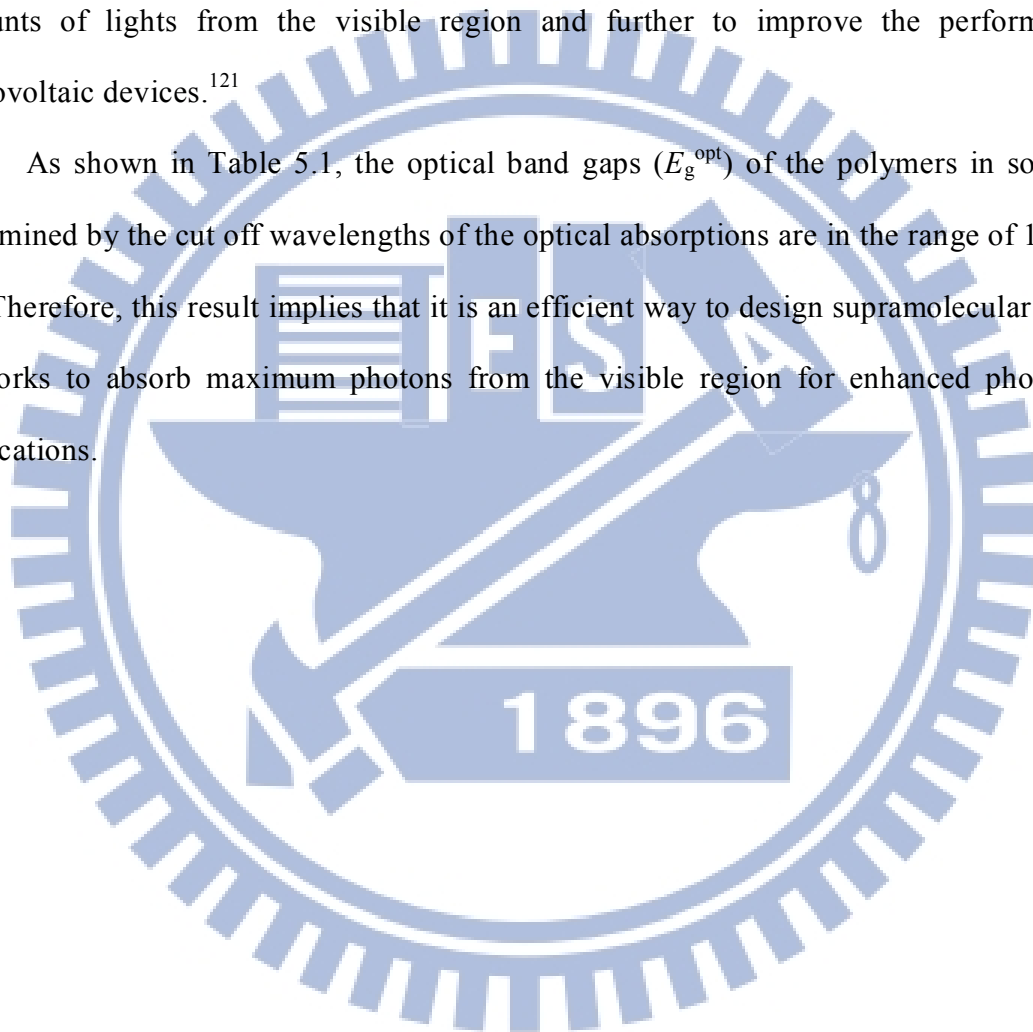
polymer networks **PBTH/C** and **PBTH/F** were considerably shifted to lower wave numbers of 1683 and 1680 cm^{-1} , respectively, and the -NH- stretching bands were significantly shifted to higher wave numbers of 3310 and 3305 cm^{-1} , respectively.¹⁰⁸ Consequently, the large shifts of wave numbers in C=O and N-H stretching bands during the formation of supramolecular polymer networks (**PBTH/C** and **PBTH/F**) indicate the presence of multiple H-bonds between polymer **PBTH** and cross-linkers (**C** and **F**).^{68a}

5.3.3 Optical Properties

The UV-visible absorption spectra of a conjugated main-chain polymer **PBTH**, π -conjugated cross-linkers **C** and **F** (in dichlorobenzene solutions and solid films), and supramolecular polymer networks **PBTH/C** and **PBTH/F** (in solid films only) are demonstrated in Figure 5.5, and their photophysical properties are summarized in Table 5.1. As shown in Figure 5.5a, the light harvesting capability of **PBTH** can be directly tuned by forming multiple H-bonds with π -conjugated cross-linkers **C** and **F**, which could be clearly identified from their absorption spectra of supramolecular polymer networks **PBTH/C** and **PBTH/F** in solid films. The absorption maxima of π -conjugated cross-linkers **C** and **F** in dichlorobenzene solutions are 379 and 369 nm, respectively, and in solid films are 419 and 409 nm, respectively. Because of the inter-chain association and π - π stacking, the absorption wavelengths of π -conjugated cross-linkers **C** and **F** in solids films generally show red-shifts of 40 and 30 nm, respectively, in contrast to those in dilute solutions.⁸² The absorption maxima of **PBTH** in the dichlorobenzene solution and solid film are found to be 523 and 535 nm, respectively, which can be attributed to the intramolecular charge transfer (ICT) from the donor to acceptor moieties.⁵²⁻⁵⁷ In solid films, UV-visible spectra of supramolecular polymer networks **PBTH/C** and **PBTH/F** are found to be 550 and 544 nm, respectively, and

red shifted about 15 and 9 nm (from **PBTH**), respectively, due to the enhanced π - π stacking and efficient charge transfer between polymer **PBTH** and cross-linkers (**C** and **F**).¹²⁰ A new peak was formed in the visible region of **PBTH/C** and **PBTH/F** which are mainly attributed to the cross-linkers (**C** and **F**) which helps **PBTH/C** and **PBTH/F** to harvest sufficient amounts of lights from the visible region and further to improve the performance of photovoltaic devices.¹²¹

As shown in Table 5.1, the optical band gaps (E_g^{opt}) of the polymers in solid films determined by the cut off wavelengths of the optical absorptions are in the range of 1.72-1.81 eV. Therefore, this result implies that it is an efficient way to design supramolecular polymer networks to absorb maximum photons from the visible region for enhanced photovoltaic applications.



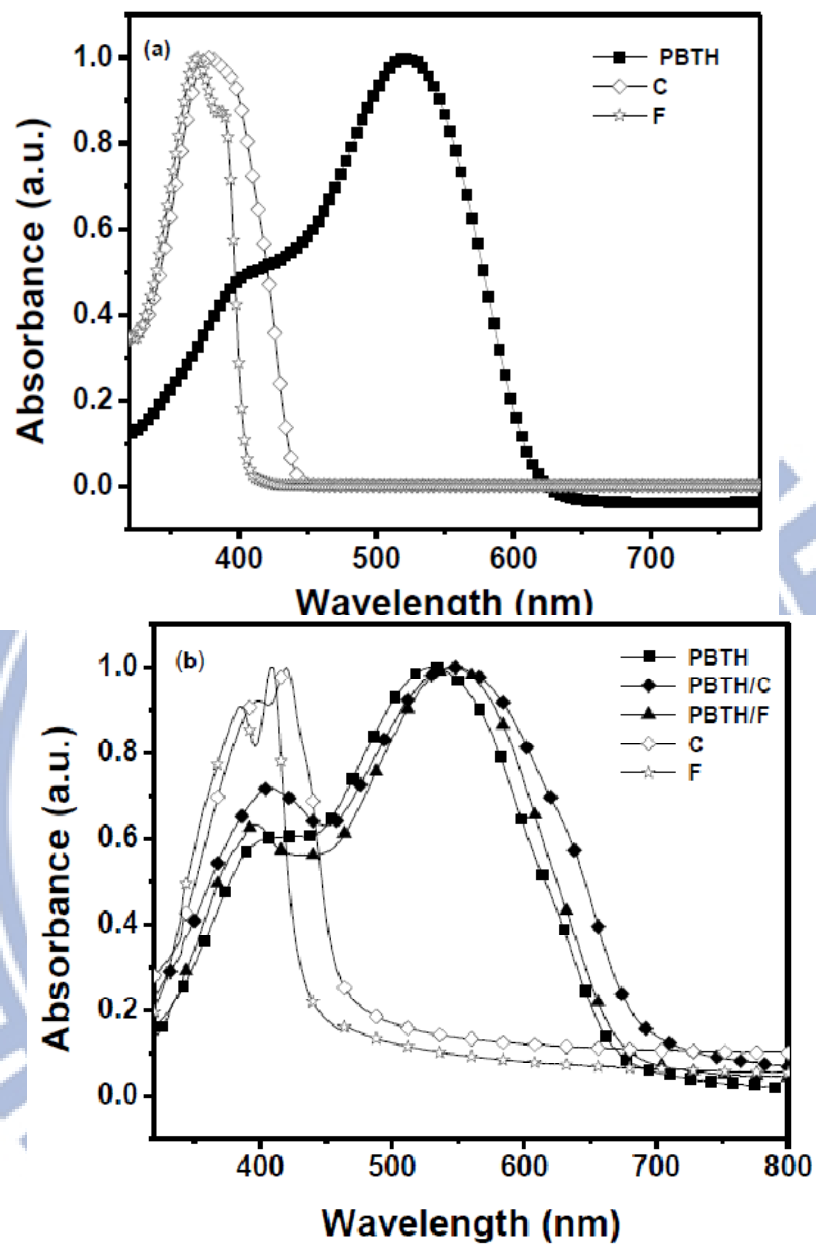


Figure 5.5 Normalized UV-vis spectra of (a) conjugated main-chain polymer **PBTH**, π -conjugated cross-linkers **C** and **F** (in dichlorobenzene solutions and solid films), and (b) supramolecular polymer networks **PBTH/C** and **PBTH/F** (in solid films only).

Table 5.1 Optical and Electrochemical Properties of Polymer PBTH and Supramolecular Polymer Networks (PBTH/C and PBTH/F).

Polymers	Solution ^a λ_{abs} (nm)	Solid film ^b λ_{abs} (nm)	$E_{\text{g}}^{\text{opt}}$ (eV)	$E_{\text{ox}}^{\text{onset}}$ (V)	$E_{\text{HOMO}}^{\text{c}}$ (eV)	$E_{\text{LUMO}}^{\text{d}}$ (eV)
C	379	419	2.58	1.26	-5.61	-3.03
F	369	409	2.66	1.49	-5.84	-3.18
PBTH	523	535	1.81	0.55	-4.90	-3.09
PBTH/C	-	407, 550	1.72	0.66	-5.01	-3.29
PBTH/F	-	396, 544	1.75	0.68	-5.03	-3.28

^aIn dichlorobenzene. ^bSpin coated from dilute dichlorobenzene solution on glass surface. ^cHOMO = $[-(E_{\text{onset}} - E_{\text{onset}}(\text{FC}/\text{FC}^+ \text{ vs. Ag/Ag}^+)) - 4.8]$ eV where 4.8 eV is the energy level of ferrocene below the vacuum level and $E_{\text{onset}}(\text{FC}/\text{FC}^+ \text{ vs. Ag/Ag}^+) = 0.45\text{eV}$. ^d $E_{\text{LUMO}} = E_{\text{HOMO}} + E_{\text{g}}^{\text{opt}}$.

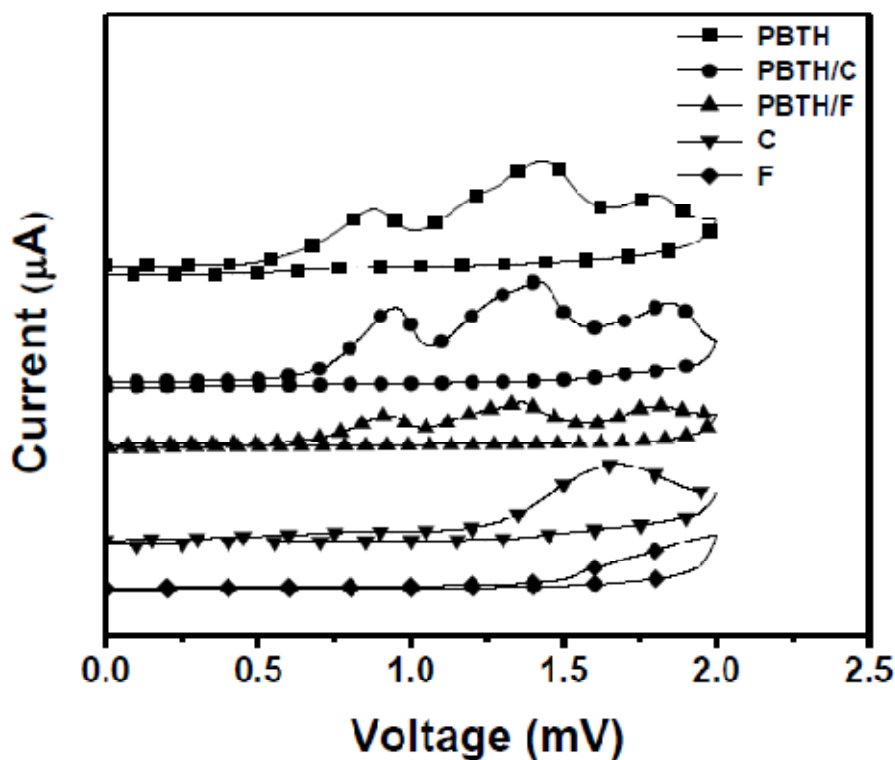


Figure 5.6 Cyclic voltammograms of PBTH, PBTH/C, PBTH/F, C and F in solid films at a scan rate of 100 mV/s.

5.3.4. Electrochemical Properties

To investigate the redox behavior of polymer (**PBTH**) and supramolecular polymer networks (**PBTH/C** and **PBTH/F**) and their electronic states, i.e., the highest occupied molecular orbital (HOMO) and lowest unoccupied molecular orbital (LUMO) levels, the electrochemical properties of polymers were investigated by cyclic voltammetry (CV) measurements polymer films in acetonitrile containing 0.1 M tetrabutylammonium hexafluorophosphate (Bu_4NPF_6) at a potential scanning rate of 100 mV/s. The oxidation cyclic voltammograms of all polymers are shown in Figure 5.6, and their electrochemical properties, such as the onset oxidation potentials ($E_{\text{ox}}^{\text{onset}}$), HOMO and LUMO levels of polymers, are summarized in Table 5.1. It can be seen that all polymers **PBTH**, **PBTH/C**, and **PBTH/F** possessed three irreversible oxidation peaks, and π -conjugated cross-linkers **C** and **F** possessed irreversible oxidation peaks at positive potentials. The $E_{\text{ox}}^{\text{onset}}$ values were found to be 0.55, 0.66, 0.68, 1.26, and 1.49 V for **PBTH**, **PBTH/C**, **PBTH/F**, **C**, and **F**, respectively. The HOMO energy levels were estimated by the oxidation potentials from the reference energy level of ferrocene according to the following equation⁶⁷

$$E_{\text{HOMO}} = [-(E_{\text{ox}} - E_{\text{onset}}(\text{FC}/\text{FC}^+ \text{ vs. Ag}/\text{Ag}^+)) - 4.8] \text{ eV}$$

Where 4.8 eV is the energy level of ferrocene below the vacuum level and $E_{\text{onset}}(\text{FC}/\text{FC}^+ \text{ vs. Ag}/\text{Ag}^+) = 0.45 \text{ eV}$ and E_{ox} is the oxidation potential of each polymer. The HOMO levels of polymer **PBTH**, supramolecular polymer networks (**PBTH/C** and **PBTH/F**), and π -conjugated cross-linkers (**C** and **F**) were found to be -4.90, -5.01, -5.03, -5.61, and -5.84 V, respectively. Obviously, the supramolecular incorporation of electron rich building blocks, such as carbazole and fluorene units, enhanced oxidation potentials of **PBTH/C** and **PBTH/F**

and lowered the HOMO levels due to their deep-laying HOMO energy levels.^{112,122} The LUMO levels of **PBTH**, **PBTH/C**, and **PBTH/F** were obtained from their optical band gaps, and the HOMO energy levels were calculated by using the following equation¹²³

$$E_{\text{LUMO}} = E_{\text{HOMO}} + E_{\text{g}}^{\text{opt}}$$

The LUMO energy levels were found to be -3.09, -3.29, -3.28, -3.03, and -3.18 eV for **PBTH**, **PBTH/C**, **PBTH/F**, **C**, and **F** respectively, and which depends on the strength of acceptors.¹²⁴ The low HOMO levels of **PBTH/C** and **PBTH/F** from **PBTH** is an advantage for attaining high V_{oc} values in solar cell devices, because the V_{oc} value is directly proportional to the difference between the HOMO level of each donor polymer and the LUMO level of the acceptor derivative (PC_{71}BM).¹²⁵ On the other hand, the LUMO energy level of the electron donor (polymer) has to be positioned above the LUMO energy level of PC_{71}BM at least 0.3 eV, so the exciton binding energy of the polymer could be overcome and resulted in efficient electron transfer from donor to acceptor.

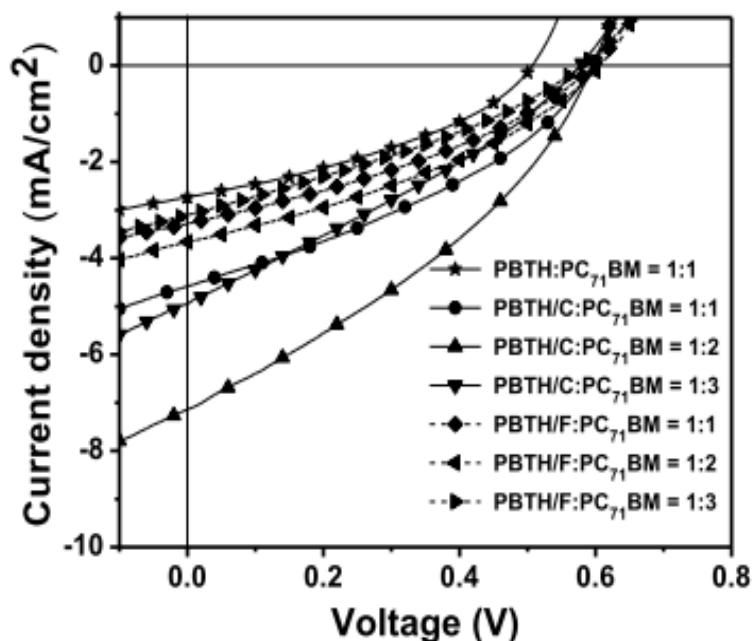


Figure 5. 7 $J-V$ characteristics of PBTH, PBTH/C, and PBTH/F under illumination of AM 1.5 at 100 mW/cm^2 .

5.3.5 Photovoltaic Properties

To investigate the photovoltaic properties of a conjugated main-chain polymer (PBTH) and supramolecular polymer networks (PBTH/C and PBTH/F) in PSC devices, the bulk heterojunction (BHJ) solar cell devices were fabricated by using polymers as electron donors and PC₇₁BM as an electron acceptor with a device configuration of ITO/PEDOT:PSS(30 nm)/(copolymers):PC₇₁BM(1:1w/w)(~90 nm)/Ca(30 nm)/Al(100 nm). In order to obtain a better absorption coefficient in visible region, PC₇₁BM was chosen as electron acceptor rather than PC₆₁BM.¹²⁵ To achieve better performance in PSC devices, chlorobenzene was chosen as the solvent to obtain the blended polymer active layers with good film qualities. Figure 5.7 shows the $J-V$ curves of polymer solar cell (PSC) devices

under the condition of AM 1.5 at 100 mW/cm², and the open circuit voltage (V_{oc}), short circuit current density (J_{sc}), fill factor (FF), and power conversion efficiency (PCE) values are summarized in Table 5.2.

Table 5.2 Photovoltaic Properties of Polymer PBTH and Supramolecular Polymer Networks (PBTH/C and PBTH/F).

Weight Ratio of Polymer to PC ₇₁ BM	V_{oc} (V)	J_{sc} (mA/cm ²)	FF	PCE (%)
PBTH : PC ₇₁ BM = 1:1	0.51	2.73	0.36	0.52
PBTH/C : PC ₇₁ BM = 1:1	0.60	4.58	0.35	0.97
PBTH/C : PC ₇₁ BM = 1:2	0.60	7.16	0.36	1.56
PBTH/C : PC ₇₁ BM = 1:3	0.58	4.97	0.30	0.87
PBTH/F : PC ₇₁ BM = 1:1	0.60	3.28	0.35	0.68
PBTH/F : PC ₇₁ BM = 1:2	0.61	3.66	0.36	0.80
PBTH/F : PC ₇₁ BM = 1:3	0.58	3.09	0.32	0.57

The obtained PCE value of conjugated main-chain polymer **PBTH** was found to be 0.52% with $V_{oc} = 0.51$ V, $J_{sc} = 2.81$ mA/cm², and FF = 0.36. However, a similar alternating copolymer reported by Li et al., which consisted of DTP and **M3** units, only achieved a lower PCE value of 0.06% and a V_{oc} of 0.26 V.⁶⁴ In addition, a polymer similar to **PBTH** was reported to possess a PCE value of 0.69% and a V_{oc} value of 0.40 V.¹¹⁴ The lower V_{oc} value (0.51 V) of polymer **PBTH** was because of its higher HOMO level (-4.90 eV), whereas its supramolecular polymer networks **PBTH/C** and **PBTH/F** showed improved V_{oc} values (0.60 and 0.61V, respectively) due to of their lower HOMO levels (-5.01 and -5.03 eV, respectively) by the supramolecular design. The PCE values of PSC devices containing **PBTH/C** and **PBTH/F** with PC₇₁BM in a weight ratio of 1:1 were found to be 0.97% and 0.68%, respectively. Hence, both supramolecular polymer networks **PBTH/C** and **PBTH/F** showed improved J_{sc} values owing to the enhanced crystallinities compared with **PBTH**,

which can be further verified by the powder X-ray diffraction (XRD) patterns. As demonstrated in Figure 5.8, the XRD patterns of polymer (**PBTH**) and supramolecular polymer networks (**PBTH/C** and **PBTH/F**) were analyzed. Compared with a single weak peak in the small angle region of polymer **PBTH**, both sharp peaks at the small angle region and broad peaks at the wide angle region were observed in supramolecular polymer networks **PBTH/C** and **PBTH/F**. Thus, the crystallinities of the supramolecular polymer networks **PBTH/C** and **PBTH/F** were much improved due to the presence of multiple hydrogen-bonds, which enhanced the chain-reorganization and self-assembled behavior and thus to induce higher PCE values of H-bonded polymer network (**PBTH/C** and **PBTH/F**).^{67,68}

The photovoltaic properties of **PBTH**, **PBTH/C**, and **PBTH/F** were investigated initially using a 1:1 weight ratio of polymer:PC₇₁BM, then different blending ratios of polymer:PC₇₁BM were applied to optimize their PCE values of **PBTH/C** and **PBTH/F**. As illustrated in Table 5.2, the maximum PCE values of 1.56% and 0.80% were obtained in the PSC devices containing **PBTH/C** and **PBTH/F**, respectively, with a weight ratio of polymer:PC₇₁BM=1:2, where the photovoltaic properties of **PBTH/C** with the optimum PCE value (1.56%) possessed $V_{oc} = 0.60$ V, $J_{sc} = 7.16$ mA/cm², and FF = 0.36. Indeed, the weight ratios between polymer donors and PC₇₁BM acceptor played a key role in the PCE values of all PSC devices.^{98,126} However, by increasing the weight ratios of PC₇₁BM in supramolecular polymer networks **PBTH/C** or **PBTH/F** (i.e., polymer:PC₇₁BM=1:3 w/w), both J_{sc} and PCE values were reduced (see Table 5.2), which might be attributed to the reduced interfacial area of exciton dissociation and the insufficient percolation for charge transport in blended films.^{98,127}

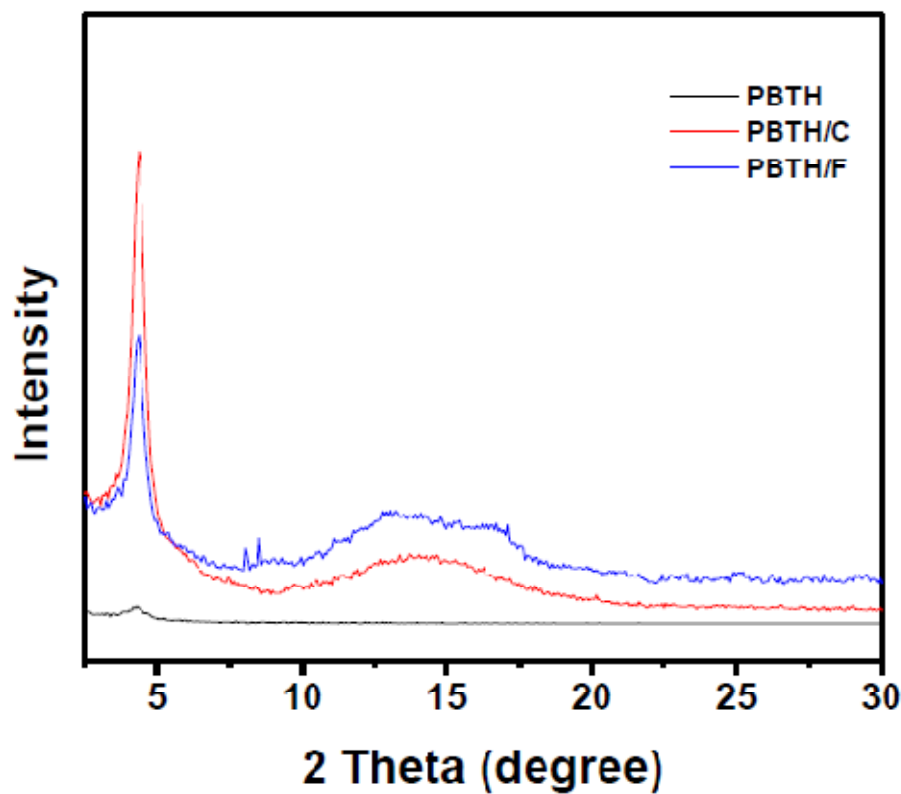


Figure 5.8 X-ray diffraction patterns of polymer **PBTH** and supramolecular polymer networks (**PBTH/C** and **PBTH/F**) in solid powders.

Interestingly, compared with polymer **PBTH** (with $V_{oc} = 0.51$ V), the V_{oc} value of the solar cell devices containing supramolecular polymer networks **PBTH/C** and **PBTH/F** (as polymer:PC₇₁BM=1:1 w/w) increased to 0.60 V. The suramolecular design resulting in an increase of 0.09 V in V_{oc} is a good agreement with the HOMO levels (see Table 1) of -4.9, -5.01, and -5.03 eV for **PBTH**, **PBTH/C**, and **PBTH/F**, respectively.¹²⁷ Various parameters improved in the suramolecular design, such as more efficient light harvests, lower HOMO energy levels, and higher crystallinities, are responsible for the enhancement of V_{oc} and J_{sc} values in PSC devices containing supramolecular polymer networks **PBTH/C** and **PBTH/F** in contrast to polymer **PBTH**. The enhanced photovoltaic properties of supramolecular polymer networks

PBTH/C and **PBTH/F** indicate that the supramolecular approach is one of an ideal design for high-performance donor-acceptor polymer solar cells.

4. Conclusions

In summary, we have developed novel supramolecular polymer networks **PBTH/C** and **PBTH/F** based on the formation of multiple hydrogen bonds between conjugated main-chain polymer **PBTH** and uracil-based conjugated cross-linkers **C** and **F** (in proper molar amounts) through complementary melamine and uracil moieties. The supramolecular formation of multiple hydrogen bonds successfully characterized by IR, and UV-Vis spectra measurements. The supramolecular concept has been successfully applied to tune the photophysical, electrochemical, and photovoltaic properties of supramolecular polymer networks **PBTH/C** and **PBTH/F** compared with polymer **PBTH**. The power conversion efficiencies (PCE) values of PSC devices containing supramolecular polymer networks **PBTH/C** and **PBTH/F** (as polymer:PC₇₁BM=1:1 w/w) are found to be 0.97 and 0.68%, respectively, in contrast to 0.52% for polymer **PBTH**. The optimum photovoltaic performance with the highest PCE value of 1.56 % was obtained in the PSC device containing supramolecular polymer networks **PBTH/C** as polymer:PC₇₁BM=1:2 w/w. This supramolecular design is an encouraging approach on the further improvements of any most excellent donor-acceptor photovoltaic polymers to be in conjunction with efficient conjugated cross-linkers complementarily through supramolecular interactions for future polymer solar cell applications.

Chapter 6

In conclusion, a series of conjugated main-chain copolymers consisting of 2,7-carbazole electron-donating unit and bithiazole electron-accepting unit were synthesized by Pd(0)-catalyzed Stille coupling polymerization. Carbazole-based polymers exhibited broad absorption bands located in the UV and visible regions from 300 to 600 nm with optical band gaps of 1.93–1.99 eV. The HOMO and LUMO energy levels of the polymers can be finely tuned via the molecular engineering of donor/acceptor moieties and conjugated linkers inside the copolymers, which possessed relatively lower HOMO levels for PSC applications. The BHJ photovoltaic devices utilizing polymers **P1-P4** as electron donors and PC₆₁BM as electron acceptors were fabricated, and the optimization of PSC devices with **P4**:PC₇₁BM in different weight ratios were investigated. Finally, the photovoltaic device bearing an active layer of polymer blend **P4**:PC₇₁BM (1:1.5 w/w) showed the best power conversion efficiency (PCE) value of 1.01%, with a short circuit current density (J_{sc}) of 4.83 mA/cm², a fill factor (FF) of 35%, and V_{oc} = 0.60 V under 100 mW/cm² of AM 1.5 white-light illumination. AFM images revealed that there were a better mixing between polymers and PC₇₁BM to generate a less scale phase separation. Although the PCE values of all PSC devices were not sufficiently high, the tunable optoelectronic properties could be achieved by the structural modifications of electron donor and acceptor units.

In conclusion, we could tune molecular energy levels, morphologies, and device preferemances by a new and straight-forward approach to introducing multiple H-bonded supramolecular structures. The broader light absorption (an extra blue absorption from H-bonded crosslinker **F** and the red-shifted absorption from H-bonded main-chain polymer **PBT**), lower HOMO level (to have a higher V_{oc} value), higher hole mobility, larger crystallinity, and better

morphology in H-bonded polymer network **PBT/F** induces better photovoltaic properties than that containing polymer **PBT**. The preliminary photovoltaic performance showed the solar cell device containing 1:1 wt. ratio of **PBT/F** and [6,6]-phenyl C₇₁ butyric acid methyl ester (PC₇₁BM) offers the best power conversion efficiency (PCE) value of 0.86% with a short-circuit current density (J_{sc}) of 4.97 mA/cm², an open circuit voltage (V_{oc}) of 0.55 V, and a fill factor (FF) of 31.5%. The highly directional multiple H-bonded strategy between melamine and uracil motifs significantly increased self-assembled behavior as well as π - π stackings, which is an encouraging method for the future researches to adjust the photovoltaic properties of polymer solar cell devices.

In conclusion, we could tune molecular energy levels, morphologies, and device preferemances by a new and straight-forward approach to introducing multiple H-bonded supramolecular structures. The broader light absorption (an extra blue absorption from H-bonded crosslinker **F** and the red-shifted absorption from H-bonded main-chain polymer **PBT**), lower HOMO level (to have a higher V_{oc} value), higher hole mobility, larger crystallinity, and better morphology in H-bonded polymer network **PBT/F** induces better photovoltaic properties than that containing polymer **PBT**. The preliminary photovoltaic performance showed the solar cell device containing 1:1 wt. ratio of **PBT/F** and [6,6]-phenyl C₇₁ butyric acid methyl ester (PC₇₁BM) offers the best power conversion efficiency (PCE) value of 0.86% with a short-circuit current density (J_{sc}) of 4.97 mA/cm², an open circuit voltage (V_{oc}) of 0.55 V, and a fill factor (FF) of 31.5%. The highly directional multiple H-bonded strategy between melamine and uracil motifs significantly increased self-assembled behavior as well as π - π stackings, which is an encouraging method for the future researches

to adjust the photovoltaic properties of polymer solar cell devices.

In summary, we have developed novel supramolecular polymer networks **PBTH/C** and **PBTH/F** based on the formation of multiple hydrogen bonds between conjugated main-chain polymer **PBTH** and uracil-based conjugated cross-linkers **C** and **F** (in proper molar amounts) through complementary melamine and uracil moieties. The supramolecular formation of multiple hydrogen bonds successfully characterized by IR, and UV-Vis spectra measurements. The supramolecular concept has been successfully applied to tune the photophysical, electrochemical, and photovoltaic properties of supramolecular polymer networks **PBTH/C** and **PBTH/F** compared with polymer **PBTH**. The power conversion efficiencies (PCE) values of PSC devices containing supramolecular polymer networks **PBTH/C** and **PBTH/F** (as polymer:PC₇₁BM=1:1 w/w) are found to be 0.97 and 0.68%, respectively, in contrast to 0.52% for polymer **PBTH**. The optimum photovoltaic performance with the highest PCE value of 1.56 % was obtained in the PSC device containing supramolecular polymer networks **PBTH/C** as polymer:PC₇₁BM=1:2 w/w. This supramolecular design is an encouraging approach on the further improvements of any most excellent donor-acceptor photovoltaic polymers to be in conjunction with efficient conjugated cross-linkers complementarily through supramolecular interactions for future polymer solar cell applications.

References

1. Delgado, J. L.; Bouit, P. A.; Filippone, S.; Herranz, M. A.; Marín, N. *Chem. Commun.* **2010**, *46*, 4853; (b) For further information about solar energy, see the International Energy Agency Photovoltaic Power Systems Program at: www.iea-pvps.org.
2. Goswami, D. Y. *Advances in Solar Energy: An annual Review of Research and Development* **2003**, Vol. 15.
3. Becquerel, A. E. *Compt. Rend. Acad. Sci.* **1839**, *9*, 561.
4. Pulfrey, D. L. *Photovoltaic Power Generation*, Van Nostrand Reinhold, New York **1978**.
5. Ohl, R. S.; Silver, L. *U.S. Patent* 2402662, **1946**.
6. Chapin, D. M.; Fuller, C. S.; Pearson, G. L. *J. Appl. Phys.* **1954**, *25*, 676.
7. Tang, C. W.; Albrecht, A. C. *The Journal of Chemical Physics* **1975**, *62*, 2139.
8. Tang, C. W. *Applied Physics Letters* **1986**, *48*, 183.
9. (a) Green, M. A.; Emery, K.; Hishikawa, Y.; Warta, W. *Prog. Photovolt. Res. Appl.* **2010**, *18*, 346; (b) Service, R. F. *Science* **2011**, *332*, 293.
10. Lin, L. Y.; Chen, Y. H.; Huang, Z. H.; Lin, H. W.; Chou, S. H.; Lin, F.; Chen, C. W.; Yi-Hung Liu, Y. H.; Wong, K. T. *J. Am. Chem. Soc.* **2011**, *133*, 15822.
11. Chen, H. Y.; Hou, J.; Zhang, S.; Liang, Y.; Yang, G.; Yang, Y.; Yu, L.; Wu, Y.; Li, G. *Nat Photonics* **2009**, *3*, 649; (b) Gendron, D.; Leclerc, M. *Energy Environ Sci.* **2011**, *4*, 1225.
12. Kietzke, T. *Advances in OptoElectronics* doi:10.1155/2007/40285, Article ID 40285, 1.
13. Hoppe, H.; Sariciftci, N. S. *Advances in Polymer Science* **2008**, *214*, 1.
14. Brabec, C. J.; Sariciftci, N. S.; Hummelen, J. C. *Adv. Funct. Mater.* **2001**, *11*, 15.
15. Thompson, B. C.; Fréchet, J. M. J. *Angew. Chem. Int. Ed.* **2008**, *47*, 58.
16. Blouin, N.; Michaud, A.; Leclerc, M. *Adv. Mater.* **2007**, *19*, 2295.

17. Coakley, K. M.; McGehee, M. D. *Chem. Mater.* **2004**, *16*, 4533.
18. Parker, I. D. *J. Appl. Phys.* **1994**, *75*, 1656.
19. Marks, R. N.; Halls, J. J. M.; Bradley, D. D. C.; Friend, R. H.; Homes, A. B. *J. Phys.: Condens. Matter* **1994**, *6*, 1379.
20. Green, M. A.; Emery, K.; Hishikawa, Y.; Warta, W. *Prog. Photovolt. Res. Appl.* **2010**, *18*, 346.
21. Sariciftci, N. D.; Braun, D.; Zhang, C.; Srdanov, V. I.; Heeger, A. J.; Stucky, G.; Wudl, F. *Appl. Phys. Lett.* **1993**, *62*, 585.
22. Pettersson, L. A. A.; Roman, L. S.; Inganäs, O. *J. Appl. Phys.* **1999**, *86*, 487.
23. Yu, G.; Heeger, A. J. *J. Appl. Phys.* **1995**, *78*, 4510.
24. Halls, J. J. M.; Walsh, C. A.; Greenham, N. C.; Marseglia, E. A.; Friend, R. H.; Moratti, S. C.; Holmes, A. B. *Nature* **1995**, *376*, 498.
25. Kannan, B.; Castelino, K.; Majumdar, A. *Nano Lett.* **2003**, *3*, 1729.
26. Günes, S.; Neugebauer, H.; Sariciftci, N. S. *Chem. Rev.* **2007**, *107*, 1324.
27. Mühlbacher, D.; Scharber, M.; Morana, M.; Zhu, Z.; Waller, D.; Gaudiana, R.; Brabec, C. J. *Adv. Mater.* **2006**, *18*, 2884.
28. Winder, C.; Sariciftci, N. S. *J. Mater. Chem.* **2004**, *14*, 1077.
29. Kitamura, C.; Tanaka, S.; Yamashita, Y., *Chem. Mater.* **1996**, *8*, 570.
30. Ajayaghosh, A. *Chem. Soc. Rev.* **2003**, *32*, 181.
31. Bundgaard, E.; Krebs, F. C. *Sol. Energy Mater. Sol. Cells* **2007**, *91*, 954.
32. Mühlbacher, D.; Scharber, M.; Morana, M.; Zhu, Z.; Waller, D.; Gaudiana, R.; Brabec, C. J. *Adv. Mater.* **2006**, *18*, 2884.
33. Chen, J. W.; Cao, Y. *Acc. Chem. Res.* **2009**, *42*, 1709.

34. Kim, Y.; Cook, S.; Tuladhar, S. M.; Choulis, S. A.; Nelson, J.; Durrant, J. R.; Bradley, D. D. C.; Giles, M.; McCulloch, I.; Ha, C.; Ree, M. *Nat. Mater.* **2006**, *5*, 197.
35. Gadisa, A.; Oosterbaan, W. D.; Vandewal, K.; Bolsee, J.C.; Bertho, S.; D'Haen, J.; Lutsen, L.; Vanderzande, D.; Manca, J. V. *Adv. Funct. Mater.* **2009**, *19*, 3300.
36. Lenes, M.; Wetzelaer, G. A. H.; Kooistra, F. B.; Veenstra, S. C.; Hummelen, J. C.; Blom, P. W. M. *Adv. Mater.* **2008**, *20*, 2116.
37. Dennler, G.; Scharber, M.; Brabec, C. J. *Adv. Mater.* **2009**, *21*, 1323.
38. Brédas, J. L.; Beljonne, D.; Coropceanu, V.; Cornil, J. *Chem. Rev.* **2004**, *104*, 4971.
39. Cai, W.; Gong, X.; Cao, Y. *Sol. Energy Mater. Sol. Cells* **2007**, *94*, 114.
40. Singh, T. B.; Marjanovic, N.; Matt, G. J.; Günes, S.; Sariciftci, N. S.; Ramil, A. M.; Andreev, A.; Sitter, H.; Schwödiauer R.; Bauer, S. *Org. Electron.* **2005**, *6*, 1199.
41. Hoppe, H.; Sariciftci, N. S. *J. Mater. Chem.* **2006**, *16*, 45.
42. Shaheen, S.; Brabec, C. J.; Sariciftci, N. S.; Padinger, F.; Fromherz, T.; Hummelen, J. C. *Appl. Phys. Lett.* **2001**, *78*, 841.
43. Li, G.; Shrotriya, V.; Huang, J. S.; Yao, Y.; Moriarty, T.; Emery, K.; Yang, Y. *Nat. Mater.* **2005**, *4*, 86.
44. Zhou, S.; Yang, L.; Stoneking, S.; You, W. *ACS Appl. Mater. Interfaces* **2010**, *2*, 1377;
45. Blouin, N.; Michaud, A.; Gendron, D.; Wakim, S.; Blair, E.; Neagu-Plesu, R.; Belletête, M.; Durocher, G.; Tao, Y.; Leclerc, M. *J. Am. Chem. Soc.* **2008**, *130*, 732.
46. Park, S. H.; Roy, A.; Beaupre, S.; Cho, S.; Coates, N.; Moon, J. S.; Moses, D.; Leclerc, M.; Lee, K.; Heeger, A. J. *Nat. Photonics* **2009**, *3*, 297.

47. Gendron, D.; Morin, P. O.; Najari, A.; Leclerc, M. *Macromol. Rapid Commun.* **2010**, *31*, 1090.
48. Zhou, E.; Cong, J.; Yamakawa, S.; Wei, Q.; Nakamura, M.; Tajima, K.; Yang, C.; Hashimoto, K. *Macromolecules* **2010**, *43*, 2873.
49. Qin, R.; Li, W.; Li, C.; Du, C.; Veit, C.; Schleiemacher, H. F.; Andersson, M.; Bo, Z.; Liu, Z.; Inganäs, O.; Wuerfel, U.; Zhang, F. *J. Am. Chem. Soc.* **2009**, *131*, 14612.
50. Yi, H.; Johnson, R. G.; Iraqi, A.; Mohamad, D.; Royce, R.; Lidzey, D. G. *Macromol. Rapid Commun.* **2008**, *29*, 1804.
51. Yue, W.; Zhao, Y.; Shao, S.; Tian, H.; Xie, Z.; Geng, Y.; Wang, F. *J. Mater Chem.* **2009**, *19*, 2199.
52. Zhou, E.; Nakamura, M.; Nishizawa, T.; Zhang, Y.; Wei, Q.; Tajima, K.; Yang, C.; Hashimoto, K. *Macromolecules* **2008**, *41*, 8302.
53. Zhou, E.; Wei, Q.; Yamakawa, S.; Zhang, Y.; Tajima, K.; Yang, C.; Hashimoto, K. *Macromolecules* **2010**, *43*, 821.
54. Zhou, E.; Wei, Q.; Yamakawa, S.; Zhang, Y.; Tajima, K.; Yang, C.; Hashimoto, K. *Chem. Mater.* **2009**, *21*, 4055.
55. Chen, L.; Deng, D.; Nan, Y.; Shi, M.; Chan, P. K. L.; Chen, H. *J. Phy. Chem. C* **2011**, *115*, 11282.
56. Zhou, E.; Cong, J.; Tajima, K.; Hashimoto, K. *Chem. Mater.* **2010**, *22*, 4890.
57. Hu, X.; Shi, M.; Zuo, L.; Nan, Y.; Liu, Y.; Fu, L.; Chen, H. *Polymer* **2011**, *52*, 2559.
58. Zhou, H.; Yang, L.; Stuart, A. C.; Price, S. C.; Liu, S.; You, W. *Angew. Chem. Int. Ed.* **2011**, *50*, 2995.
59. Price, S. C.; Yang, L.; Zhou, H.; Stuart, A. C.; You, W. *J. Am. Chem. Soc.* **2011**, *133*, 4625.

60. Chu, T. Y.; Lu, J.; Beaupré, S.; Zhang, Y.; Pouliot, J. R.; Wakim, S.; Zhou, J.; Leclerc, M.; Li, Z.; Ding, J.; Tao, Y. *J. Am. Chem. Soc.* **2011**, *133*, 4250.
61. Wang, H.; Shi, Q.; Lin, Y.; Fan, H.; Cheng, P.; Zhan, X.; Li, Y.; Zhu, D. *Macromolecules* **2011**, *44*, 4213.
62. Yang, M.; Peng, B.; Liu, B.; Zou, Y.; Zhou, K.; He, Y.; Pan, C.; Li, Y. *J. Phys. Chem. C* **2010**, *114*, 17989.
63. Lee, J.; Jung, B. J.; Lee, S. K.; Lee, J. I.; Cho, H. J.; Shim, H. K. *J. Polym. Sci Part A: Polym. Chem.* **2005**, *43*, 1845.
64. Zhang, M.; Fan, H.; Guo, X.; He, Y.; Zhang, Z.; Min, J.; Zhang, J.; Zhao, G.; Zhan, X.; Li, Y. *Macromolecules* **2010**, *43*, 5706.
65. Zhang, M.; Fan, H.; Guo, X.; He, Y.; Zhang, Z. G.; Min, J.; Zhang, J.; Zhao, G.; Zhan, X.; Li, Y. *Macromolecules* **2010**, *43*, 8714.
66. Shi, Q.; Fan, H.; Liu, Y.; Chen, J.; Ma, L.; Hu, W.; Shuai, Z.; Li, Y.; Zhan, X. *Macromolecules* **2011**, *44*, 4230.
67. Li, K. C.; Huang, J. H.; Hsu, Y. C.; Huang, P. J.; Chu, C. W.; Lin, J. T.; Ho, K. C.; Wei, K. H.; Lin, H. C. *Macromolecules* **2009**, *42*, 3681.
68. a) Greef, T. F. A. D.; Smulders, M. M. J.; Wolfs, M.; Schenning, A. P. H. J.; Sijbesma, R. P.; Meijer, E. W. *Chem. Rev.* **2009**, *109*, 5687; (b) Lianes-Pallas, A.; Palma, C. -A.; Piot, L.; Belbakra, A.; Listorti, A.; Prato, D. M.; Samorì, P.; Armaroli, N.; Bonifazi, D. *J. Am. Chem. Soc.* **2009**, *131*, 509; (c) González-Rodríguez, D.; Schenning, A. P. H. *J. Chem. Mater.* **2011**, *23*, 310.
69. (a) Bonifazi, D.; Kiebele, A.; Stöhr, M.; Cheng, F.; Jung, T.; Diederich, F.; Spillmann, H. *Adv. Funct. Mater.* **2007**, *17*, 1051; (b) Surin, M.; Samorì, P. *Small* **2007**, *3*, 190.

70. Wiesenauer, E. F.; Edwards, J. P.; Scalfani, V. F.; Travis S. Bailey, T. S.; Gin, D. L. *Macromolecules* **2011**, *44*, 5075.
71. (a) Wessendorf, F.; Grimm, B.; Guldi, D. M.; Hirsch, A. *J. Am. Chem. Soc.* **2010**, *132*, 10786; (b) Seitz, W.; Jiménez, Á. J.; Carbonell, E.; Grimm, B.; Salomé, M.; -Morgade, R.; Guldi, D. M.; Torres, T. *Chem. Commun.* **2010**, *46*, 127.
72. (a) Chen, Y.Y., Tao, Y. T.; Lin, H. C. *Macromolecules* **2006**, *39*, 8559; (b) Padhy, H.; Sahu, D.; Chiang, I. H.; Patra, D.; Kekuda, D.; Chu, C. -W.; Lin, H. -C. *J. Mater. Chem.*, **2011**, *21*, 1196; (c) Nair, K. P.; Breedveld, V.; Weck, M. *Macromolecules* **2011**, *44*, 3346.
73. (a) Schenning, A. P. H. J.; Herrikhuyzen, J.; Jonkheijm, P.; Chen, Z.; F. Würthner; Meijer, E. W. *J. Am. Chem. Soc.* **2002**, *124*, 10252; (b) Jonkheijm, P.; Stutzmann, N.; Chen, Z.; Leeuw, D. M.; Meijer, E. W.; Schenning, A. P. H. J.; Würthner, F. *J. Am. Chem. Soc.* **2006**, *128*, 9535.
74. (a) El-ghayoury, A.; Schenning, A. P. H. J.; Hal, P. A. V.; Duren, J. K. J. V.; Janssen, R. A. J.; Meijer, E. W. *Angew. Chem. Int. Ed.* **2001**, *40*, 3660; (b) Jonkheijm, P.; Duren, J. K. J. V.; Kemerink, M.; Janssen, R. A. J.; Schenning, A. P. H. J.; Meijer, E. W. *Macromolecules* **2006**, *39*, 784.
75. (a) Mazzio, K. A.; Yuan, M.; Okamoto, K.; Luscombe, C. K. *ACS Appl. Mater. Interfaces* **2011**, *3*, 271; (b) Loser, S.; Bruns, C. J.; Miyauchi, H.; Ortiz, R. P.; Facchetti, A.; Stupp, S. I.; Marks, T. J. *J. Am. Chem. Soc.* **2011**, *133*, 8142.
76. (a) Liang, T. C.; Chiang, I. H.; Yang, P. J.; Kekuda, D.; Chu, C. W.; Lin, H. C. *J. Polym. Sci. Part A: Polym. Chem.* **2009**, *47*, 5998; (b) Sahu, D.; Padhy, H.; Patra, D.; Kekuda, D.; Chu, C. W.; Chiang, I. H.; Lin, H. C. *Polymer* **2010**, *51*, 6182.
77. Po, R.; Maggini, M.; Camaioni, N. *J. Phys. Chem. C* **2010**, *114*, 695.

78. Zhag, S.; Guo, Y.; Fan, H.; Liu, Y.; Chen, H. -Y.; Yang, G.; Zhan, X.; Liu, Y.; Li, Y.; Yang, Y. *J. Polym. Sci Part A: Polym. Chem.* **2009**, *47*, 5498.
79. Zhou, E.; Cong, J.; Tajima, K.; Yang, C.; Hashimoto, K. *Macromol Chem Phys* **2011**, *212*, 305.
80. (a) Greef, T. F. A. D.; Smulders, M. M. J.; Wolffs, M.; Schenning, A. P. H. J.; Sijbesma, R. P.; Meijer, E. W. *Chem. Rev.* **2009**, *109*, 5687; (b) González-Rodríguez, D.; Schenning, A. P. H. J. *Chem. Mater.* **2011**, *23*, 310.
81. (a) Cheng, Y. J.; Yang, S. H.; Hsu, C. S. *Chem. Rev.* **2009**, *109*, 5868; (b) Bundgaard, E.; Krebs, F. C. *Sol Energy Mater Solar Cells* **2007**, *91*, 954.; (c) Shrotriya, V. *Nat. Photonics* **2009**, *3*, 447.
82. (a) Velusami, M.; Huang, J. H.; Hsu, Y. C.; Chou, H. H.; Ho, K. C.; Wu, P. L.; Chang, W. H.; Lin, J. T.; Chu, C. W. *Organic Letters* **2009**, 4898; (b) Huang, J. H.; Velusami, M.; Ho, K. C.; Lin, J. T.; Chu, C. W. *J. Mater. Chem.* **2010**, *20*, 2820.
83. (a) Daun, C.; Cai, W.; Huang, F.; Zhang, J.; Wang, M.; Yang, T.; Zhong, C.; Gong, X.; Cao, Y. *Macromolecules* **2010**, *43*, 5262; (b) Boudreault, P. T.; Michaud, A.; Leclerc, M. *Macromol. Rapid Commun.* **2007**, *28*, 2176.
84. (a) Mühlbacher, D.; Scharber, M.; Morana, M.; Zhu, Z.; Waller, D.; Gaudiana, R.; Brabec, C. *Adv. Mater.* **2006**, *18*, 2884; (b) Peet, J.; Kim, J. Y.; Coates, N. E.; Ma, W. L.; Moses, D.; Heeger, A. J.; Bazan, G. C. *Nat. Mater* **2007**, *6*, 497.
85. (a) Chen, M. H.; Hou, J.; Hong, Z.; Yang, G.; Sista, S.; Chen, L. M.; Yang, Y. *Adv. Mater.* **2009**, *21*, 4238; (b) Gadisa, A.; Mammo, W.; Andersson, L. M.; Admassive, S.; Zhang, F.; Andersson, M. R.; Inganäs, O. *Adv. Funct. Mater.* **2007**, *17*, 3836.

86. (a) Tang, W. ; Kietzke, T.; Vemulamada P.; Chen, Z. -K. *J. Polym. Sci. Part A: Polym. Chem.* **2007**, *4*, 5266; (b) Huang, J. H.; Li, K. C.; Wei, H. Y.; Chen, P. Y.; Lin, L.Y.; Kekuda, D.; Lin, H. C.; Ho, K. C.; Chu, C. W. *Organic Electronics* **2009**, *10*, 1109.
87. Blouin, N.; Michaud, A.; Leclerc, M. *Adv. Mater.* **2007**, *19*, 2295.
88. Wong, W. Y.; Wang, X. Z.; He, Z.; Chen, K. K.; Djurišić, A. B.; Cheung, K. Y.; Yip, C. T.; Ng, A. M. C.; Xi, Y. Y.; Mak, C. S. K.; Chan, W. K. *J. Am. Chem. Soc.* **2007**, *129*, 14372.
89. Wei, Y.; Yang, Y.; Yeh, J. M. *Chem. Mater* **1996**, *8*, **2659**.
90. (a) Chan, S. H.; Chen, C. P.; Chao, T. C.; Ting, C.; Lin, C. S.; Ko, B. T. *Macromolecules* **2008**, *41*, 5519; (b) Jung, I. H.; Yu, J.; Jeong, E.; Kwon, S.; Kong, H.; Lee, K.; Woo, H.Y.; Shim, H.K. *Chem. Eur J.* **2010**, *16*, 3743.
91. (a) Liang, Y.; Wu, Y.; Feng, D.; Tsai, S.T.; Son, H.J.; Li, G.; Yu, L. *J. Am. Chem. Soc.* **2009**, *131*, 56; (b) Jung, I. H.; Kim, H.; Park, M, J.; Kim, B.; Park, J, H.; Jeong, E.; Woo, H. Y.; Yoo, S.; Shim, H. K. *J. Polym. Sci Part A: Polym. Chem.* **2010**, *48*, 1423.
92. Baek, N. S.; Hau, S. K.; Yip, H. L.; Acton, O.; Chen, K. S.; Jen, A. K. Y. *Chem. Mater.* **2008**, *20*, 5734.
93. (a) Zhou, Y. H.; Wang, Y. N.; Wu, W, C.; Wang, H.; Han, L.; Tian, W.J.; Bassler, H. *Sol. Energy Mater Sol. Cells* **2007**, *91*, 1842; (b) Liu, J.; Shi, Y. J.; Yang, Y. *Adv. Funct. Mater.* **2001**, *11*, 420.
94. Li, Y.; Xue, L.; Li, H.; Xu, B.; Wen, S.; Tian, W. *Macromolecules* **2009**, *42*, **4491**.
95. Liu, J.; Zhang, R.; Osaka, I.; Mishra, S.; Javier, A. E.; Smilgies, D. M.; Kowalewski, T.; McCullough, R. D. *Adv. Funct. Mater.* **2009**, *19*, 3427.
96. Patra, D.; Sahu, D.; Padhy, H.; Kekuda, D.; Chu, C. W.; Lin, H. C. *J. Polym. Sci Part A: Polym. Chem.* **2010**, *48*, 5479.

97. Jung, I. H.; Jung, Y. K.; Lee, J.; Park, J. H.; Woo, H. Y.; Lee, J. -I.; Chu, H. Y.; Shim, H. K. *J. Polym. Sci. Part A: Polym. Chem.* **2008**, *46*, 7148.
98. Sahu, D.; Patra, D.; Padhy, H.; Huang, J. H.; Chu, C. W.; Lin, H. C. *J. Polym. Sci Part A: Polym. Chem.* **2010**, *48*, 5812.
99. Zhang, X.; Steckler, T. T.; Dasari, R. R.; Ohira, S.; Potscavage, W. J.; Jr, Tiwari, S. P.; Coppée, S. Ellinge, S.; Barlow, S.; Brédas, J. -L.; Kippelen, B.; Reynolds, J. R.; Marder, S. R. *J. Mater. Chem.* **2010**, *20*, 123.
100. Roncali, J. *Chem Rev.* **1997**, *97*, 173.
101. Huo, L.; He, C.; Han, M.; Zhou, E.; Li, Y. *J. Polym. Sci. Part A: Polym. Chem.* **2007**, *45*, 3861.
102. Price, S. C.; Stuart, A. C.; You, Y. *Macromolecules* **2010**, *43*, 4609; (b) Ding, P.; Chu, C. C.; Liu, B.; Peng, B.; Zou, Y.; He, Y.; Zhou, K.; Hsu, C. S. *Macromol. Chem. Phys.* **2010**, *211*, 2555.
103. Hou, J.; Chen, T. L.; Zhang, S.; Chen, H. -Y.; Yang, Y. *J. Phys. Chem. C* **2009**, *113*, 1601.
104. Kleinhenz, N.; Yang, L.; Zhou, H.; Price, S. C.; You, W. *Macromolecules* **2011**, *44*, 872.
105. Chen, Y. C.; Yu, C. Y.; Fan, Y. L.; Hung, L. I.; Chen, C. P.; Ting, C.; *Chem. Commun.* **2010**, *46*, 6503.
106. Li, Y.; Li, Z.; Wang, C.; Li, H.; Lu, H.; Xu, B.; Tian, W. *J. Polym. Sci. Part A: Polym. Chem.* **2008**, *46*, 2765.
107. (a) Piot, L.; Palma, C. A.; Pallas, A. L.; Prato, M.; Szekrényes, Z.; Kamarás, K.; Bonifazi, D.; Samori, P. *Adv. Funct. Mater.* **2009**, *19*, 1207; (b) Kuo, C. Y.; Su, M. S.; Ku, C. S.; Wang, S. M.; Lee, H. Y.; Wei, K. H. *J. Mater. Chem.* **2011**, *21*, 11605.

108. (a) Delbosc, N.; Reynes, M.; Dautel, O. J.; Wantz, G.; Porte, J. P. L.; Moreau, J. J. E. *Chem. Mater.* **2010**, *22*, 5258; (b) Liu, Y.; Xiao, S.; Li, H.; Liu, H.; Lu, F.; Zhaung, J.; Zhu, D. *J. Phys. Chem. B*, **2004**, *108*, 6256.
109. Patra, D.; Sahu, D.; Padhy, H.; Kekuda, D.; Chu, C. W.; Lin, H. C. *J. Polym. Sci. Part A: Polym. Chem.* **2010**, *48*, 5479.
110. Li, Z.; Pei, J.; Li, Y.; Xu, B.; Deng, M.; Liu, Z.; Li, H.; Lu, H.; Li, Q.; Tian, W. *J. Phys. Chem. C* **2010**, *114*, 18270.
111. (a) Padhy, H.; Sahu, D.; Patra, D.; Pola, M. K.; Huang, J. H.; Chu, C. W.; Wei, K. H.; Lin, H. C. *J. Polym. Sci. Part A: Polym. Chem.* **2011**, *49*, 3417; (b) Padhy, H.; Huang, J. H.; Sahu, D.; Patra, D.; Kekuda, D.; Chu, C. W.; Lin, H. C. *J. Polym. Sci. Part A: Polym. Chem.* **2010**, *48*, 4823.
112. Wu, J. S.; Cheng, Y. J.; Dubosc, M.; Hsieh, C. H.; Chang, C. Y.; Hsu, C. S. *Chem. Commun.* **2010**, *46*, 3259.
113. Zhang, Y.; Hau, S. K.; Yip, H. L.; Sun, Y.; Action, O.; Jen, A. K. Y. *Chem. Mater.* **2010**, *22*, 2696.
114. Patra, D.; Sahu, D.; Padhy, H.; Kekuda, D.; Chu, C. W.; Wei, K. H.; Lin, H. C. *Macromol. Chem. Phys.* **2011**, *212*, 1960.
115. (a) Li, Y.; Xu, B.; Li, H.; Cheng, W.; Xue, L.; Chen, F.; Lu, H.; Tian, W. *J. Phys. Chem. C* **2011**, *115*, 2386; (b) Li, Y.; Li, Z.; Wang, C.; Li, H.; Lu, H.; Xu, B.; Tian, W. *J. Polym. Sci. Part A: Polym. Chem.* **2010**, *48*, 2765.
116. (a) Shunmugam, R.; Gabriel, G. J.; Amaer, K. A.; Tew, G. N. *Macromol. Rapid. Commun.* **2010**, *31*, 784; (b) Yan, P.; Chowdhury, A.; Holman, M. W.; Adams, D. M. *J. Phys. Chem. B* **2005**, *109*, 724.

117. (a) Boudreault, P. L.T.; Najari, A.; Leclerc, M.; *Chem. Mater.* **2011**, *23*, 456; (b) Wang, E.; Wang, M.; Wang, L.; Duan, C.; Zhang, J.; Cai, W.; He, C.; Wu, H.; Cao, Y. *Macromolecules* **2009**, *42*, 4410.
118. Würthner, F.; Chen, Z.; Hoeben, F. J. M.; Peter Osswald, P.; You, C. C.; Jonkheijm, P.; Herrikhuyzen, J. V.; Schenning, A. P. H. J.; Schoot, P. P. A. M. V. D.; Meijer, E. W.; Beckers, E. H. A.; Meskers, S. C. J.; Janssen, R. A. J. *J. Am. Chem. Soc.* **2004**, *126*, 10611.
119. Hoeben, F. J. M.; Zhang, J.; Lee, C. C.; Pouderoijen, M. J.; Wolfs, M.; Würthner, F.; Schenning, A. P. H. J.; Meijer, E. W.; Feyter, S. D. *Chem. Eur. J.* **2008**, *14*, 8579.
120. Yagai, S.; Kubota, S.; Unoike, K.; Karatsu, T.; Kitamura, A. *Chem. Commun.* **2008**, 4466.
121. Khlyabich, P. P.; Burkhart, B.; Ng, C. F.; Thompson, B. C. *Macromolecules* **2011**, *44*, 5079.
122. (b) Li, W.; Qin, R.; Yi, Zhou, Y.; Andersson, M.; Li, F.; Zhang, C.; Li, B.; Liu, Z.; Bo, Z.; Zhang, F. *Polymer* **2010**, *51*, 3031; (c) Inaganäs, O.; Zhang, F.; Andersson, M. R. *Acc. Chem. Res.* **2009**, *4*, 1731.
123. Zhang, J.; Cai, W.; Huang, F.; Wang, E.; Zhong, C.; Liu, S.; Wang, M.; Duan, C.; Yang, T.; Cao, Y. *Macromolecules* **2011**, *44*, 894; (b) Zhao, W.; Kai, W.; Xu, R.; Yang, W.; Gong, X.; Wu, H.; Cao, Y. *Polymer* **2010**, *51*, 3196.
124. Tamilavan, V.; Sakthivel, P.; Li, Y.; Song, M.; Kim, C. H.; Jin, S. H. *J. Polym. Sci. Part A Polym. Chem.* **2010**, *48*, 3169.
125. (a) Wang, E.; Ma, Z.; Zhang, Z.; Henriksson, P.; Inaganäs, O.; Zhang, F.; Andersson, M. R. *Chem. Commun.* **2011**, 47, 4908; (b) Tamilavan, V.; Song, M.; Jin, S. H.; Hyun, M. H. *Polymer* **2011**, *52*, 2384.

126. Walker, B.; Tamayo, A. B.; Dang, X. D.; Zalar, P.; Seo, J. H.; Garcia, A.; Tantiwiwat, M. Nguyen, T. Q. *Adv. Funct. Mater.* **2009**, *19*, 3063.
127. (a) Guo, X.; Xin, H.; Kim, F.S.; Liyanage, A. D. T.; Jenekhe, S. A.; Watson, M. D. *Macromolecules* **2011**, *44*, 269; (b) Zhang, G.; Fu, Y.; Zhang, Q.; Xie, Z. *Polymer* **2010**, *51*, 2313.



Curriculum Vitae

Personal Details:

Name: Dhananjaya Patra
Date of Birth: 9th June, 1981
Nationality: Indian
Email: itspilu@gmail.com
Contact no: +886-911842964 (Taiwan), +91-6819-270122 (India)
Permanent address: At: Khillabadi, Po: Sorada Dist: Ganjam, Odisha, 761008, (India)



Education:

2007-2011: National Chiao Tung University, Hsinchu, Taiwan
Ph.D. studies at Department of Materials Science and Engineering
2002-2004: Berhampur University, Orissa, India
M.Sc studies at Department of Chemistry at S.K.C.G. College,
Paralakhemundi
1998-2001: Berhampur University, Orissa, India
B.Sc studies at Science College, Hinjilicut

Work Experience:

Dec.2004 to Aug. 2005: Working as a R & D Chemist in **Themis Medicare Ltd., Vapi.**

Aug.2005 to June 2006: Working as a Quality Assurance staff in **Mapra Laboratory Pvt. Ltd., Daman** (an ARISTO group).

June2006 to June 2007: Working as a Quality Control Management staff in **Jupiter Remedies, Daman (Cipla group).**

Publications:

1. **Dhananjaya Patra**, Duryodhan Sahu, Harihara Padhy, Dhananjay Kekuda, Chih-Wei Chu and Hong-Cheu Lin*, "Synthesis and Applications of 2,7-Carbazole-Based Conjugated Main-Chain Copolymers Containing Electron Deficient Bithiazole Units for Organic Solar Cells" *Journal of Polymer Science: Part A: Polymer Chemistry*, **2010**, *48*, 5479–5489.
2. **Dhananjaya Patra**, Duryodhan Sahu, Harihara Padhy, Dhananjay Kekuda, Chih-Wei Chu*, Kung-Hwa Wei and Hong-Cheu Lin* "Fine Tuning of HOMO Energy Levels for Low-Band-Gap Photovoltaic Copolymers Containing Cyclopentadithienopyrrole and Bithiazole Units" *Macromol. Chem. Phys.*, **2011**, *212*, 1960–1970.
3. **Dhananjaya Patra**, Mohan Ramesh, Duryodhan Sahu, Harihara Padhy, Chih-Wei Chu*, Kung-Hwa Wei, Hong-Cheu Lin* "Synthesis and Applications of a Novel Supramolecular Polymer Network with Multiple H-bonded Melamine Pendants and Uracil Cross-linkers" Accepted in "*Journal of Polymer Science: Part A: Polymer Chemistry*, **2012**, doi: 10.1002/pola.25853.
4. **Dhananjaya Patra**, Duryodhan Sahu, Mohan Ramesh, Harihara Padhy, Chih-Wei Chu*, Kung-Hwa Wei and Hong-Cheu Lin* "Enhancement of Photovoltaic Properties in Supramolecular Polymer Networks Featuring a Solar Cell Main-Chain Polymer H-Bonded with Conjugated Cross-Linkers" Submitted to *Polymer*, **2011**.
5. Harihara Padhy, Jen-Hsien Huang, Duryodhan Sahu, **Dhananjaya Patra**, Dhananjay Kekuda, Chih-Wei Chu and Hong-Cheu Lin*, "Synthesis and applications of low-bandgap conjugated polymers containing phenothiazine donor and various benzodiazole acceptors for polymer solar cells" *Journal of Polymer Science: Part A: Polymer Chemistry*, **2010**, *48*, 4823–4834.
6. Duryodhan Sahu, Harihara Padhy, **Dhananjaya Patra**, Jen-Hsien Huang, Chih-Wei Chu and Hong-Cheu Lin*, "Synthesis and characterization of novel low-bandgap triphenylamine-based conjugated polymers with main-chain donors and pendent acceptors for organic photovoltaics" *Journal of Polymer Science: Part A: Polymer Chemistry*, **2010**, *48*, 5812–5823.
7. Duryodhan Sahu, Harihara Padhy, **Dhananjaya Patra**, Dhananjay Kekuda, Chih-Wei Chu, I-Hung Chiang, and Hong-Cheu Lin*, "Synthesis and application of H-Bonded cross-linking polymers containing a conjugated pyridyl H-Acceptor side-chain polymer and various carbazole-based H-Donor dyes bearing symmetrical cyanoacrylic acids for organic solar cells" *Polymer*, **2010**, *51*, 6182-6192.
8. Duryodhan Sahu, Harihara Padhy, **Dhananjaya Patra**, Jen-Fu. Yin, Ying-Chan. Hsu, Jiann.-T'Suen. Lin, Kuang-Lieh Lu, Kung-Hwa Wei, and Hong-Cheu Lin*, "Synthesis and applications of novel acceptor-donor-acceptor organic dyes with dithienopyrrol- and fluorine-cores for dye-sensitized solar cells" *Tetrahedron* **2011**, *67*, 303-311.

9. Harihara Padhy, Duryodhan Sahu, I-Hung Chiang, **Dhananjaya Patra**, Dhananjay Kekuda, Chih-Wei Chu and Hong-Cheu Lin*, “Synthesis and Applications of Main-Chain Ru^{II} Metallo-Polymers Containing Bis-terpyridyl Ligands with Various Benzodiazole Cores for Solar Cells” *J. Mater. Chem.* **2011**, *21*, 1196-1205.
10. Harihara Padhy, Duryodhan Sahu, **Dhananjaya Patra**, Murali Krishna Pola, Jen-Hsien Huang, Chih-Wei Chu, Kung-Hwa Wei and Hong-Cheu Lin*, “Synthesis and Applications of Cyano-Vinylene-Based Polymers Containing Cyclopentadithiophene and Dithienosilole Units for Photovoltaic Cells” *Journal of Polymer Science: Part A: Polymer Chemistry*, **2011**, *49*, 3417–3425.
11. Hsuan-Chih Chu, Duryodhan Sahu, Ying-Chan Hsu, Harihara Padhy, **Dhananjaya Patra**, Jiann.-T’Suen. Lin, Dibyendu Bhattacharya, Kuang-Lieh Lu, Kung-Hwa Wei, and Hong-Cheu Lin*, “Structural planarity and conjugation effects of novel symmetrical acceptor-donor-acceptor Organic Sensitizers on Dye-Sensitized Solar Cells” *Dyes and pigments*, **2011**, doi:10.1016/j.dyepig.2011.09.012.
12. Harihara Padhy, Mohan Ramesh, **Dhananjaya Patra**, Rudrakanta Satapathy, Murali krushna Pola, Hsuan- Chih Chu, Chih -Wei Chu*, Kung- Hwa Wei and Hong-Cheu Lin*, “Synthesis of Main-Chain Metallo-Copolymers Containing Donor and Acceptor Bis-Terpyridyl Ligands for Photovoltaic Applications” *Macromol. Rapid Commun.*, **2012**, doi: 10.1002/marc.201100752.

